Entanglement Entropy of Scalar Fields in Causal Set Theory

by

Yasaman Kouchekzadeh Yazdi

A thesis
presented to the University of Waterloo
in fulfillment of the
thesis requirement for the degree of
Doctor of Philosophy
in
Physics

Waterloo, Ontario, Canada, 2017

Examining Committee Membership

The following served on the Examining Committee for this thesis. The decision of the Examining Committee is by majority vote.

- External Examiner: Professor Steven Carlip
- Supervisors: Professors Niayesh Afshordi and Rafael Sorkin
- Internal Member: Professor Roger Melko
- Internal-external Member: Professor Florian Girelli
- Other Member: Professor Robert Myers

This thesis consists of material all of which I authored or co-authored: see Statement of Contributions included in the thesis. This is a true copy of the thesis, including any required final revisions, as accepted by my examiners.

I understand that my thesis may be made electronically available to the public.

Statement of Contributions

The publications on which this thesis is based (all of which I authored or co-authored) are:

- **Chapter 4:** Mehdi Saravani, Rafael D. Sorkin, and Yasaman K. Yazdi. Spacetime entanglement entropy in 1 + 1 dimensions. Class. Quant. Grav., 31(21):214006, 2014.
- **Chapters 4, 5 and 6:** Rafael D. Sorkin and Yasaman K. Yazdi. Entanglement Entropy in Causal Set Theory. arXiv:1611.10281. 2016.
- **Appendices A and B:** Yasaman K. Yazdi and Achim Kempf. Towards Spectral Geometry for Causal Sets. Class. Quant. Grav., 34(9):094001, 2017.
- **Appendix D:** Yasaman K. Yazdi. Zero Modes and Entanglement Entropy. JHEP, 04:140, 2017.

Appendix C consists of a collection of unpublished calculations by me.

Abstract

Entanglement entropy is now widely accepted as having deep connections with quantum gravity. It is therefore desirable to understand it in the context of causal sets, especially since they provide the UV cutoff needed to render entanglement entropy finite in a natural and covariant manner. Defining entropy in a causal set is not straightforward because the type of canonical hypersurface-data on which definitions of entanglement typically rely is not available in a causal set. Instead, we appeal to a more global expression given in [1] which, for a gaussian scalar field, expresses the entropy of a spacetime region in terms of the field's correlation function within that region.

We first consider this spacetime entropy for a $1+1$-dimensional "causal diamond" in a flat continuous spacetime immersed in the vacuum within a larger causal diamond (our choice of vacuum being the Sorkin-Johnston vacuum described more fully in Chapter 2). The spacetime entropy of the smaller diamond in this case measures (when interpreted spatially) the entanglement between a line-segment and its complement within a larger line-segment. In this situation we carry out the computation numerically for a massless scalar field. The required ultraviolet cutoff is implemented as a truncation on *spacetime* mode sums, and we find excellent agreement with the expected form of the entropy (i.e. an area law) from conformal field theory.

Carrying this formula over to a causal set, one obtains an entanglement entropy which is finite with a natural UV cutoff and Lorentz invariant. Herein we evaluate this entropy for causal sets sprinkled into a $1+1$-dimensional causal diamond in flat spacetime, and specifically for a smaller order-interval (causal diamond) within a larger concentric one. We find in the first instance an entropy that obeys a (spacetime) volume law instead of the expected (spatial) area law. We find, however, that one can obtain the expected area law by following a prescription for truncating the eigenvalues of a certain "Pauli-Jordan" operator and the projections of their eigenfunctions on the Wightman function that enters into the entropy formula.

We also study the "entropy of coarse-graining" generated by thinning out the causal set, and we compare it with what one obtains by similarly thinning out a chain of harmonic oscillators, finding the same "universal" behaviour in both cases.

Acknowledgements

First and foremost I would like to thank my supervisors Niayesh Afshordi and Rafael Sorkin. I could not have asked for better advisors than you. Thank you for all you have taught me and for making my graduate studies the positive experience that it has been.

I thank my friends: Ravi Kunjwal, Yangang Chen, Miguel Zilhão, Heidar Moradi, Mansour Karami, Farbod Kamiab, Sebastian Mizera, Laura Eilers, Jonah Miller, Siavash Aslanbeigi, and Markus Hauru. Squash games, movie nights, dinner parties, and lunch/dinner discussions in the bistro with you will be missed.

I am thankful to Sumati Surya for her hospitality at the Raman Research Institute in Bangalore during two visits and for organizing meetings where many fruitful discussions about causal set theory took place. I thank my collaborators Mehdi Saravani and Achim Kempf. I thank Fay Dowker for sharing her insights about my work. I thank Robert Mann for his helpful comments on my research during my committee meetings, and I thank the members of my defence committee: Steven Carlip, Florian Girelli, Roger Melko, and Robert Myers.

I would like to thank the friendly staff at Perimeter Institute, especially Dawn Bombay, Anne Little, and Joy Montgomery. Thank you to my office mates and friends Chiamaka Okoli and Naty Altamirano.

I thank my parents and sister for their support and encouragement.

Finally, I would like to thank Anton. Thank you for your love and support throughout the years. It has been very important to me. Also thank you for so often listening to me talk about my research. Your questions and comments allow me to sharpen my thoughts.

Dedication

Dedicated to my father.

Table of Contents

List of Tables

List of Figures

Chapter 1

Introduction

Entanglement entropy is widely believed to be an important clue to a better understanding of quantum gravity. Beginning with the original proposal that black hole entropy may be entanglement entropy in whole or in part [2], and continuing through the current surge of interest excited by Van Raamsdonk's ideas on deriving the spacetime metric from quantum entanglement [3, 4], evidence has been accumulating that entanglement entropy has the potential to unveil some of the mysteries surrounding the interplay between the Lorentzian kinematics of general relativity and the interference-laden dynamics of quantum theory.

Despite this history, it is only recently that a workable definition of entanglement entropy has been formulated for causal sets [1]. It is customary to conceive of entropy in a quantum field theory as defined relative to a spacelike surface Σ on which the momentary state of the field is represented by a density-matrix $\rho(\Sigma)$. For some purposes a more global notion of entropy would be preferable. For one thing, the notion of state at a moment of time might not survive in quantum gravity, and it seems in special jeopardy in relation to discrete theories, including causal sets [5] and others. Moreover, even in flat spacetimes, quantum fields are believed to be too singular to be meaningfully restricted to lower dimensional submanifolds, and in the context of quantum gravity with its fluctuating causal structure, this problem can only become worse. A more global conception of entropy is also called for if one aims at a path-integral or "histories-based" formulation of quantum mechanics. And such a conception would seem especially fitting in connection with black holes, whose very definition is global in character.

But over and above all these considerations stands the question of an ultraviolet "cut-off". If one seeks to compute, for example, the entropy of entanglement of a scalar field between the interior and exterior of a black hole, one inevitably encounters a divergent

answer that traces its existence to the infinitely many high frequency modes of the field in the neighbourhood of the horizon. Within a particular Cauchy surface Σ, one can cut these modes off at some given wavelength λ but there is no guarantee that one would obtain the same answer if one tried to use the same cutoff with a different hypersurface. And without such a guarantee, it seems hard to feel fully confident in basic results like the proportionality of entanglement entropy to area [2, 6].

Thus arises the need for a covariant (locally Lorentz invariant) cutoff or — better still — a more fundamental theory of spacetime structure that would furnish nature's own regularization scheme. Based on evidence from causal sets and such attempts as non-commutative geometry, one can anticipate that an entropy defined this way would need to refer to whole regions of spacetime rather than simply hypersurfaces. (For example, the spatio-temporal volume-element is invariant, but the spatial volume-element is not, a basic underpinning of causal set theory.) The need for a covariant discreteness or other covariant cutoff thus gives rise to a further need for a definition of entropy that does not rely on the notion of state on a hypersurface.

Recently, an expression of this kind has been derived, which, for a gaussian scalar field (a free scalar field in a gaussian state), deduces an entropy for an arbitrary region R of spacetime from the correlation function of the field within that region, $\langle 0|\phi(x)\phi(x')|0\rangle$, where $|0\rangle$ is the given gaussian state [1]. When R is globally hyperbolic with Cauchy surface Σ, the resulting entropy can be identified with that of Σ, but unlike with previous formalizations of the entropy concept, this expression is *covariant* in the sense that it involves only space-time quantities[1]. This is the definition of entropy we primarily use in this thesis.

We begin in Chapter 2 with an introduction to and some background on causal set theory and quantum field theory on a causal set. Here we also introduce much of the terminology that will be referred to throughout this thesis. We then review in Chapter 3 conventional entanglement entropy results and introduce the spacetime definition of entropy which we will be working with. Chapter 4 discusses the entanglement entropy of a causal diamond in 1+1-dimensional continuum flat spacetime, using the spacetime entropy definition. The properties of this new definition of entropy are determined in this setup. We find that, indeed, the entanglement entropy of a scalar field restricted to a smaller diamond inside a bigger diamond scales with an area law in terms of the UV cutoff

[1]This "covariant" entropy agrees formally with the usual one [7, 8] in situations where both can be defined, but it applies also to non-globally hyperbolic spacetime regions, to causal sets, and more generally to any algebra with bosonic generators, as illustrated by the quantum theories we study herein. The "new" entropy is also new in the sense that it demands a different kind of UV cutoff, and each different way of introducing a cutoff is technically a different definition of entropy.

(the conventional result). This result serves as an important test of the new definition of entanglement entropy, and is a key step to applying the definition in other theoretically interesting settings. It is also an important result to compare future work to, such as the causal set result presented in Chapter 5.

The causal set entropy results in Chapter 5 are the main results of this thesis. This is the first time entanglement entropy has been successfully calculated in causal set theory, and opens the door to calculate entanglement entropy in many fundamental settings in quantum gravity. We specifically consider the entropy of a causal set sprinkled into a $1+1$-dimensional causal diamond in flat spacetime. Despite the ingredients for this work being readily available from previous works, we had to overcome considerable technical difficulty to obtain physically meaningful results. It turns out that a naive application of the spacetime entropy definition to causal sets leads to a counter-intuitive spacetime-volume scaling (as opposed to an entropy which scales as the spatial area in the limit of small discreteness scale). We show below how to obtain the anticipated area law by means of a suitable truncation scheme. We also put forward an intuitive explanation of how the pre-truncation volume-scaling arises, and of why it should be regarded as spurious from the point of view of the continuum.

The entropy calculations in the causal set are easily amenable to restrictions of the field functions to subsets which are not necessarily connected subregions of spacetime. For example, we can consider a collection of disjoint subregions or a coarse-grained subset of a whole region. In connection to this, in Chapter 6 we study the entropy of coarse-graining in the causal set by considering subsets which are more dilute versions of the original causal set. We also compare our results to those obtained from coarse-graining a chain of harmonic oscillators. When a comparison is possible between the causal set and harmonic oscillator cases, the results agree with one another. We find that this entropy of coarse-graining demonstrates universal properties. The entropy scales quadratically with the number of degrees of freedom in the system, and a maximum entropy is reached when around half the degrees of freedom remain in the system.

Much of the work presented here falls into the broader program of studying scalar field theory on a fixed background causal set. In this context many useful operators such as the retarded Green function and Feynman propagator have been defined and studied. The Feynman propagator expresses the strength of the correlations between quantum field fluctuations at pairs of points. Since these correlations drop with the invariant distance of the two points, the Feynman propagator in effect provides a measure for the invariant distance between points in spacetime. The Feynman propagator could therefore substitute for the metric. Correspondingly, instead of using rulers and clocks (which in any case do not exist at extremely small scales) it is possible, in principle, to measure distances in spacetime

by measuring the correlations of quantum fluctuations of fields [9]. In Appendix A, we show for 2-dimensional spacetimes described by causal sets that the Feynman propagator does indeed contain all metric information: knowing the Feynman propagator is to know the causal set. The Feynman propagator on causal sets therefore provides, in this sense, a quantitative measure of the invariant distances between events of its causal set.

In Appendix B we comment on how rich in information these operators' spectra are. We consider spacetimes described by causal sets and we calculate the spectra of their correlators and d'Alembert operators, or more accurately, of their self-adjoint and anti-self-adjoint parts. We find numerical evidence that these spectra contain a large amount of geometric information: It occurs relatively rarely that, for example, the d'Alembertian spectra of two distinct causal sets coincide. Indeed, we find numerical evidence that, in general, the more geometrically different two causal sets are, the more their spectra differ. This means that the spectral distances of causal sets could serve as a measure of their geometric similarity. We discuss the potential for using this fact to do Lorentzian spectral geometry with these causal set operators.

In the course of arriving at the main result of this thesis, several studies were made of the causal set and continuum entropies calculated with the spacetime formula of [1]. As a means of having a record of these observations, and also because some of these results are interesting in their own right, a collection of these miscellaneous calculations are placed in Appendix C.

Finally, Appendix D contains a detailed study of the effect of zero modes on entanglement entropy within a simple 1d system of a chain of harmonic oscillators. Throughout this thesis, we primarily work with a free massless scalar field in a causal diamond of two-dimensional Minkowski spacetime. While this theory is well-defined in the spacetime regions we consider, it is useful to keep in mind that the free massless scalar field theory in full two-dimensional Minkowski spacetime or a finite region with periodic boundary conditions is an ill-defined theory due to the presence of a zero mode. In the example we study in this appendix, a mass regulator is necessary to avoid an infrared divergence due to a zero mode. We also comment on a surprising contribution of the zero mode to the UV-scaling of the entanglement entropy.

Chapter 2

Causal Set Theory

2.1 Definition and Properties

The causal structure of a spacetime contains a lot of information. This was recognized early on. Approaches to describing relativity using causal structure are as old as relativity itself. One such early work (perhaps the earliest) is that of Alfred Arthur Robb [10, 11]. Starting with a small number of postulates involving before and after relations between spacetime elements, he gets far with defining concepts such as null and parallel lines and planes, and proving numerous theorems involving them[1]. His work is limited to flat spacetime but it would be interesting to explore the extent to which his results and similar ones can be extended to curved spacetimes.

Later work by Hawking [12] and Malament [13] has been crucial for confirming the fruitfulness of these approaches. They proved theorems that show that the causal structure of a spacetime, together with a conformal factor, determine the metric of a Lorentzian spacetime uniquely. Therefore instead of starting with the metric and finding the lightcones associated to it, one can go the other way around: using the before and after relations amongst all events one can recover the conformal metric. Furthermore, if one has a measure for the conformal factor as well then one can recover the entire metric and spacetime from this information. This is what causal set theory [5] does. It is perhaps the most developed

[1] To get a taste of his work, an example definition for the boundary of the future lightcone of a point in Minkowski spacetime is: If A is some element of the spacetime, then an element X will be said to be on the future lightcone of A if it is either identical with A, or else provided there exists at least one element Y distinct from A and neither *before* nor *after* A such that X is *after* both A and Y but is not *after* any other element which is *after* both A and Y.

theory of spacetime in this spirit of viewing causal structure as fundamental. Its aim, moreover, is to go beyond the classical description of spacetime and to describe its quantum nature as well.

Causal set theory was independently found by 't Hooft [14] and Myrheim [15] in the late 1970's and Bombelli et. al [5] in the 1980's. It is an approach to quantum gravity where the deep structure of spacetime is discrete and causal structure is fundamental. It is a theory of discrete spacetime elements or 'atoms' and the causal relations amongst them. The causal relations amongst the elements yield the information about the conformal metric and the number of elements in a region encodes the conformal volume factor of that region[2]. In short[3]: *Order+Number=Geometry.* The discrete elements and the ordering relation induced by the causal structure together form a partially ordered set, $\mathcal{C}$. The set $\mathcal{C}$ and the ordering relation $\preceq$ satisfy

- Reflexivity: for all $X \in \mathcal{C}$, $X \preceq X$.
- Antisymmetry: for all $X, Y \in \mathcal{C}$, $X \preceq Y \preceq X$ implies $X = Y$.
- Transitivity: for all $X, Y, Z \in \mathcal{C}$, $X \preceq Y \preceq Z$ implies $X \preceq Z$.
- Local finiteness: for all $X, Y \in \mathcal{C}$, $|I(X, Y)| < \infty$, where $|\cdot|$ denotes cardinality and $I(X, Y)$ is the causal interval defined by $I(X, Y) := \{Z \in \mathcal{C} | X \preceq Z \preceq Y\}$.

We write $X \prec Y$ if $X \preceq Y$ and $X \neq Y$. The antisymmetry condition ensures that there are no closed timelike curves.

A fundamental conjecture of causal set theory (called the "Hauptvermutung" [18]) is that two very different manifolds could not approximate the same causal set. It should also be mentioned that in general, an arbitrary causal set may not embed in any Lorentzian manifold with a metric [18]. It remains an open question how manifoldlike causal sets may arise from suitable dynamical laws [19, 20]. One can, however, study causal sets created by "sprinkling" elements in a spacetime according to a Poisson process. A sprinkling generates a causal set from a given Lorentzian manifold $\mathcal{M}$ by placing points at random in $\mathcal{M}$ via a

[2] While the causal structure information is readily available in the continuum, there is no obvious way to extract the information about the conformal factor there. There is still much that can be done with causal structure in the continuum without a conformal factor. In [16] for example a notion of global hyperbolicity is defined using causal concepts, and in [17] a proof of the positive energy theorem is given using similar concepts.

[3] A slogan by R. Sorkin.

Poisson process with "density" ρ, such that the probability of having N points in a region of spacetime volume V is $P(N) = \frac{(\rho V)^N}{N!} e^{-\rho V}$. This produces a causal set whose elements are the sprinkled points and whose partial order relation is that of the manifold's causal relation restricted to the sprinkled points. The expected total number of elements in the causal set will be $N = \rho V_{\mathcal{M}}$.

Causal set theory is unique in that it discretizes spacetime while preserving local Lorentz invariance. This is in contrast to a regular lattice type of discretization of spacetime. Under a boost, a regular lattice would have regions with high densities and other regions with large voids, thus violating Lorentz invariance. A causal set, in contrast, would still have a uniform distribution of elements everywhere after a boost, due to the random nature of the Poisson sprinkling [18].

In practice one can thus use the sprinkling process to obtain physically meaningful causal sets corresponding to any spacetime of interest, without needing to know how they would dynamically arise.

In this thesis we will primarily consider $2d$ flat causal sets. A causal set consisting of points sprinkled into a region of $\mathbb{M}^2$ (2d Minkowski) is shown in Figure 2.1. As evident from the figure, this causal set simply looks like a random lattice.

A useful way to represent a causal set is through its causal matrix C or link matrix L. The causal matrix is defined by

$$C_{xy} = \begin{cases} 1, & \text{for } x \prec y \\ 0 & \text{otherwise} \end{cases} \tag{2.1}$$

We use the notation throughout this thesis, for example in writing C_{xy} above, that x and y refer to the indices of C corresponding to spacetime elements x and y.

A link (or nearest neighbour relation) is a relation $x \prec y$ such that there exists no $z \in \mathcal{C}$ with $x \prec z \prec y$. We then say that x and y are nearest neighbours $x \prec\!\!* \, y$. The link matrix, L, is defined by

$$L_{xy} = \begin{cases} 1, & \text{for } x \prec\!\!* \, y \\ 0 & \text{otherwise} \end{cases} \tag{2.2}$$

One can always choose a labelling (called a *natural labelling*) to ensure that C and L are both strictly upper triangular. A *chain* of length n is a sequence $x_0 \prec x_1 \prec x_2 \prec ... \prec x_n$. A *path* of length n is a sequence $x_0 \prec\!\!* \, x_1 \prec\!\!* \, x_2 \prec\!\!* \, ... \prec\!\!* \, x_n$.

A 10-element causal set represented by its Hasse diagram is shown in Figure 2.2. In a Hasse diagram, the causal set elements are represented as points, and lower elements

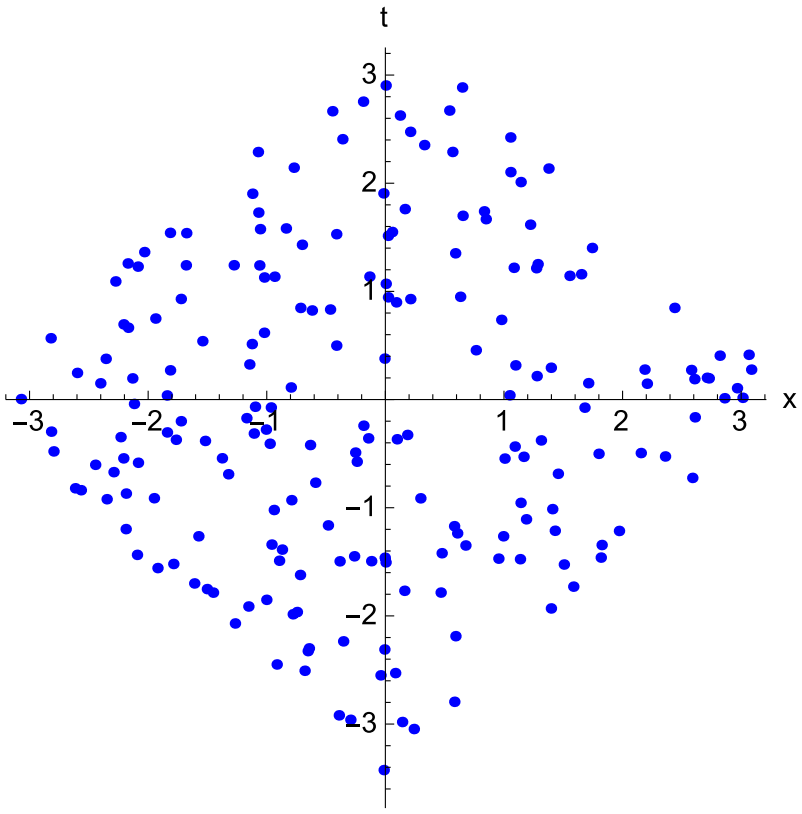

Figure 2.1: A causal set formed by sprinkling 200 elements into a finite interval in $1+1$ dimensional Minkowski spacetime.

precede higher elements. The lines are the links (the relations not implied by transitivity). The causal matrix and link matrix for this causal set are given below. The rows and columns have been ordered alphabetically with respect to the element labels in Figure 2.2.

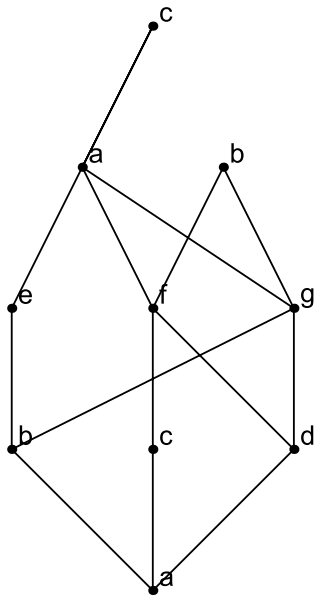

Figure 2.2: Hasse diagram of a 10-element causal set. Lower elements precede higher elements and lines are drawn in for links.

$$C = \begin{pmatrix} 0 & 1 & 1 & 1 & 1 & 1 & 1 & 1 & 1 & 1 \\ 0 & 0 & 0 & 0 & 1 & 0 & 1 & 1 & 1 & 1 \\ 0 & 0 & 0 & 0 & 0 & 1 & 0 & 1 & 1 & 1 \\ 0 & 0 & 0 & 0 & 0 & 1 & 1 & 1 & 1 & 1 \\ 0 & 0 & 0 & 0 & 0 & 0 & 0 & 0 & 0 & 1 \\ 0 & 0 & 0 & 0 & 0 & 0 & 0 & 1 & 1 & 1 \\ 0 & 0 & 0 & 0 & 0 & 0 & 0 & 1 & 1 & 1 \\ 0 & 0 & 0 & 0 & 0 & 0 & 0 & 0 & 0 & 1 \\ 0 & 0 & 0 & 0 & 0 & 0 & 0 & 0 & 0 & 0 \\ 0 & 0 & 0 & 0 & 0 & 0 & 0 & 0 & 0 & 0 \end{pmatrix} \tag{2.3}$$

$$L = \begin{pmatrix} 0 & 1 & 1 & 1 & 0 & 0 & 0 & 0 & 0 & 0 \\ 0 & 0 & 0 & 0 & 1 & 0 & 1 & 0 & 0 & 0 \\ 0 & 0 & 0 & 0 & 0 & 1 & 0 & 0 & 0 & 0 \\ 0 & 0 & 0 & 0 & 0 & 1 & 1 & 0 & 0 & 0 \\ 0 & 0 & 0 & 0 & 0 & 0 & 0 & 0 & 0 & 1 \\ 0 & 0 & 0 & 0 & 0 & 0 & 0 & 1 & 1 & 0 \\ 0 & 0 & 0 & 0 & 0 & 0 & 0 & 1 & 1 & 0 \\ 0 & 0 & 0 & 0 & 0 & 0 & 0 & 0 & 0 & 1 \\ 0 & 0 & 0 & 0 & 0 & 0 & 0 & 0 & 0 & 0 \\ 0 & 0 & 0 & 0 & 0 & 0 & 0 & 0 & 0 & 0 \end{pmatrix} \tag{2.4}$$

A causal set is rich in information. This information extends beyond the binary information of whether or not two elements are causally related. For example, there is much information in the abundance of m-element order-intervals[4]. In [21] Surya and Glaser obtain analytic expressions for the expectation value of these interval abundances (for arbitrary m) for causal sets that embed into an Alexandrov interval in d-dimensional flat spacetime. They found the characteristics of these abundances to be a good indicator of manifoldlikeness and of flatness.

Sometimes the shorthand "causet" will be used instead of causal set.

2.2 Quantum Field Theory on a Causal Set

In the ultimate theory of quantum gravity, many of the questions we would like to answer are of a "spacetime" nature. Thus we would like our framework to be covariant. In order for any quantum theory to respect covariance, the most promising route seems to be to adopt the path integral formalism of quantum theory rather than the canonical or Hamiltonian approach [22–24]. The Hamiltonian approach involves evolution over time slices and is thus not manifestly covariant. It is therefore difficult to imagine how this approach could be meaningful if there is no fixed background spacetime. On the other hand, the path integral approach allows allows one to consider histories with certain spacetime properties and from different spacetimes in a covariant manner. It is the aim of causal set quantum gravity to realize quantum theory in its path integral or histories formulation.

[4] An order-interval (also called causal diamond or Alexandrov neighborhood) is the intersection of the future of a point p with the past of a point $q \succ p$.

Classical dynamics for causal sets has been developed in terms of stochastic sequential growth models [25,26]. In these sequential growth models, causal sets are built one element at a time. The dynamics consists of assigning physically motivated (for example based on covariance and causality) probabilities to different ways a new element can be added to the existing causal set.

A quantum generalization of this scheme to a path integral over causal sets has not yet been achieved. How to define and interpret a quantum path integral over causal sets, whether by a generalization of such classical sequential growth models or by other means, remains an open problem of the theory in its present stage.

In the absence of a full quantum dynamics for causal sets, there are still many interesting quantum phenomena that can and have been studied. Calculations analogous to those in quantum field theory in curved spacetime, where a quantum field is considered on a fixed classical background spacetime, are possible. In particular, the theory of a free scalar field $\hat{\phi}(x)$ on a causal set has been developed in both algebraic [27] and path-integral [28] forms. A definition of entropy for the scalar field on the causal set also exists [1]. So far this definition is only in terms of algebraic operators and the histories based definition has not been constructed[5]. For this reason, for the remainder of this thesis we will focus on the algebraic formulation of scalar field theory on a causal set.

While, as mentioned above, in the ultimate theory of quantum gravity we would like to follow the path integral formalism, at the level of a fixed background causal set or spacetime, the path integral and algebraic approaches are in agreement.

2.3 The Sorkin-Johnston Prescription

In this subsection we introduce the theory of a free scalar field in a gaussian state[6]. We define this theory using the Sorkin-Johnston (SJ) prescription, which we will describe below. In defining a scalar field theory in the continuum, the typical starting point is the Klein Gordon equation and the equal-time commutation relations. The SJ prescription does not take this route and is instead based on the retarded Green function and the spacetime volume-element. The causal set, due to its spatio-temporal discreteness, requires spacetime quantities in order to define the field theory. The retarded Green function provides the

[5] We mean a path integral or histories formulation of entropy without the use of Wick rotations.

[6] A gaussian state is one for which Wick's rule holds: All higher order n-point functions can be determined from the two-point function of the theory. Therefore, the two-point function determines the theory in full.

necessary spacetime information to achieve this (and in fact in a more manifestly covariant manner compared to the usual continuum approach). The spacetimes we consider are globally hyperbolic, so that they have a unique retarded Green function. We will use the signature $-+++$ (and the analogous variants in dimensions other than $3+1$) throughout.

The retarded Green function of a free scalar field theory of mass $m \geq 0$ in a d-(spacetime) dimensional continuum spacetime satisfies [29]

$$(\Box - m^2)G_R^{(d)}(x, x') = -\frac{\delta^{(d)}(x - x')}{\sqrt{-g(x')}}, \tag{2.5}$$

where $x = (t, \vec{x})$. $G_R^{(d)}(x, x')$ is zero unless $x' \prec x$. For the massless $1 + 1$d theory (which we will mostly be concerned with here) in the continuum, this function has the simple form [30]

$$G_R^{(2)}(x, x') = \theta(t - t')\theta(-\tau^2)\frac{1}{2}, \tag{2.6}$$

i.e it has the value of $\frac{1}{2}$ if x is in the future lightcone of x', and it is 0 otherwise. θ is the Heaviside theta function and τ is the proper time. For the massless $1 + 1$d theory on a causal set the retarded Green function is given by [27]

$$G_R := \frac{1}{2}C\left(I + \frac{m^2}{2\rho}C\right)^{-1}, \tag{2.7}$$

where the constant ρ is the sprinkling density, C is the causal matrix and I is the identity matrix. That (2.7) with $m = 0$ will agree with (2.6) is evident from the definition of C we gave in Section 2.1. For high causal set densities, (2.7) is also in agreement with the massive retarded Green function in $1 + 1$d continuum spacetimes [30]:

$$G_{R,m}^{(2)}(x, x') = \theta(t - t')\theta(-\tau^2)\frac{1}{2}J_0(m\sqrt{-\tau^2}), \tag{2.8}$$

where J_0 is a zeroth order Bessel function of the first kind.

It is worth digressing here to briefly review how (2.7) can be obtained as a sum over chains (as shown in [27]). The picture to have in mind is that of a point particle sequentially travelling (forward in time) along a chain from one element of the causal set to another. Any given trajectory consists of a number of "hops" from one element to the next and a number of "stops" at each element. For a trajectory of length n there are n hops and $n - 1$ stops (the endpoints are not considered as stops). Assigning constant amplitudes for the hops and stops as a and b respectively, the full amplitude of a length n trajectory

is $a^n b^{n-1}$. To obtain the total amplitude of going from x to y we sum over chains (of all possible lengths) between them. This total amplitude is then given by the K_{xy} entry of the matrix

$$K := \sum_{n=1}^{N} b^{n-1} a^n C^n = aC \left(I - b\, aC\right)^{-1}, \tag{2.9}$$

where $\left(C^n\right)_{xy}$ yields the number of chains of length n from x to y [31]. The sum index in (2.9) is over a finite range because the causal set is finite. What now remains is to choose a and b appropriately (if this is at all possible) such that K_{xy} resembles the continuum propagator. It turns out that this is possible and dimensional analysis helps to a large extent determine the values of a and b. The continuum propagators have mass dimension $\left[G^{(d)}_{R,m}\right] = M^{d-2}$. Comparing this to $[a^n b^{n-1}]$ for all n we have $[a] = M^{d-2}$ and $[b] = M^{2-d}$ so that $[ab] = 1$. The dimensionful constants we have in a causal set are the density (where $[\rho] = M^d$) and the particle mass m (where $[m] = M$). If we further assume that a is independent of particle mass we have that $a = A\rho^{1-2/d}$, where A is a (dimensionless) constant. In $2d$, a comparison with the continuum function (2.6) shows that for the massless theory we have $A = \frac{1}{2}$, and $a = \frac{1}{2}$. Further analysis (see [27] for details) shows that for the massive theory in 2d, $a = \frac{1}{2}$ and $b = -\frac{m^2}{\rho}$ are the correct amplitudes.

The field commutator, also called the Pauli-Jordan function[7] is defined as

$$\Delta := G_R - G_A, \tag{2.10}$$

where G_A is the advanced Green function and is equal to the transpose of the retarded Green function. (2.10) is consistent with $[\phi(x), \phi(x')] = i\Delta(x, x')$. $i\Delta$ is anti-symmetric and Hermitian. Its non-zero eigenvalues, $\pm\lambda_i$, come in pairs of positive and negative real numbers. If we label the normalized positive and negative eigenvectors of $i\Delta$ by u_i and v_i respectively, we can also express it as

$$i\Delta = \sum_i \lambda_i u_i u_i^\dagger - \lambda_i v_i v_i^\dagger. \tag{2.11}$$

Restricting to the positive eigenspace of $i\Delta$, we can define a two-point correlation function or Wightman function for the theory

$$W := \mathrm{Pos}(i\Delta) = \sum_i \lambda_i u_i u_i^\dagger. \tag{2.12}$$

[7] Δ is also sometimes referred to as the "causal propagator", but we will not use this term for it.

This is the Sorkin-Johnston (SJ) prescription for getting a Wightman function. With any choice of Wightman function W there comes a definition of vacuum state [29]. The choice of vacuum state that this prescription leads to is called the SJ state [27, 28]. This prescription is just as well applicable to any globally hyperbolic continuum spacetime. See for example [32–34]. Furthermore, for large causal set densities, the SJ procedure in causal sets will yield results in agreement with the continuum results. In static spacetimes the SJ state corresponds to the state invariant under the timelike Killing vector of the spacetime [32]. In general spacetimes without a symmetry there is little to guide what is a good choice for a vacuum, but the SJ prescription works just as well to define a state in these situations. Whether or not the SJ states in such spacetimes without symmetry are "good" states, insofar as the question can objectively be posed, is not known. A property of interest to us regarding the SJ state is that it is a *pure* state [35]. This will allow us to use it as our reference state with respect to which entanglement entropies will be defined and computed.

The Feynman propagator, in terms of the operators we have just defined, is [27]

$$G_F = G_R + iW. \tag{2.13}$$

In Appendix A, we show that this Feynman Green function G_F contains the complete information about the causal set, at least for the 2-dimensional case [36].

In cases where these operators are known in causal set theory, they have been shown to agree with their continuum counterparts in the limit of large density (see eg. [27, 33]).

Alternatively, the SJ vacuum and Wightman function are defined by the three conditions [33]:

- *commutator:* $i\Delta(x,x') = W(x,x') - W^*(x,x')$
- *positivity:* $\int_{\mathcal{M}} dV \int_{\mathcal{M}} dV' f^*(x) W(x,x') f(x') \geq 0$
- *orthogonal supports:* $\int_{\mathcal{M}} dV'\, W(x,x')\, W(x',x'')^* = 0,$

where $\int dV = \int d^d x \sqrt{-g(x)}$.

These conditions have the meaning that W is the positive part of $i\Delta$, thought of as an operator on the Hilbert space of square integrable functions $L^2(\mathcal{M}, dV)$ [28]. This allows us to describe a direct construction of W from the Pauli-Jordan function [27, 28, 32]. In practice, the above three conditions do not help us calculate the SJ Wightman function.

If we have a candidate W we can use the conditions to test whether or not it is the SJ Wightman function. Otherwise, to compute W^{SJ} we would go through the steps (2.10) to (2.12).

It would be interesting to apply this prescription to a black hole spacetime or causal set and see what its preferred state is there.

Chapter 3

Entanglement Entropy

Entanglement entropy has been an important topic in various fields of theoretical physics for some time, and interest continues to grow in this deep and useful concept. Especially in the quantum gravity community, many believe that the key insight that will help us connect quantum mechanics and general relativity, will come from entanglement entropy.

In quantum field theory and AdS/CFT many important theorems involving entanglement entropy, such as strong subadditivity [37], have been proved [7, 8, 38–40]. Also in condensed matter theory, important applications of entanglement entropy include investigating topological order [41, 42] as well as properties of Fermi surfaces [43], where quantum phase transitions are characterized by the entanglement entropy of the system.

In gravity, there is also the question of black hole entropy and whether all of it or most of it is entanglement entropy. As mentioned in the introduction, the earliest works conjecturing that this might be the case are by R. Sorkin [2, 6]. Many others have thought about this as well (e.g. [44]), but we do not have a final answer to this question yet.

For these reasons, in the quantum gravity approach of causal set theory, we are also interested in addressing this question of black hole entropy and also the broader questions surrounding the role that entanglement entropy might play in arriving at a consistent quantum gravity theory.

Ordinarily, entropy is defined by the formula

$$S = \mathrm{Tr}\rho \ln \rho^{-1}, \tag{3.1}$$

where ρ is a density matrix evaluated on a Cauchy hypersurface Σ. If Σ is divided into two complementary subregions A and B, such as in Figure 3.1, then the reduced density

matrix for subregion A is

$$\rho_A = \mathrm{Tr}_B \rho. \tag{3.2}$$

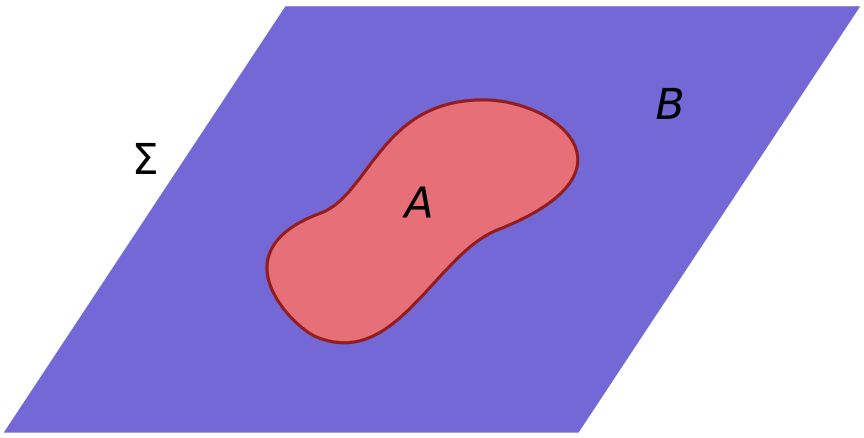

Figure 3.1: A hypersurface Σ divided into two complementary subregions A and B.

Substituting (3.2) back into (3.1), we get the entropy associated to region A as

$$S_A = -\mathrm{Tr}\rho_A \ln \rho_A \ , \tag{3.3}$$

which can be designated as the entanglement entropy between regions A and B if the original density matrix ρ was pure. We would of course get exactly the same answer if we instead traced over the degrees of freedom of A and computed S_B.

This definition of entanglement entropy does not work for a causal set, because we lack in that setting a notion of data on a hypersurface. The analogue of a spatial slice or hypersurface does exist [45]: it is the maximal anti-chain (set of unrelated elements) where all the remaining elements of the causet are either to the past or to the future of at least one element of the anti-chain, such that we cannot extend the anti-chain and have it remain an anti-chain (it is in this sense "maximal"). However, this maximal anti-chain fails to be a suitable candidate for a Cauchy surface in the causal set. As a result of the non-locality inherent in the causal set, the maximal anti-chain acts more like a Cauchy "sieve" than a surface! Many links in the causal set pass through the anti-chain without meeting any of the elements of the anti-chain. Even if this difficulty could be ignored, a hypersurface-based definition of entanglement entropy would be questionable. Essential to getting a

finite entanglement entropy is a UV cutoff, and a cutoff referred to a spacelike surface has no reason to be covariant. Two partial Cauchy surfaces sharing the same boundary would then have no reason to carry equal entanglement entropies even if their domains of dependence were the same. Fortunately, however, there exists a more covariant definition of entanglement entropy which is formally equivalent to (3.3) in a globally hyperbolic spacetime, and which does make sense for a causal set [1].

So far, this definition has been developed for the theory of a gaussian scalar field (also called a free scalar field in a quasi-free state). We briefly review this definition next. For a more detailed review, we refer the reader to [46], and for the full derivation to [1].

The goal is to express S directly in terms of the field correlators. We start by considering a single degree of freedom, with a conjugate pair of variables q and p. These variables satisfy $[q, p] = i$, and they have correlators $\langle qq\rangle$, $\langle pp\rangle$, and $Re\langle qp\rangle$.

A gaussian density matrix, in a basis of q, is

$$\rho(q, q') \equiv \langle q|\rho|q'\rangle \propto e^{\left(-\frac{A}{2}(q^2+q'^2)+\frac{iB}{2}(q^2-q'^2)-\frac{C}{2}(q-q')^2\right)}. \tag{3.4}$$

As already mentioned, the entropy will depend on ρ such that $S(\rho) = Tr\rho \ln \rho^{-1}$. Furthermore, S has to be dimensionless and invariant under unitary transformations. Given these conditions, S can only depend on the combination:

$$\langle qq\rangle\langle pp\rangle - (Re\langle qp\rangle)^2 = \frac{C}{2A} + \frac{1}{4}. \tag{3.5}$$

In [6], it was shown that the entropy takes the form

$$S = -\frac{\mu \ln \mu + (1-\mu)\ln(1-\mu)}{1-\mu} \tag{3.6}$$

with

$$\mu = \frac{\sqrt{1+2C/A}-1}{\sqrt{1+2C/A}+1}, \tag{3.7}$$

or

$$S = (\sigma + 1/2)\ln(\sigma + 1/2) - (\sigma - 1/2)\ln(\sigma - 1/2) \tag{3.8}$$

where $\pm i\sigma$ are the eigenvalues of $\Delta^{-1}R$ and where

$$i\Delta = 2Im \begin{pmatrix} \langle qq \rangle & \langle qp \rangle \\ \langle pq \rangle & \langle pp \rangle \end{pmatrix} \tag{3.9}$$

and

$$R = Re \begin{pmatrix} \langle qq \rangle & \langle qp \rangle \\ \langle pq \rangle & \langle pp \rangle \end{pmatrix}. \tag{3.10}$$

We can further simplify (3.8) by using the eigenvalues of $\Delta^{-1}W = \Delta^{-1}R + i\,I/2$ instead of those of $\Delta^{-1}R$ [1]. Calling these eigenvalues $\pm i\omega_{\pm}$ (where $\pm i\omega_{\pm} = i(1/2 \pm \sigma)$), the entropy can be written in the simpler form

$$S = \omega_+ \ln \omega_+ - \omega_- \ln \omega_- \tag{3.11}$$

To generalize (3.11) for more degrees of freedom, we simply extend it to a sum over the full spectrum of $\Delta^{-1}W$. To work with real eigenvalues we can define the operator L by

$$\Delta^{-1}W = iL, \tag{3.12}$$

and use its eigenvalues, which we call λ, to express the full entropy as the sum

$$S = \sum \lambda \ln |\lambda|. \tag{3.13}$$

(3.13) is the final expression for the entropy.

We can equivalently view the eigenvalues λ to be the solutions to the generalized eigenvalue problem

$$Wv = i\lambda\Delta v \tag{3.14}$$

and

$$\Delta v \neq 0. \tag{3.15}$$

The eigenvalues come in pairs of λ and $1 - \lambda$.

Hence we have arrived at a covariant formulation of the entropy in terms of the (spacetime) field correlators. The matrix W corresponds in the field theory to $W(x, x') = \langle 0|\phi(x)\phi(x')|0\rangle$, while Δ gives the imaginary part of W ($2\Delta = \mathrm{Im}\,(W)$) and corresponds to the commutator function defined by $i\Delta(x, x') = [\phi(x), \phi(x')]$.

[1] We work with the invertible part of Δ.

If we take the Wightman function to be the SJ one from the previous chapter, W_{SJ}, the entropy vanishes. When we use W_{SJ}, all the eigenvalues are either $\lambda = 1$, or $\lambda = 0$, and so the sum (3.13) vanishes. This is expected, since the SJ vacuum is a pure state (as stated before).

In certain cases where we restrict W and Δ to subregions within a larger region or within an entire spacetime or causal set, (3.13) can be interpreted as an entanglement entropy. In the next two chapters, (3.13) will be applied to some examples in flat two-dimensional continuum spacetimes and causal sets.

It has been known for some time that the entropy can be expressed in terms of correlators [6, 47, 48]. However the earlier papers (such as the works reviewed in Appendix D) all work with fixed-time correlators, specifically, separate correlators of canonical variables $\langle qq \rangle$, $\langle pp \rangle$ and $\langle qp \rangle$. What is different about the formulation we have just reviewed is that it relies on spacetime correlations: i.e. the Wightman function. This is also simpler since only one kind of correlation occurs: $\langle \phi\phi \rangle$.

3.1 CFT Results in $1+1$d Flat Spacetime

The entanglement entropy between a finite interval within a larger interval (such that the shorter interval has two boundaries), for a massless scalar field in $1+1$ dimensions, has been found to take the asymptotic form for $a \to 0$ [7, 8] (see also [38]),

$$S \sim \frac{1}{3} \ln[\frac{\tilde{L}}{\pi a} \sin(\frac{\pi \tilde{\ell}}{\tilde{L}})] + c_1 \ , \tag{3.16}$$

where a is a UV cutoff, $\tilde{\ell}$ is the length of the shorter interval, $\tilde{L}$ is the length of the longer interval[2], and c_1 is a non-universal constant.[3] In the limit that the smaller interval is much shorter than the larger one ($\frac{\tilde{\ell}}{\tilde{L}} \to 0$), the entropy reduces to

$$S \sim \frac{1}{3} \ln \left[\frac{\tilde{\ell}}{a} \right] + c_1 \ . \tag{3.17}$$

[2]We have placed $\sim$ over the lengths of these intervals in order to distinguish them from the half side lengths ℓ and L of the smaller and larger diamonds respectively, which will be used extensively in the next two chapters.

[3]The entropy (3.16) is supposed to be defined within an overall vacuum state, which doesn't exist in the case with periodic boundary conditions due to the presence of a zero mode. As a result of this zero mode, the entanglement entropy is IR divergent. See Appendix D for details. Presumably the CFT formulas in this case have a regularization of the zero-mode in mind, either by a small mass or otherwise, and hold the regulator fixed while sending the UV cutoff a to zero.

In this limit, S depends only on the length of the smaller interval and the UV cutoff of the theory. For the massive theory, one would expect $1/m$ to play the role of IR scale, in which case the entropy would take the form (cf. [7, 8]),

$$S \sim -\frac{1}{3} \ln[ma]. \tag{3.18}$$

These results will serve as our reference for the scaling and scaling coefficient we expect in Chapters 4 and 5.

Chapter 4

Entanglement Entropy in Continuum Diamonds

4.1 Entanglement Entropy

In this chapter, we review the main results of [46].

We wish to use (3.13) to compute the entanglement entropy of a scalar field, resulting from restricting it to a smaller causal diamond within a larger one in $1+1$d Minkowski spacetime. The setup is shown in Figure 4.1. As is evident in Figure 4.1, each diamond is the domain of dependence of the 1d interval that is its "waist" or "diameter". Thus our result for the spacetime entropy of the smaller diamond within the larger one should be compared with the CFT-results for a shorter line-segment within a longer one (reviewed in the previous chapter), where the intervals would be the diameters of the diamonds.

We need W and Δ, restricted to the smaller diamond, to solve the generalized eigenvalue problem (3.14). In Minkowski lightcone coordinates $u = \frac{t+x}{\sqrt{2}}$ and $v = \frac{t-x}{\sqrt{2}}$,

$$\Delta(u, v; u', v') = \frac{-1}{2}[\theta(u-u') + \theta(v-v') - 1], \tag{4.1}$$

and

$$W = -\frac{1}{4\pi}\ln|\Delta u \Delta v| - \frac{i}{4}\mathrm{sgn}(\Delta u + \Delta v)\theta(\Delta u \Delta v) - \frac{1}{2\pi}\ln\frac{\pi}{4L} + \epsilon + \mathcal{O}\left(\frac{\delta}{L}\right), \tag{4.2}$$

where $\epsilon \approx -0.063$ when $\ell \ll L$, and δ collectively denotes the coordinate differences $u-u', v-v', u-v', v-u'$. We set $\frac{\ell}{L} = .01$. The W in (4.2) is the SJ Wightman function

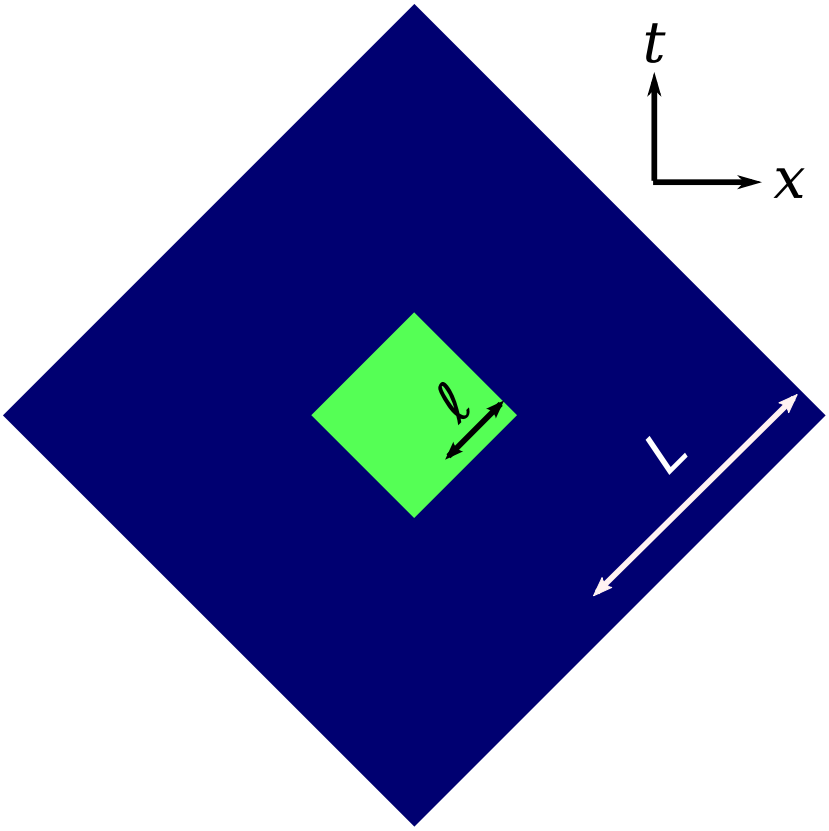

Figure 4.1: Two concentric causal diamonds.

of the scalar field in the causal diamond of side length $2L$, restricted to spacetime regions away from the boundaries. Within the smaller diamond the $\mathcal{O}\left(\frac{\delta}{L}\right)$ correction in (4.2) will be negligible, and we can write the remainder more simply as

$$W(u,v;u',v') = \lim_{\epsilon\to 0^+}(-\frac{1}{4\pi}\ln\left[-\mu^2(\Delta u - i\epsilon)(\Delta v - i\epsilon)\right]) \tag{4.3}$$

where $\mu = (\pi/4L)e^{-2\pi\epsilon_{\text{centre}}}$ is the IR scale of the large diamond. As long as the small diamond is much smaller than the large one, this approximation should be adequate. In our calculation we will use (4.3) for W, with μ taken specifically to be $\mu = 0.0116681$.

We should note here that although the construction of W_{SJ} for a causal diamond is completely well-defined, it has no finite limit as the large diamond goes to infinity.

Indeed a self-consistent Minkowski vacuum state $|0_M\rangle$ does not exist. If we try to define a vacuum in the usual way as the state annihilated by the operator coefficients of the positive frequency modes in the expansion of the field operator $\hat{\phi}(t,x)$, then we encounter an infrared divergence. We can remove the divergence by introducing a long wavelength cutoff into the integral for the Wightman function W, but the result is unphysical because it fails to be positive semidefinite as a quadratic form. Nevertheless, the resulting expression matches the general form (4.3) that we obtained as a local approximation to the SJ vacuum of the large diamond. In this sense, we can think of (4.3) as an approximate Minkowski vacuum which is valid for separations Δt and Δx that are small compared to the IR scale μ.

Returning to our calculation, we want to solve (3.14) subject to (3.15). To that end we will represent W and Δ as matrices, using the basis that diagonalizes $i\Delta$, and which consists of two families of eigenfunctions:[1]

$$\begin{aligned} f_k(u,v) &:= e^{-iku} - e^{-ikv}, & &\text{with } k = \frac{n\pi}{\ell},\ n = \pm 1, \pm 2, \ldots \\ g_k(u,v) &:= e^{-iku} + e^{-ikv} - 2\cos(k\ell), & &\text{with } k \in \mathcal{K}, \end{aligned} \tag{4.4}$$

where $\mathcal{K} = \{k \in \mathbb{R} \,|\, \tan(k\ell) = 2k\ell \text{ and } k \neq 0\}$.

Before actually embarking on the numerics, however, we need to decide on a cutoff. As we have been emphasizing, it will necessarily have a spacetime character as opposed to the purely spatial one seen, for example, in a lattice of carbon atoms. A discrete theory provides its own cutoff, but here in the continuum a naive lattice cutoff would be inconvenient and possibly inappropriate. Instead we simply truncate the matrices representing W and Δ by retaining only a finite number of eigenfunctions f_k and g_k up to a maximum value k_{max} of k. Finally, in comparing our results with (3.17), we need to translate our cutoff into a purely spatial one a. It is not certain that such a correspondence is always possible, but in this case we are expanding solutions of the wave equation, which in turn are in one-to-one correspondence with initial data specified on the spatial diameter of the causal diamond. With the modes we have retained, we can expand initial data of wavelengths longer than $\lambda_{min} \sim 1/k_{max}$ (or $2\sqrt{2}\pi/k_{max}$ if one were trying to be more precise). It is therefore natural to equate a to $1/k_{max}$, and this is what we do in the comparisons below.

In our basis, the integral-kernel $i\Delta$ is diagonal, so its representation is trivial, but for

[1] Thanks to (3.15) we need only consider functions orthogonal to the kernel of Δ, all of which consist of solutions to the wave equation. If one wanted to expand arbitrary L^2 functions, one would need to supplement the solutions, (4.4), with a basis for $\ker \Delta$.

W, we must compute $\langle f_k|W|f_{k'}\rangle$ and $\langle g_k|W|g_{k'}\rangle$[2]. The terms $\langle f_k|W|g_{k'}\rangle$ vanish, making W block diagonal in this basis, so we can treat each block separately in solving (3.14). Summing over the resulting eigenvalues λ, we obtain the entropy associated to each block. Each block contributed to the entropy roughly equally, with the g block making a slightly greater contribution. Adding the two contributions, we obtain the total entropy. In the calculations reported here, all of the eigenvalues obtained from (3.14)-(3.15) were order-one numbers of absolute value below 3, with all but a handful of the eigenvalue-pairs being very close to the values one and zero. As required for consistency we did not encounter any functions in the kernel of $i\Delta$. A typical spectrum looks like:

```
{1.43495,1.02763,1.00224,1.00036,1.00035,1.00033,1.00029,1.00028,1.00027,1.00027,1.0002,1.00016,
1.00006,1.00004,1.00001,1.,1.,1.,1.,1.,1.,1.,1.,1.,1.,1.,1.,1.,1.,1.,1.,1.,1.,1.,1.,1.,1.,1.,
1.,1.,1.,1.,1.,1.,1.,1.,1.,1.,1.,1.,1.,1.,1.,1.,1.,1.,1.,1.,1.,1.,1.,1.,1.,1.,1.,1.,1.,1.,1.,
1.,1.,1.,1.,1.,1.,1.,1.,1.,1.,1.,1.,1.,1.,1.,1.,1.,1.,1.,1.,1.,1.,1.,1.,1.,1.,1.,1.,1.,1.,1.,
1.,1.,1.,1.,1.,1.,1.,1.,1.,1.,1.,1.,0.999999,0.999998,0.999998,0.999998,0.999998,0.999998,
0.999998,0.999998,0.999998,0.999998,0.999998,0.999998,0.999998,0.999998,0.999998,0.999998,
0.999998,0.999998,0.999998,0.999997,0.999995,0.999992,0.999981,0.999968,0.999892,0.999886,
0.999877,0.999825,0.999792,0.999787,0.999778,0.999767,0.99971,0.99969,0.99967,-0.434947,
-0.027627,-0.00223413,-0.000177196,-0.0000138426,-1.02609*10^-6,-6.87856*10^-8,-4.25705*10^-9,
-2.56333*10^-10,0,0,0}
```

The resulting entropies are plotted in Figure 4.2, as a function of $\frac{\ell}{a}$. As seen in the plot, the obtained values of S are fit almost perfectly by the curve

$$S = b \ln\left[\frac{\ell}{a}\right] + c_1, \tag{4.5}$$

with $b = 0.33277$ and $c_1 = 0.70782$. This is consistent with the expected result.

For the results in this chapter, we set $\ell/L = .01$. We expect that different values of ℓ/L would only modify the value of c_1 in (4.5). In the next chapter, the same calculation is done with causal set diamonds and $\ell/L = 1/2$. The expected result (4.5) with b consistent with $1/3$ is obtained after a suitable truncation that will be discussed in the subsequent chapter. In [46] a closely related but slightly different calculation was carried out with yet a different value of ℓ/L. In that calculation, we considered a causal diamond embedded in (and touching the boundary of) a spacetime equal to the right half of 2d Minkowski space. In terms of subregions of a spacelike hypersurface, we were computing the entanglement entropy for a 1d interval at one end of a semi-infinite line, such that $\ell/L = 0$. The half-space has an advantage that it admits a true minimum energy state or vacuum, relieving us

[2] We performed the calculations in this section using Mathematica 9.0.

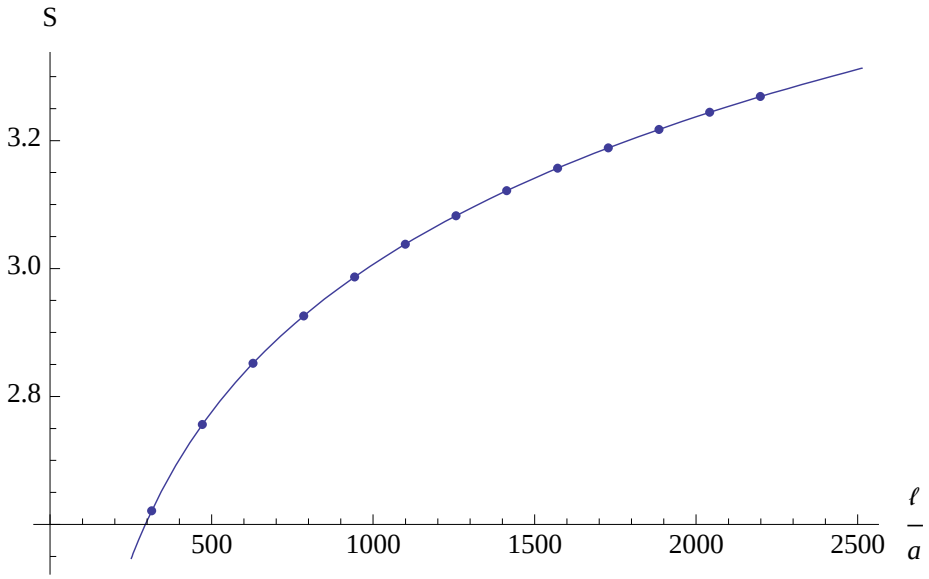

Figure 4.2: Data points represent calculated values of $S = \sum \lambda \ln|\lambda|$ in the continuum causal diamonds of Figure 4.1.

of the need for an infrared cutoff. On the other hand, the presence of a boundary requires that we choose a boundary condition. We did this by requiring the field to vanish at the boundary (Dirichlet condition).

In the half-space again we obtained an entropy scaling $S = b \ln\left[\frac{\ell}{a}\right] + c_1$ with a value for b that is consistent with the expected value of $1/6$ from CFT [7]. The coefficient is $1/6$ rather than $1/3$ because the entanglement concerns only one of the two boundaries of the smaller interval.

These examples increase our confidence that the numerics work for general values of ℓ/L.

4.2 Rényi Entropies

We can extend the results of [46] to include Rényi entropies. The spacetime definition of entropy given in [1] can be generalized for Rényi entropies of order n, $S^{(n)}$, in the following way:

$$S^{(n)} = \sum_{\lambda} \frac{-1}{1-n} \ln(\lambda^n - (\lambda - 1)^n), \tag{4.6}$$

where λ and $1-\lambda$ are solutions to the generalized eigenvalue problem (3.13). The spacetime we apply this formula to is again Figure 4.1. The expected result [49] is that the entropies should take the form:

$$S^{(n)} = \frac{1}{6}(1+\frac{1}{n})\ln(\frac{\ell}{a}) + c_n, \tag{4.7}$$

where c_n are non-universal constants.

Figures 4.3 and 4.4 show the results from (4.6) for $S^{(2)}$ and $S^{(3)}$, along with a best fit to $S = b\ln\left[\frac{\ell}{a}\right] + c$. There is in general good agreement between our best fits for b and the scaling coefficients from (4.7), with more deviation present for the higher order Rényi entropies. The scaling coefficients found from fitting the data from (4.6) to $S = b\ln\left[\frac{\ell}{a}\right] + c$ for $S^{(2)}$ to $S^{(10)}$ are:

$$\{0.24961, 0.221498, 0.206892, 0.197726, 0.191411, 0.18682, 0.183354, 0.18066, 0.178517\}, \tag{4.8}$$

and for comparison those from (4.7) are:

$$\{0.25, 0.222222, 0.208333, 0.2, 0.194444, 0.190476, 0.1875, 0.185185, 0.183333\}. \tag{4.9}$$

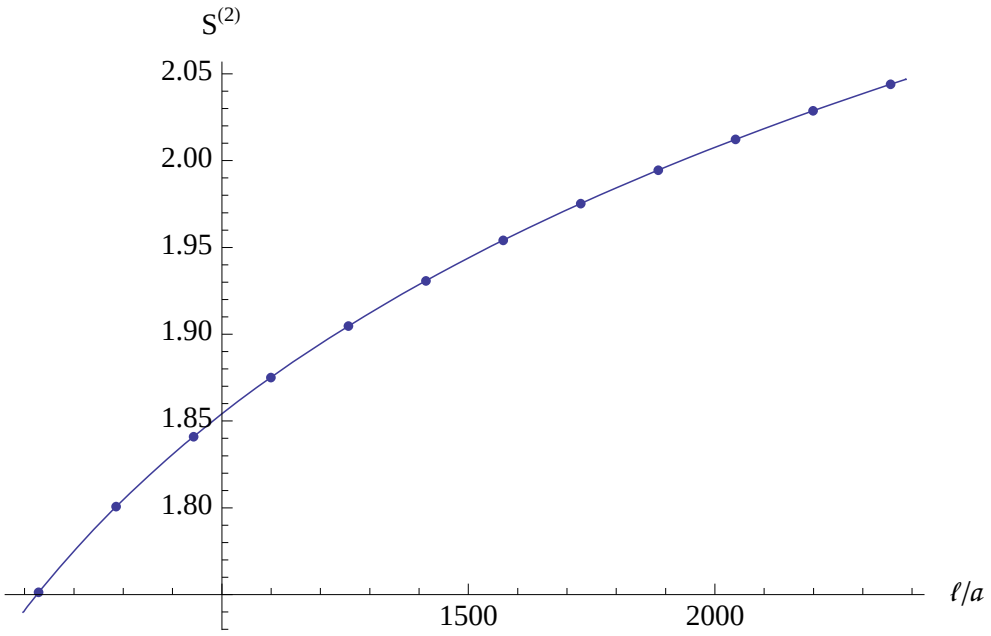

Figure 4.3: 2nd order Rényi entropy $S^{(2)}$ from (4.6) vs. ℓ/a along with a best fit to $S = b \ln\left[\frac{\ell}{a}\right] + c$.

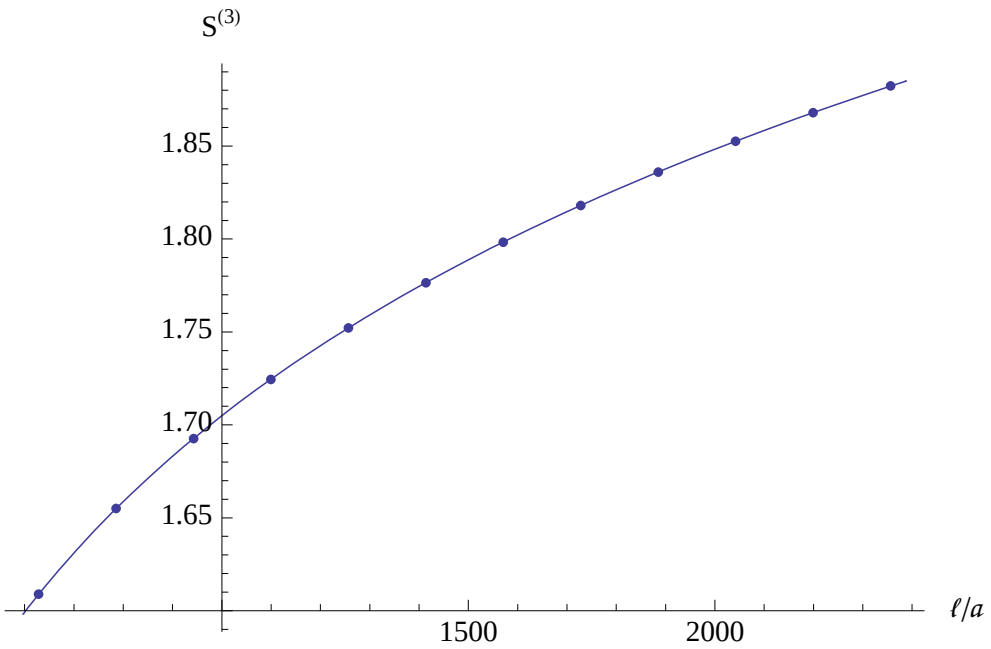

Figure 4.4: 3rd order Rényi entropy $S^{(3)}$ from (4.6) vs. ℓ/a along with a best fit to $S = b \ln\left[\frac{\ell}{a}\right] + c$.

Chapter 5

Entanglement Entropy in Causal Set Diamonds

This chapter summarizes and extends some of the main results of [50].

Consider a free gaussian scalar field living on a causal set which is well approximated by a causal diamond in a 2d Minkowski spacetime. Using the spacetime definition of entropy which was reviewed in Chapter 3, let us compute the entropy associated to a smaller causal-set causal diamond nested within a larger one. Our setup is shown in Figure 5.1, and the entropy we will compute can be interpreted as that of the entanglement between the small region and its "causal complement". In less global terms, it is the entanglement entropy between the "equator" of the smaller region, and its complement within the Cauchy surface produced by extending this equator to the larger region.

In the larger diamond, we use W_{SJ} (the Sorkin-Johnston Wightman function), which is the positive part of the operator $i\Delta$, where

$$\Delta(x, y) = G_R(x, y) - G_R(y, x), \tag{5.1}$$

$G_R(x, y)$ being the retarded Green function. As we saw in Chapter 2 (eq. (2.7)), for a (free) massless scalar field, G_R is simply related to the causal matrix: $G_R = \frac{1}{2}C$, where C is the causal matrix,

$$C_{xy} := \begin{cases} 1, & \text{if } x \prec y \\ 0, & \text{otherwise} \end{cases} \tag{5.2}$$

In solving (3.14), we restrict W and Δ to elements within the smaller diamond in Figure 5.1, keeping only the submatrices W_{xy} and Δ_{xy} such that x and y are in the smaller

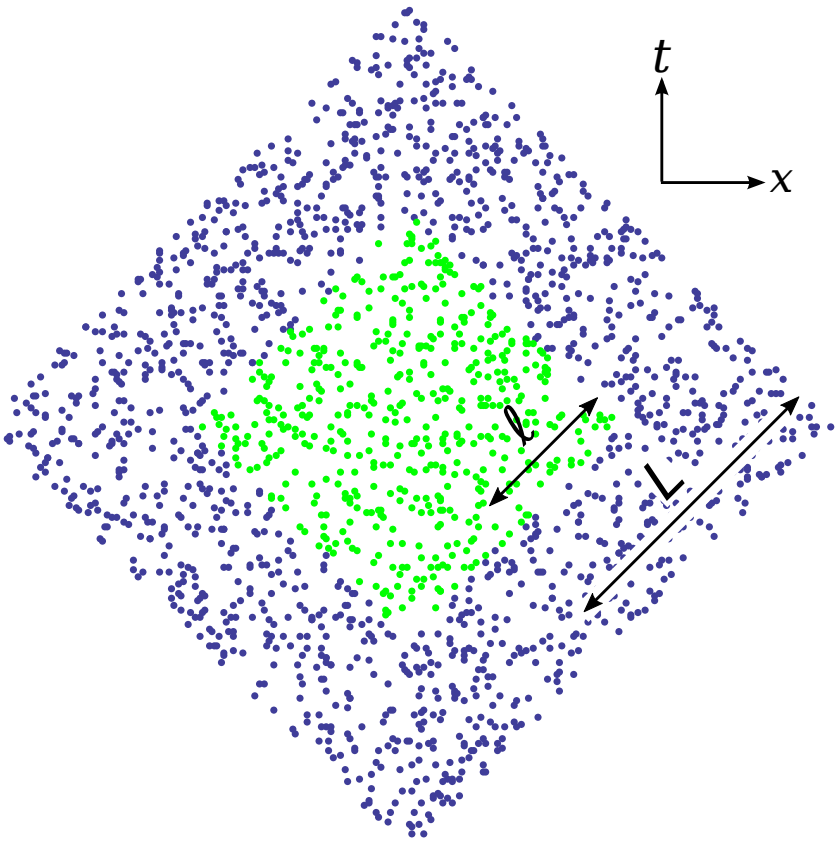

Figure 5.1: Causal sets of two causal diamonds.

diamond. In order to assess how the entropy scales with the UV cutoff, we hold the ratio of the sizes of the diamonds fixed and vary the number of elements sprinkled into them. Thus the UV cutoff (given by the discreteness length-scale, which is in this case square root of the density of elements) is proportional to $\sqrt{N}$ where N is the number of the causet elements. The UV cutoff in 2d is of course proportional to the square root of the number of elements in both the larger and the smaller diamond; we will use the number of elements in the smaller diamond, N_ℓ, to express it.

We find, via numerical simulations, that the entanglement entropy grows linearly with the number of elements in the smaller diamond, thus obeying a spacetime-volume law[1]! The expectation, of course, was that (in $1+1$d) the entropy would scale logarithmically

[1]Notice that not only is this not an area law, but it is not even a spatial volume law. A spatial volume

with the UV cutoff (which would mean logarithmic scaling with $\sqrt{N}$ and therefore with N itself), as in the continuum theory [46, 51]. Furthermore, we find that the entropy in the causet is larger in magnitude (values of order 100) in comparison with the results in the continuum (order 1 values). Two examples of this linear scaling are shown in Figures 5.2 and 5.3, for $\ell/L = 1/4$ and $\ell/L = 1/2$, respectively. The results fit $S = aN + b$ with $a = 0.46$ and $b = -3.20$ for $\ell/L = 1/4$, and $a = 0.32$ and $b = -6.64$ for $\ell/L = 1/2$.

We also find that this spacetime-volume law persists for the massive theory, in $3 + 1$ dimensions, and when working with nonlocal Green functions such as that obtained from inverting the d'Alembertian defined in [52]. See Appendix C for more details on these cases. This suggests that the spacetime-volume law is a generic feature of the direct application of (3.13)-(3.15) to causal sets.

law would mean linear growth with $\sqrt{N}$, whereas the scaling that we obtain is linear in N.

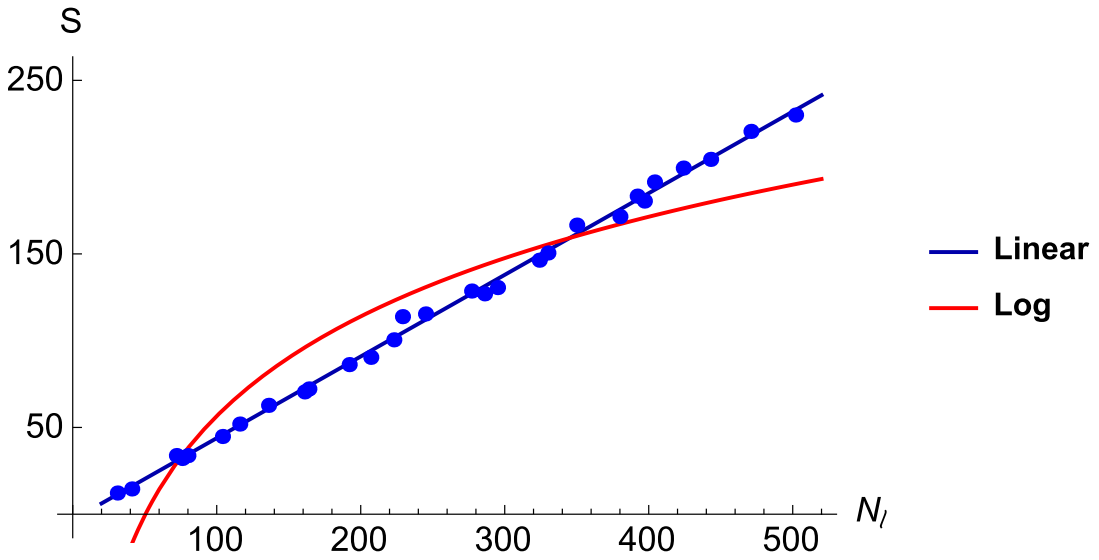

Figure 5.2: S vs N_ℓ when $\ell/L = 1/4$, along with best fits for linear and logarithmic functions. N_ℓ is the number of causet elements in the smaller diamond.

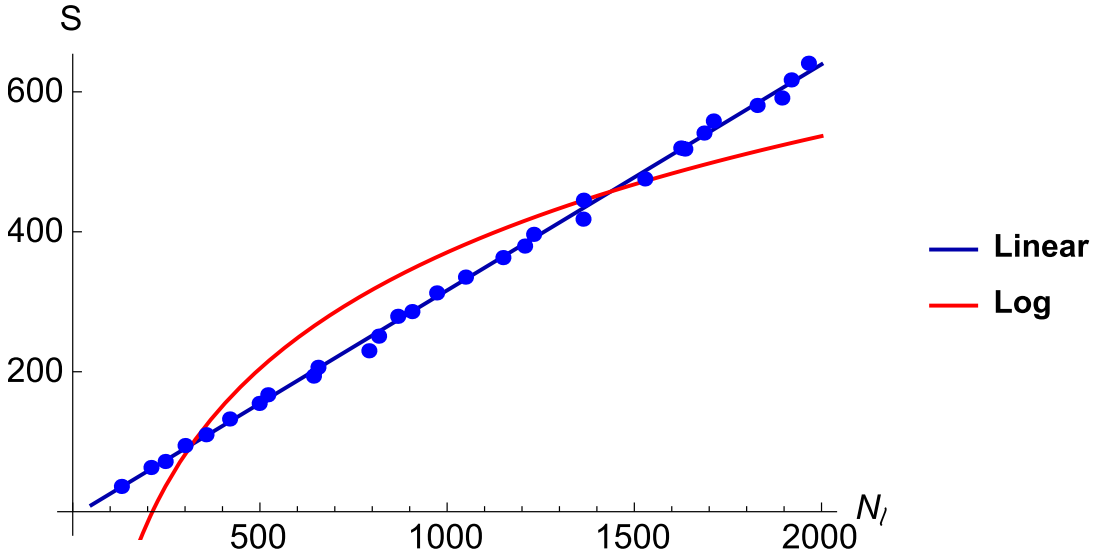

Figure 5.3: S vs N_ℓ when $\ell/L = 1/2$, along with best fits for linear and logarithmic functions. N_ℓ is the number of causet elements in the smaller diamond.

Whence comes this "extra" entropy? The spectrum of $-i\Delta^{-1}W$ on a causal set necessarily has the same form as in the continuum, in that its eigenvalues come in pairs of λ and $1-\lambda$. However, many more of these pairs contribute to the entropy than in the analogous continuum calculation. A closer look at the spectrum of $i\Delta$ reveals how this happens. In (3.14) it is crucial that we exclude functions in the kernel of $i\Delta$, for which λ would not be defined. (Doing this also ensures that we have enough constraints to enforce the equations of motion, so that only linearly independent degrees of freedom remain.) While excluding the kernel is a simple task for the continuum $i\Delta$, its meaning is not so straightforward for the causal set $i\Delta$. In the continuum, the number of "zero-modes" of $i\Delta$ is huge, but in the causet it is much smaller. Instead of strict zeroes one finds many small but finite eigenvalues that have no counterpart in the spectrum of the continuum $i\Delta$. Even though these eigenvalues are very small, they can contribute a large amount of entropy due to their being so numerous and due to the inversion of Δ in $-i\Delta^{-1}W$.

This observation leads to the idea that (as suggested to us by Siavash Aslanbeigi) these "almost zero-modes" of $i\Delta$ might be the source of the discrepancy[2] between the causet and continuum, and that they should be excluded from the entropy calculation if one aims at agreement with the continuum. If we start removing the smallest eigenvalues $\tilde{\lambda}$ of $i\Delta$, the scaling of the entropy with the cutoff indeed becomes logarithmic.[3] If the magnitude of the smallest eigenvalue we keep is approximately $\tilde{\lambda}_{min} \sim \sqrt{N}/4\pi$, then we get not only the expected scaling-law but also the expected coefficient $1/3$ [49].

An example of the logarithmic shape of the data points after the truncation of $i\Delta$ is shown in Figure 5.4 for $\ell/L = 1/2$. In Figure 5.4, the spectrum of $i\Delta$ has been truncated such that $\tilde{\lambda}_{min} \sim \sqrt{N_L}/4\pi$ in the larger diamond and $\tilde{\lambda}_{min} \sim \sqrt{N_\ell}/4\pi$ when the restriction is made to the smaller diamond, with contributions from the truncated modes being projected out of W as well. (We first truncate both Δ and W in the larger diamond (Δ being the antisymmetric part of W). We then restrict both matrices to the smaller diamond. Call these restricted matrices W^R and Δ^R. We then do a second truncation on them, based on the spectrum of Δ^R.) A fit to $S = a\ln(x) + b$, with x being $\sqrt{N_\ell}/4\pi$ in the smaller diamond yielded $a = 0.346 \pm 0.028$ and $b = 1.883 \pm 0.035$, consistent with the continuum value of $a = 1/3$. It is worth emphasizing that the truncation has to be done both in the larger diamond and in the smaller diamond.

With hindsight we can understand why the magnitude of the smallest eigenvalue has to be $\sim \sqrt{N}/4\pi$ for consistency with the continuum results. The spectrum of $i\Delta$ in the

[2] We say "discrepancy" and not "error" since we don't wish to take a position on which, if either, of the two entropies is the "correct" one.

[3] We use $\tilde{\lambda}$ to refer to the spectrum of $i\Delta$, to avoid confusion with λ which are the eigenvalues of $-i\Delta^{-1}W$ that go into (3.13).

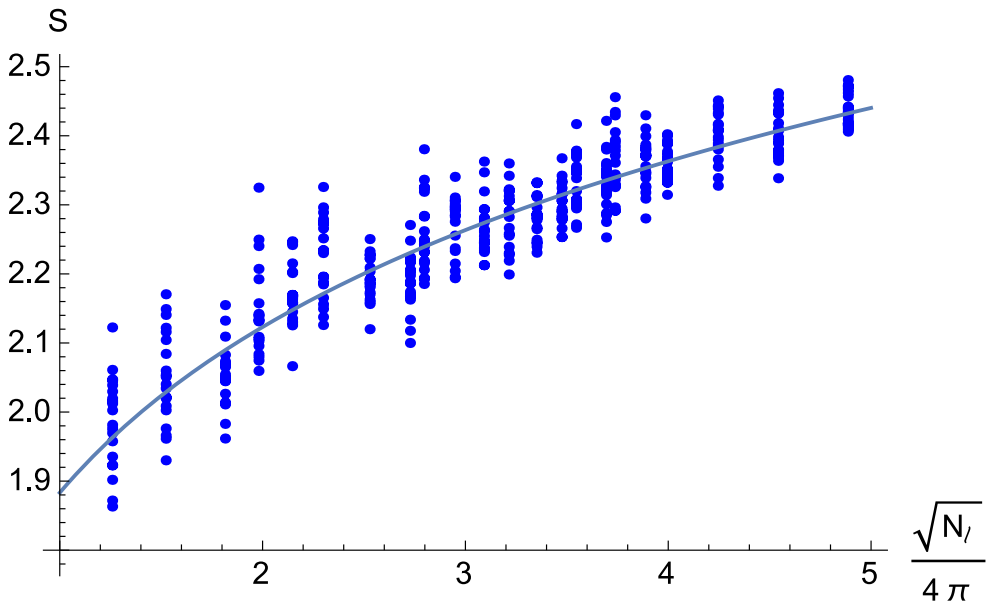

Figure 5.4: S vs. $\sqrt{N_\ell}/4\pi$, after the spectrum of $i\Delta$ has been truncated such that $\tilde{\lambda}_{min} \sim \sqrt{N_L}/4\pi$ in the larger diamond and $\tilde{\lambda}_{min} \sim \sqrt{N_\ell}/4\pi$ in the smaller diamond.

continuum has dimensions of area, while its spectrum in the causal set is dimensionless. This dimensional observation, together with a comparison of the largest eigenvalues of $i\Delta$ between continuum and causal set, shows that the two spectra can be related by a density factor: $\tilde{\lambda}^{cs} = \rho\tilde{\lambda}^{cont}$, where $\rho = N_\ell/4\ell^2$. Converting our $\tilde{\lambda}^{cs}_{min}$ to a $\tilde{\lambda}^{cont}_{min}$ (in the small diamond), we find

$$\begin{aligned} \tilde{\lambda}^{cont}_{min} &= \tilde{\lambda}^{cs}_{min}/\rho \\ &= \sqrt{N_\ell}/4\pi\rho \\ &\sim \frac{\ell^2}{\pi\sqrt{N_\ell}}, \end{aligned} \tag{5.3}$$

This is precisely[4] the minimum eigenvalue which we retained in the continuum, after imposing our cutoff on the wavelength of the eigenmodes of $i\Delta$. This was reviewed in the previous chapter. Eigenvalues smaller than $\tilde{\lambda}^{cs}_{min}$ thus correspond to solutions beyond the cutoff, and are the ones we wish to exclude.

[4]When we identify $\pi\sqrt{N_\ell}/\ell$ as k_{max}.

Another way to think of where the $\sqrt{N}/4\pi$ comes from is the following. On one hand, the causet provides a fundamental length given (in 2d) by $\rho^{-1/2}$, and in this sense it serves as a "low pass filter" in relation to the continuum. On the other hand, in the continuum we know exactly the relation between wavelength and eigenvalue for eigenfunctions of Δ in a causal diamond. If by means of this relation, we convert a cutoff at wavelength $\rho^{-1/2}$ into a cutoff on the spectrum of Δ, we obtain the truncation rule stated above.

Truncating the spectrum of $i\Delta$ in the causal set by requiring its smallest eigenvalue to be $\tilde{\lambda}_{min} \sim \sqrt{N}/4\pi$ reduces the size of the spectrum from $\sim N$ to $\sim \sqrt{N}$. Thus, a large number of these approximate kernel-modes need to be eliminated if one wishes to recover an area law.

Figure 5.5 compares the positive spectrum of $i\Delta$ in the causal set with that in the continuum, using a log-log plot. The causal set in this case comprises 200 elements sprinkled with a density of 50. The red dots are the continuum eigenvalues, the blue dots those of the causet appropriately rescaled by a factor of $1/\rho$ for the comparison, the green dashed line is at $\tilde{\lambda}^{cs} = \sqrt{N}/4\pi$ (where we would expect the causet spectrum to end if it were to agree with the continuum), and the purple dashed line is where $\tilde{\lambda}^{cs} = \sqrt{N}/8\pi$. As one sees, the eigenvalues above the green dashed line are in good agreement between causet and continuum, but in very poor agreement below it. In particular, there is a "break" in the causet spectrum around where the truncation has to be done. Evidently, this spectral feature could also be used as a guide for where to apply the truncation.

In general, then, one can expect to recover continuum-cum-cutoff behaviour from the causal set by modifying the condition $i\Delta\, v \neq 0$ in (3.15) to $i\Delta\, v \neq \tilde{\lambda}_0 v$ when $\tilde{\lambda}_0 < \sqrt{N}/4\pi$ and projecting out these near-zero modes from W as well.

The necessity of this truncation in the full diamond can also be seen by considering the entropy associated to restricting the scalar field to the upper half triangle of the (full) causal diamond[5]. We would expect the entropy in the triangle to vanish, as it shares the same approximate Cauchy surface (diameter of the diamond) with the causal diamond. Without truncating $i\Delta$, however, we find that there is a large non-zero entropy associated to the restriction to the triangle. After truncating $i\Delta$ we eliminate this excess entropy and obtain the expected small and statistically vanishing entropy.

In Figure 5.6, we have repeated our analysis with a cutoff value smaller than $\tilde{\lambda}^{cs} = \sqrt{N}/4\pi$ by a factor of 2. A fit to $S = a\ln(x) + b$, with x being $\sqrt{N_\ell}/8\pi$ in the smaller diamond yielded $a = 0.351 \pm 0.089$ and $b = 5.036 \pm 0.043$, still consistent with the continuum

[5]Ian Jubb and Dionigi Benincasa suggested the entropy of the triangle as a useful test of the truncation scheme presented here.

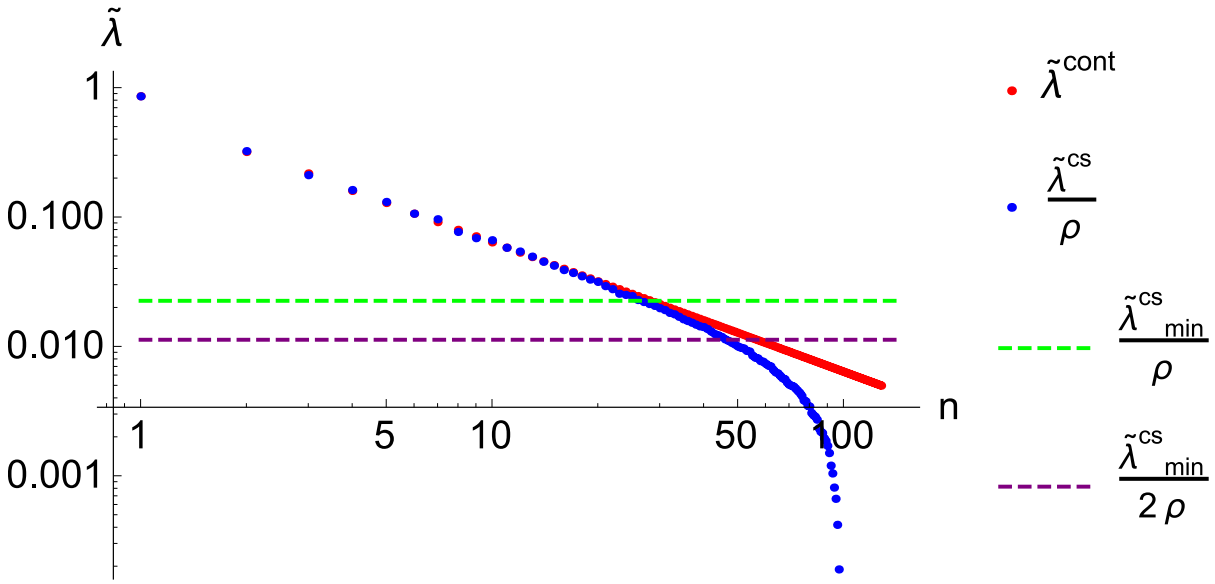

Figure 5.5: Comparison of the positive spectrum of $i\Delta$ in the continuum and causal set. The causal set has 200 elements and a density of 50. The green dashed line is where $\tilde{\lambda}^{cs} = \sqrt{N}/4\pi$ and the purple dashed line is where $\tilde{\lambda}^{cs} = \sqrt{N}/8\pi$.

value of $a = 1/3$. Therefore the truncation procedure is not too sensitive to lowering the location of the truncations (at least by an order one factor).

It may interest the reader to know that the work of this chapter commenced shortly after the preprint of [1] appeared, and in particular, prior to the analogous continuum calculation [46] presented in the previous chapter. Besides our interest in the causal set result, the main reason for this was based on practicality. When all the ingredients that go into the spacetime entropy definition (essentially G_R and the spacetime or causal set itself) are available (as they were for both the causal set and continuum cases studied here), the causal set calculation is computationally much simpler than the continuum one. Upon first attempting the causal set calculation, however, instead of the expected spatial area law the spacetime-volume law mentioned above was found. The failure of our initial attempts (some of which are described in Appendix C) to understand this result led to the subsequent undertaking of the computationally more difficult but physically more familiar continuum calculation of Chapter 4. After completing the continuum calculation and establishing that the result there exhibited the expected spatial area law (thus also verifying the spacetime formula of [1] in a concrete example), we returned our attention to

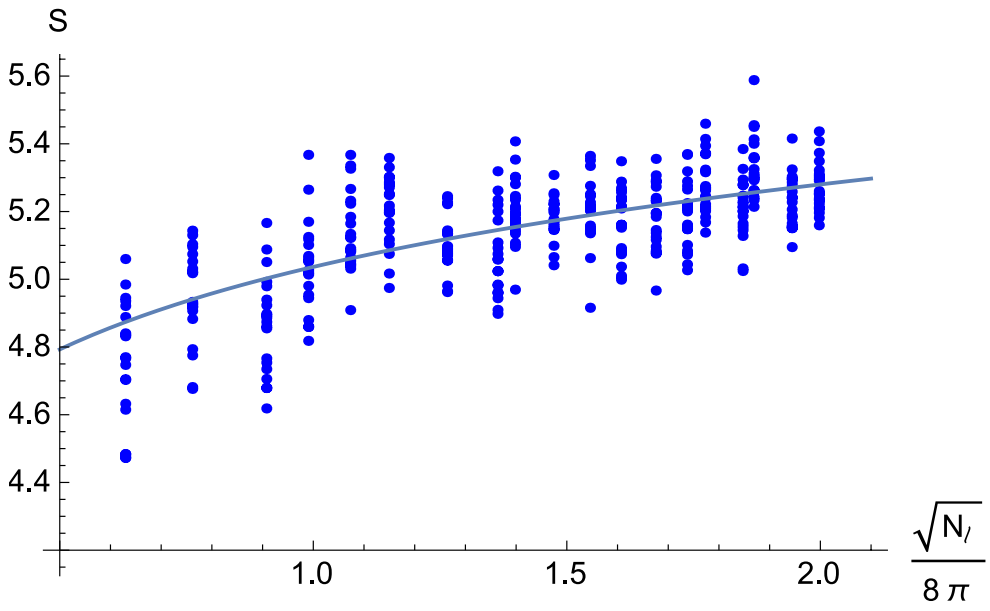

Figure 5.6: S vs. $\sqrt{N_\ell}/8\pi$, after the spectrum of $i\Delta$ has been truncated such that $\tilde{\lambda}_{min} \sim \sqrt{N_L}/8\pi$ in the larger diamond and $\tilde{\lambda}_{min} \sim \sqrt{N_\ell}/8\pi$ in the smaller diamond.

understanding the causal set calculation.

We have presented here a prescription for the recovery of the spatial area law in the causal set calculation, in agreement with the continuum results. As described above, this prescription, involving projecting out the contributions from the small but finite eigenvalues of Δ, in hindsight seems reasonable. The road to arriving at this resolution was a rather long one, however, because while a single truncation of Δ was a resolution we tried early on, the more subtle need for two truncations was not foreseen by us so early. Instead, in the course of arriving at this result, numerous other variations of both the causal set and continuum calculations were studied first. While many of the insights gained from these alternative calculations did not end up directly contributing to our final resolution of the volume law puzzle, they are interesting in their own right and may prove useful in future work. Therefore, we have collected a summary of some of these miscellaneous calculations and observations in Appendix C.

Finally, we would like to emphasize that it remains an open question whether or not the extra entropy in the causal set that leads to the volume law is physical. If it were to really be there and be an entanglement entropy, then one thing that would need to be addressed

is where the complementary subregions in the sense of Figure 3.1 are. An important property of (bipartite) entanglement entropy is that it is equal in both the subregion and its complement. One might naively expect the complement of the inner diamond in Figure 5.1 to be the green subset of either Figure 5.7 (the domains of dependence of the complement of the "Cauchy surface") or Figure 5.8 (the spacetime volume complement[6]). Restrictions of the scalar field to either of these obvious choices for complementary subregions does not yield an entropy equal to the entropy within the inner diamond. Notice that either of these complementary regions would be appropriate in the continuum case, since they both contain the complement of the Cauchy surface of the inner diamond. There may yet exist a reasonable choice of a complementary region, but it will have to be more subtle than the regions in Figure 5.7 and 5.8. The difficulty in identifying two complementary subregions in the causal set, with equal entanglement entropies, may also be a reflection of the fact that the entanglement entropy in the causal set is not bipartite. If it is not bipartite, further investigation is necessary to determine the nature of the entropy, and if there is a bipartite contribution that may be identified with entanglement entropy. Furthermore, if one would like to study black hole entropy and if the conjecture that black hole entropy is entanglement entropy is correct, one would need to show how an area law arises for a causal set black hole.

[6]This spacetime complement has the additional drawback that (even in the continuum) the operators in the two complementary subregions do not commute with one another. Therefore, it doesn't fit as well the standard notion of entanglement.

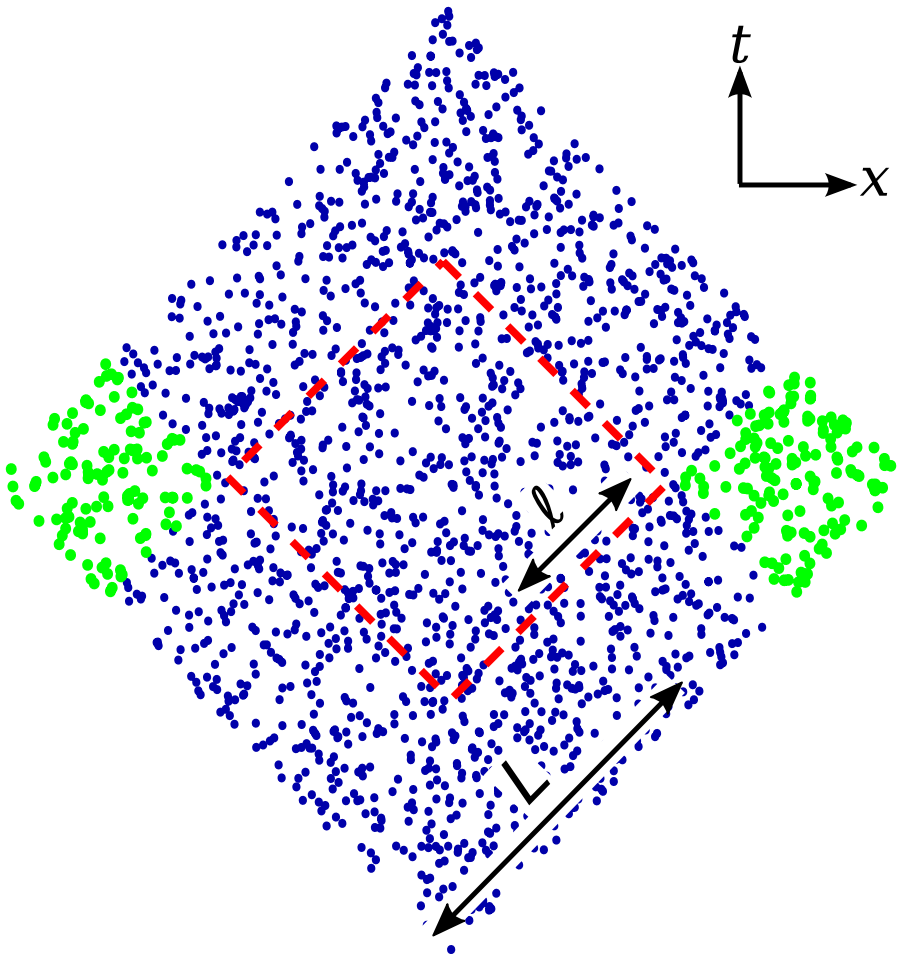

Figure 5.7: The domains of dependence of the complement of the "Cauchy surface" in the causal diamond.

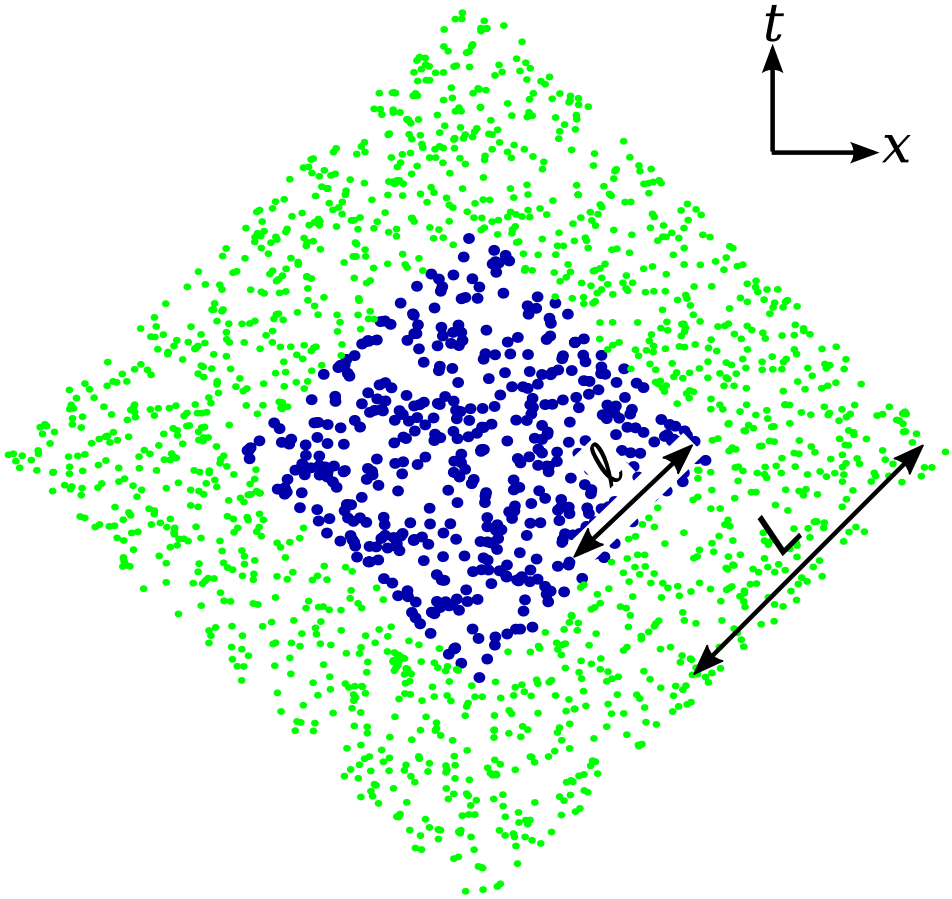

Figure 5.8: The spacetime volume of the complement of the inner causal diamond.

Chapter 6

Entropy of Coarse-Graining

This chapter summarizes some of the results of [50]. We study the entropy of coarse-graining by decimation and blocking. We study decimation in both causal sets and a chain of harmonic oscillators, and blocking in a chain of harmonic oscillators. There is no known way to coarse-grain by blocking in a causal set. We use the SJ vacuum state and the entropy definition (3.13) for the causal set calculation, and the formalism of [6] (also reviewed in Appendix D) for the oscillator calculations.

6.1 Coarse-Graining by Decimation

The Lagrangian for the chain of oscillators we consider is

$$\mathcal{L} = \frac{1}{2}\left(\sum_{N=1}^{N_{max}} \hat{\dot{q}}_N^2 - \sum_{N,M=1}^{N_{max}} V_{MN}\,\hat{q}_N\,\hat{q}_M\right) = \frac{1}{2}\sum_{N=1}^{N_{max}} [\hat{\dot{q}}_N^2 - m^2\hat{q}_N^2 - k(\hat{q}_{N+1} - \hat{q}_N)^2], \tag{6.1}$$

where k is the coupling strength between the oscillators, and in terms of the spatial UV cutoff a, $k = 1/a^2$ [53]. We set $k = 10^6$. We consider the massless theory with periodic boundary conditions and mass regulator[1] $m^2 = 10^{-6}$.

In coarse-graining by decimation, we iteratively remove 10% of the causet elements and oscillators. In the causet we remove each element with probability 0.1, and in the chain of oscillators we remove each oscillator with probability 0.1. In more detail, at first

[1] A mass regulator is introduced since the $m = 0$ theory is IR divergent [54]. See Appendix D for more details.

we divide the oscillators and causal set elements into two subsets: one subset containing (approximately) 90% of the oscillators and causet elements, and the other (complementary) subset containing the remaining (approximately) 10%. This division is done randomly, so the oscillators in one subset may not necessarily have all of their nearest neighbours from the full chain in that subset. Similarly, the elements of the subset of the causal set are randomly chosen. Then we compute the entanglement entropy between the two subsets. This is our first (non-zero) entropy data point. Subsequently, we divide the subset containing $\sim 90\%$ of the original oscillators and causet elements into two subsets containing $\sim 90\%$ and $\sim 10\%$ of them. We then group this second $\sim 10\%$ subset with the first $\sim 10\%$ subset, such that in terms of the original number of oscillators, our two subsets at this second iteration contain $\sim 81\%$ and $\sim 19\%$ of the total number of original oscillators and elements. The entanglement entropy between these two subsets gives us our second (non-zero) entropy data point. Similarly, each n^{th} time we carry this out, we will have $\sim 0.9^n$ and $\sim 1 - 0.9^n$ of the original number of oscillators and causet elements in the two subsets whose entanglement entropy we compute.

A simple relation is obtained in both the oscillator and the causet cases. The entropy depends quadratically on the number of degrees of freedom (DoF's) remaining after coarse-graining. Initially, when all DoF's are present, the entropy is 0. It rises and reaches a maximum when about half of the DoF's remain, after which it drops, symmetrically, until it reaches 0 again when there are no more DoF's left.

The causal set result without truncating $i\Delta$ and W is shown in Figure 6.1, where the entropy is plotted versus the number of elements remaining in the causal diamond. Initially the diamond contained 4048 sprinkled elements and had a density of 10.12. The results fit $S = aN^2 + bN + c$ with $a = -1.5 \times 10^{-4}$, $b = 0.60$, and $c = 7.0$.

The causal set result with truncated[2] $i\Delta$ and W is shown in Figure 6.2, where the entropy is plotted versus the square root of the number of elements remaining in the causal diamond. Initially the diamond contained 4048 sprinkled elements. The results fit $S = aN + b\sqrt{N} + c$ with $a = -0.0019$, $b = 0.12$, and $c = -0.40$.

[2]The first truncation in the full diamond is done identically to that used in Chapter 5. In other words, we make sure that $i\Delta$ does not have any eigenvalues smaller than $\sqrt{N}/4\pi$, where N is the total number of causal set elements. We similarly project out the contributions of the eigenfunctions corresponding to eigenvalues smaller than this cut from W. The second truncation, however, is different from that used in Chapter 5. This is because our subset here is no longer a smaller diamond. Our subset in this case lives in the same larger diamond, so in our second truncation we use the same minimum eigenvalue of $\sqrt{N}/4\pi$ for the $i\Delta$ restricted to the more dilute subset. N is again the number of elements in the original full diamond (as opposed to the number of elements in the diluted subset). Similarly we project out their corresponding eigenfunctions from the restricted W as well.

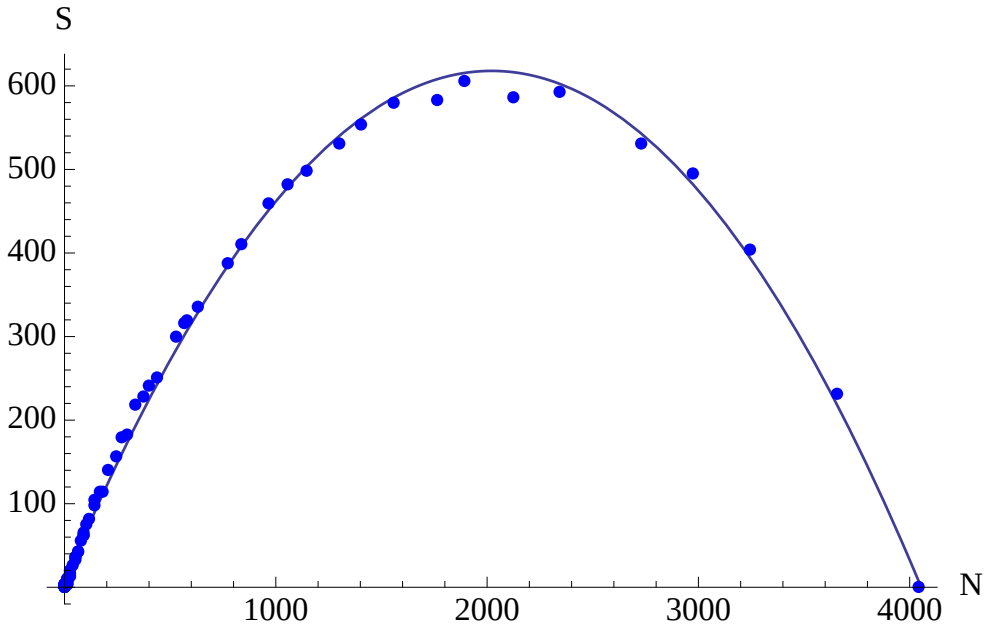

Figure 6.1: S vs. N in a causet under coarse-graining (without truncating $i\Delta$ and W) by decimation: we remove elements with probability 0.1.

It should be noted that the DoF's in terms of which we get a parabolic relation for the entropy of course-graining are different for the truncated and full $i\Delta$ and W. For the full $i\Delta$ and W the DoF's are counted by the number of elements remaining in the diamond, N, and for the truncated $i\Delta$ and W they are counted by $\sqrt{N}$.

The result for the chain of oscillators is shown in Figure 6.3, where the entropy is plotted versus the number of oscillators remaining in the chain. Initially the chain contained 1000 oscillators. The results fit $S = aN^2 + bN + c$ with $a = -5.1 \times 10^{-4}, b = 0.51, c = 5.4$.

6.2 Coarse-Graining by Blocking

In coarse-graining by blocking, we rewrite the q_i's in terms of $Q_i^{\pm}$'s defined as $Q_1^{\pm} \equiv (q_1 \pm q_2)/2$, $Q_2^{\pm} \equiv (q_3 \pm q_4)/2$, ... We then discard all Q^-'s, thus reducing the DoF's by half. In the next iteration we work in terms of $(Q_1^+ \pm Q_2^+)/2$, $(Q_3^+ \pm Q_4^+)/2$... and repeat. The result for the entropy of coarse-graining by blocking in a chain of oscillators is shown in Figure 6.4. The entropy is shown versus the number of oscillators remaining in the

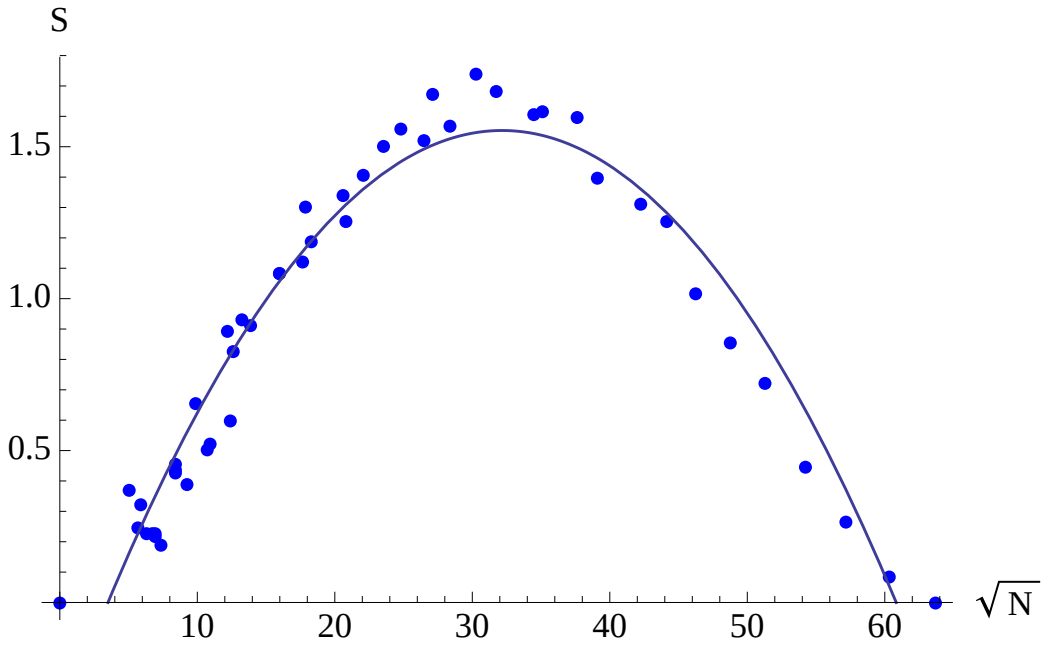

Figure 6.2: S vs. $\sqrt{N}$ in a causet under coarse-graining (with truncated $i\Delta$ and W) by decimation: we remove elements with probability 0.1.

chain. Initially the chain contained 2^{14} oscillators. The results fit $S = aN^2 + bN + c$ with $a = -9.4 \times 10^{-6}$, $b = 0.15$, and $c = -0.36$.

Thus entropy of coarse-graining by both decimation and blocking have led to a parabolic dependence on the number of remaining DoF's, in our examples. Our results suggest that this entropy of coarse-graining might have universal properties that would be interesting to investigate further. We frequently deal with coarse-grained versions of certain systems, and there seems to be an entropy associated to this coarse-graining which has universal properties that would be useful to understand.

Our choices of parameters (ρ for the causal set, and m and k for the oscillators) in this chapter were arbitrary. As we change the values of these parameters (as long as the UV cutoffs ρ and k remain large such that the asymptotic form of the entropy in (3.16) holds, and as long as the mass, m, remains finite in order to avoid the infrared divergence discussed in Appendix D), the qualitative results of this chapter do not change (as my own unpublished investigations have shown). The magnitude of the maximum of the quadratic relation (Figures 6.1–6.4) will, however, depend on the choices for these parameters. It

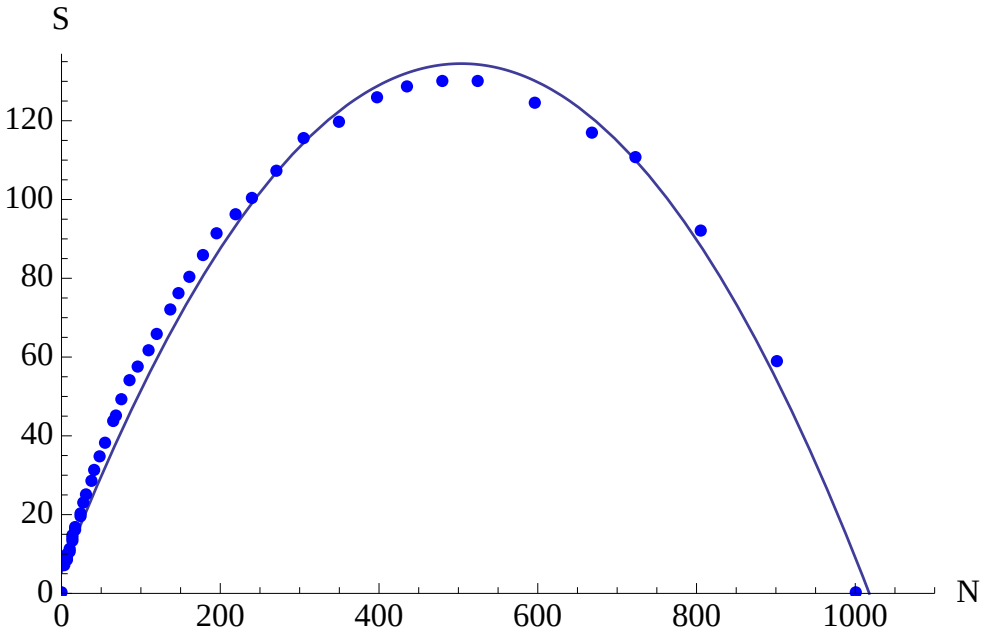

Figure 6.3: S vs. N in a chain of oscillators under coarse-graining by decimation: we remove elements with probability 0.1.

would be interesting to analyze how this maximum scales with each of these parameters. We defer this study to future work.

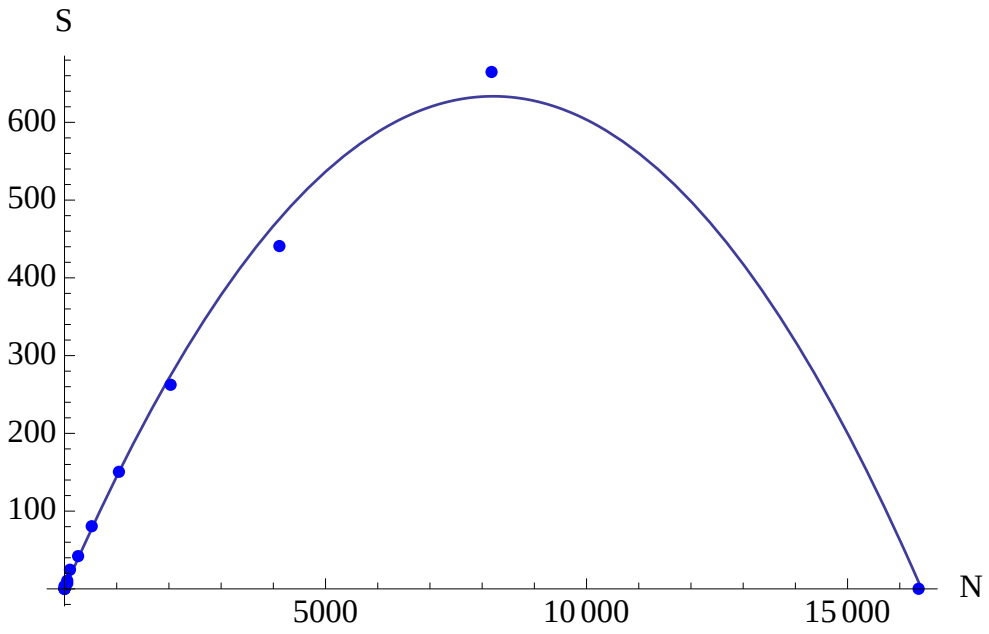

Figure 6.4: S vs. N in a chain of oscillators under coarse-graining by blocking.

Chapter 7

Conclusions

In the present thesis, we have studied (primarily by computer simulations) the entanglement entropy of a free scalar field in causal sets well approximated by regions of $1+1$d flat spacetime. Initially we found unexpectedly that instead of the conventional spatial area law (logarithmic scaling of entropy with the UV cutoff), a spacetime-volume scaling was obtained. We attributed this difference between the causet and the continuum, to a difference in the near-zero part of the spectrum of $i\Delta$. With this in mind, we identified, in the causet case, a minimum eigenvalue of $i\Delta$ which answers to the fundamental discreteness scale embodied in the causet itself. And we found that when the spectrum of $i\Delta$ was truncated there (and the contributions of these parts removed from W as well), the continuum area law was recovered.

With these findings, we are beginning to understand entanglement entropy in causal set theory. This is important for causal sets, of course, but it also demonstrates an important point of principle, namely that the UV cutoff needed to render entanglement entropy finite can be introduced without undermining Lorentz symmetry. The way now seems open to begin to address questions which hinge on understanding the entropy of entanglement associated with black hole horizons, ultimately the question whether most or all of the horizon entropy can be traced to entanglement of one sort or another.

Work is also underway to find the entropy associated to the event horizon of an observer in de Sitter spacetime [55]. The retarded Green function in $3+1$d de Sitter spacetime has recently been found [56] and makes possible the entropy calculation in $3+1$d. Also soon to appear is an application of the truncation scheme presented in Chapter 5 to the Pauli-Jordan function derived from the retarded Green functions which are inverses of the nonlocal causal set d'Alembertians discussed in Appendices B and C [57].

It is not yet known how the truncation scheme in Chapter 5 will be generalized to higher dimensions and for arbitrary spacetime regions. One speculation is that in d spacetime dimensions, the magnitude of the smallest eigenvalue is always of the order of $N^{1/d}$. Another simple possibility for the generalization of the truncation scheme is to include the largest $N^{(d-1)/d}$ eigenvalues (possibly with a pre-factor that could depend on the shape of the region) in d spacetime dimensions. Both of these possibilities are currently under investigation. Ultimately, however, to successfully generalize this truncation scheme we would need to gain a better understanding of the asymptotic (in the UV regime) nature of the eigenfunctions and spectrum of $i\Delta$ in a general setting. Some ideas in this direction (involving a conjecture that these eigenvalues resemble a class of wavepackets and/or wavelets) are being pursued.

The spacetime entropy of Chapter 3 is so far defined only for the case of Gaussian states. It is not yet known how the definition could be generalized for interacting theories. A perturbative calculation for interacting theories could potentially be done along the same lines as the case for a Gaussian state (i.e. using Green functions). Also, perhaps if the entropy definition could be recast into a path integral language[1], it could be more easily generalized to the non-Gaussian case.

The methods we have used in our simulations could also prove valuable in a continuum context, as they illustrate how simulating entanglement entropy via sprinkled causal sets can expedite calculations which would otherwise be more tedious.

Additionally, if the extra entropy really is there under certain conditions, it would be an interesting phenomenological property of causal sets and may lead to new insights when better understood.

We also found that the entropy of coarse-graining, obtained by considering a diluted subset of causal set elements or harmonic oscillators within a chain, demonstrates universal properties. This entropy scales quadratically with the number of degrees of freedom in the system, and a maximum entropy is reached when around half the degrees of freedom remain. In many systems it happens that coarse-graining occurs either by some procedure or experimental limitations. Information is lost as a result of this coarse-graining and the entropy we have found could be a useful measure of this. It would be interesting to further explore the implications of this entropy.

[1]For example, if the entropy could be expressed as the sum over some function of the eigenvalues of a decoherence functional or some other quantity closely related to the path integral

References

[1] R. D. Sorkin, *Expressing entropy globally in terms of (4D) field-correlations*, *J. Phys. Conf. Ser.* **484** (2014) 012004, [arXiv:1205.2953].

[2] R. D. Sorkin, *1983 paper on entanglement entropy: "On the Entropy of the Vacuum outside a Horizon"*, *ArXiv e-prints* (Feb., 2014) [arXiv:1402.3589].

[3] M. Van Raamsdonk, *Building up spacetime with quantum entanglement*, *Gen. Rel. Grav.* **42** (2010) 2323–2329, [arXiv:1005.3035]. [Int. J. Mod. Phys.D19,2429(2010)].

[4] T. Faulkner, M. Guica, T. Hartman, R. C. Myers, and M. Van Raamsdonk, *Gravitation from Entanglement in Holographic CFTs*, *JHEP* **03** (2014) 051, [arXiv:1312.7856].

[5] L. Bombelli, J. Lee, D. Meyer, and R. Sorkin, *Space-Time as a Causal Set*, *Phys. Rev. Lett.* **59** (1987) 521–524.

[6] L. Bombelli, R. K. Koul, J. Lee, and R. D. Sorkin, *A Quantum Source of Entropy for Black Holes*, *Phys. Rev.* **D34** (1986) 373–383.

[7] P. Calabrese and J. Cardy, *Entanglement entropy and conformal field theory*, *J. Phys.* **A42** (2009) 504005, [arXiv:0905.4013].

[8] P. Calabrese and J. L. Cardy, *Entanglement entropy and quantum field theory*, *J. Stat. Mech.* **0406** (2004) P06002, [hep-th/0405152].

[9] M. Saravani, S. Aslanbeigi, and A. Kempf, *Spacetime Curvature in terms of Scalar Field Propagators*, *Phys. Rev.* **D93** (2016), no. 4 045026, [arXiv:1510.0272].

[10] A. A. Robb, *A Theory of Time and Space*. Cambridge: University Press, 1914.

[11] A. A. Robb, *Geometry Of Time And Space*. At The University Press, 1936.

[12] S. W. Hawking, A. R. King, and P. J. Mccarthy, *A New Topology for Curved Space-Time Which Incorporates the Causal, Differential, and Conformal Structures*, *J. Math. Phys.* **17** (1976) 174–181.

[13] D. B. Malament, *The class of continuous timelike curves determines the topology of spacetime*, *Journal of Mathematical Physics* **18** (July, 1977) 1399–1404.

[14] G. 't Hooft, *Quantum Gravity: A Fundamental Problem and Some Radical Ideas*, pp. 323–345. Springer US, Boston, MA, 1979.

[15] J. Myrheim, "Statistical Geometry." CERN-TH-2538.

[16] R. D. Sorkin and E. Woolgar, *A Causal order for space-times with C0 Lorentzian metrics: Proof of compactness of the space of causal curves*, *Class. Quant. Grav.* **13** (1996) 1971–1994, [gr-qc/9508018].

[17] R. Penrose, R. D. Sorkin, and E. Woolgar, *A Positive mass theorem based on the focusing and retardation of null geodesics*, gr-qc/9301015.

[18] R. D. Sorkin, *Causal sets: Discrete gravity*, in *Lectures on quantum gravity. Proceedings, School of Quantum Gravity, Valdivia, Chile, January 4-14, 2002*, pp. 305–327, 2003. gr-qc/0309009.

[19] J. Henson, *The Causal set approach to quantum gravity*, gr-qc/0601121.

[20] P. Wallden, *Causal sets dynamics: Review & outlook*, *Journal of Physics: Conference Series* **453** (2013), no. 1 012023.

[21] L. Glaser and S. Surya, *Towards a Definition of Locality in a Manifoldlike Causal Set*, *Phys. Rev.* **D88** (2013), no. 12 124026, [arXiv:1309.3403].

[22] R. D. Sorkin, *Forks in the road, on the way to quantum gravity*, *Int. J. Theor. Phys.* **36** (1997) 2759–2781, [gr-qc/9706002].

[23] S. W. Hawking, *Quantum Gravity and Path Integrals*, *Phys. Rev.* **D18** (1978) 1747–1753.

[24] F. Dowker, J. Henson, and P. Wallden, *A histories perspective on characterizing quantum non-locality*, *New J. Phys.* **16** (2014) 033033, [arXiv:1311.6287].

[25] D. P. Rideout and R. D. Sorkin, *A Classical sequential growth dynamics for causal sets*, *Phys. Rev.* **D61** (2000) 024002, [gr-qc/9904062].

[26] D. P. Rideout, *Dynamics of causal sets*. PhD thesis, Syracuse U., 2001. gr-qc/0212064.

[27] S. P. Johnston, *Quantum Fields on Causal Sets*. PhD thesis, Imperial Coll., London, 2010. arXiv:1010.5514.

[28] R. D. Sorkin, *Scalar Field Theory on a Causal Set in Histories Form*, *J. Phys. Conf. Ser.* **306** (2011) 012017, [arXiv:1107.0698].

[29] N. D. Birrell and P. C. W. Davies, *Quantum Fields in Curved Space*. Cambridge Monographs on Mathematical Physics. Cambridge University Press, 1982.

[30] Y. Egorov and M. Shubin, *Partial Differential Equations II: Elements of the Modern Theory. Equations with Constant Coefficients*. Encyclopaedia of Mathematical Sciences. New York, 1994.

[31] R. P. Stanley, *Enumerative Combinatorics: Volume 1*. Cambridge University Press, New York, NY, USA, 2nd ed., 2011.

[32] N. Afshordi, S. Aslanbeigi, and R. D. Sorkin, *A Distinguished Vacuum State for a Quantum Field in a Curved Spacetime: Formalism, Features, and Cosmology*, *JHEP* **08** (2012) 137, [arXiv:1205.1296].

[33] N. Afshordi, M. Buck, F. Dowker, D. Rideout, R. D. Sorkin, and Y. K. Yazdi, *A Ground State for the Causal Diamond in 2 Dimensions*, *JHEP* **10** (2012) 088, [arXiv:1207.7101].

[34] S. Aslanbeigi and M. Buck, *A preferred ground state for the scalar field in de Sitter space*, *JHEP* **08** (2013) 039, [arXiv:1306.3231].

[35] R. D. Sorkin, *From Green Function to Quantum Field*, arXiv:1703.0061.

[36] Y. K. Yazdi and A. Kempf, *Towards Spectral Geometry for Causal Sets*, *Class. Quant. Grav.* **34** (2017), no. 9 094001, [arXiv:1611.0994].

[37] M. Headrick and T. Takayanagi, *A Holographic proof of the strong subadditivity of entanglement entropy*, *Phys. Rev.* **D76** (2007) 106013, [arXiv:0704.3719].

[38] S. Ryu and T. Takayanagi, *Holographic derivation of entanglement entropy from AdS/CFT*, *Phys. Rev. Lett.* **96** (2006) 181602, [hep-th/0603001].

[39] H. Casini, M. Huerta, and R. C. Myers, *Towards a derivation of holographic entanglement entropy*, *JHEP* **05** (2011) 036, [arXiv:1102.0440].

[40] R. C. Myers and A. Sinha, *Seeing a c-theorem with holography*, *Phys. Rev.* **D82** (2010) 046006, [arXiv:1006.1263].

[41] A. Kitaev and J. Preskill, *Topological entanglement entropy*, *Phys. Rev. Lett.* **96** (2006) 110404, [hep-th/0510092].

[42] S. V. Isakov, M. B. Hastings, and R. G. Melko, *Topological entanglement entropy of a Bose-Hubbard spin liquid*, *Nature Physics* **7** (Oct., 2011) 772–775, [arXiv:1102.1721].

[43] B. Swingle, *Entanglement Entropy and the Fermi Surface*, *Phys. Rev. Lett.* **105** (2010) 050502, [arXiv:0908.1724].

[44] M. Srednicki, *Entropy and area*, *Phys. Rev. Lett.* **71** (1993) 666–669, [hep-th/9303048].

[45] S. Major, D. Rideout, and S. Surya, *Spatial hypersurfaces in causal set cosmology*, *Class. Quant. Grav.* **23** (2006) 4743–4752, [gr-qc/0506133].

[46] M. Saravani, R. D. Sorkin, and Y. K. Yazdi, *Spacetime entanglement entropy in 1 + 1 dimensions*, *Class. Quant. Grav.* **31** (2014), no. 21 214006, [arXiv:1311.7146].

[47] H. Casini and M. Huerta, *Entanglement entropy in free quantum field theory*, *J. Phys.* **A42** (2009) 504007, [arXiv:0905.2562].

[48] A. Dhar, K. Saito, and P. Hänggi, *Nonequilibrium density-matrix description of steady-state quantum transport*, *Phys. Rev. E* **85** (Jan, 2012) 011126.

[49] P. Calabrese and J. Cardy, *Entanglement entropy and conformal field theory*, *J. Phys.* **A42** (2009) 504005, [arXiv:0905.4013].

[50] R. D. Sorkin and Y. K. Yazdi, *Entanglement Entropy in Causal Set Theory*, arXiv:1611.1028.

[51] A. Chandran, C. Laumann, and R. D. Sorkin, *When is an area law not an area law?*, *Entropy* **18** (2016) 240, [arXiv:1511.0299].

[52] R. D. Sorkin, *Does locality fail at intermediate length-scales*, gr-qc/0703099.

[53] H. Goldstein, *Classical Mechanics*. Addison-Wesley Publishing Company, Reading, MA, 2nd ed., 1980.

[54] Y. K. Yazdi, *Zero Modes and Entanglement Entropy*, *JHEP* **04** (2017) 140, [arXiv:1608.0474].

[55] S. N. Ahmed, R. D. Sorkin, S. Surya, and Y. K. Yazdi (in preparation).

[56] S. N. Ahmed, F. Dowker, and S. Surya, *Scalar Field Green Functions on Causal Sets*, arXiv:1701.0721.

[57] D. Benincasa, A. Belenchia, M. Letizia, and S. Liberati (in preparation).

[58] P. Gilkey, *The spectral geometry of operators of dirac and laplace type*, in *Handbook of Global Analysis* (D. Krupka and D. Saunders, eds.). Elsevier Science, 2011.

[59] J. Milnor, *Eigenvalues of the Laplace Operator on Certain Manifolds*, *Proceedings of the National Academy of Science* **51** (Apr., 1964) 542.

[60] M. Panine and A. Kempf, *Towards spectral geometric methods for Euclidean quantum gravity*, *PRD* **93** (Apr., 2016) 084033, [arXiv:1601.0751].

[61] M. Kac, *Can one hear the shape of a drum?*, *The American Mathematical Monthly* **73** (1966), no. 4 1–23.

[62] K. Datchev and H. Hezari, *Inverse problems in spectral geometry*, *ArXiv e-prints* (Aug., 2011) [arXiv:1108.5755].

[63] S. Aslanbeigi, M. Saravani, and R. D. Sorkin, *Generalized causal set d'Alembertians*, *JHEP* **06** (2014) 024, [arXiv:1403.1622].

[64] F. Dowker and L. Glaser, *Causal set d'Alembertians for various dimensions*, *Class. Quant. Grav.* **30** (2013) 195016, [arXiv:1305.2588].

[65] D. M. T. Benincasa and F. Dowker, *The Scalar Curvature of a Causal Set*, *Phys. Rev. Lett.* **104** (2010) 181301, [arXiv:1001.2725].

[66] I. Chavel, *Eigenvalues in Riemannian Geometry*. Pure and Applied Mathematics. Elsevier Science, 1984.

[67] P. B. Gilkey, *The Spectral geometry of a Riemannian manifold*, *J. Diff. Geom.* **10** (1975), no. 4 601–618.

[68] S. W. Hawking, *Quantum gravity and path integrals*, *Phys. Rev. D* **18** (Sep, 1978) 1747–1753.

[69] G. Landi and C. Rovelli, *Gravity from Dirac eigenvalues*, *Mod. Phys. Lett.* **A13** (1998) 479–494, [gr-qc/9708041].

[70] A. Kempf, *Quantum Gravity on a Quantum Computer?*, *Found. Phys.* **44** (2014) 472–482, [arXiv:1302.3680].

[71] A. Kempf, *Information-theoretic natural ultraviolet cutoff for spacetime*, *Phys. Rev. Lett.* **103** (2009) 231301, [arXiv:0908.3061].

[72] A. Kempf, *Spacetime could be simultaneously continuous and discrete in the same way that information can*, *New J. Phys.* **12** (2010) 115001, [arXiv:1010.4354].

[73] T. Jacobson, *Entanglement Equilibrium and the Einstein Equation*, *Phys. Rev. Lett.* **116** (2016), no. 20 201101, [arXiv:1505.0475].

[74] N. Lashkari, M. B. McDermott, and M. Van Raamsdonk, *Gravitational dynamics from entanglement 'thermodynamics'*, *JHEP* **04** (2014) 195, [arXiv:1308.3716].

[75] S. Carlip, *Dimensional reduction in causal set gravity*, *Class. Quant. Grav.* **32** (2015), no. 23 232001, [arXiv:1506.0877].

[76] A. Eichhorn and S. Mizera, *Spectral dimension in causal set quantum gravity*, *Class. Quant. Grav.* **31** (2014) 125007, [arXiv:1311.2530].

[77] A. Belenchia, D. M. T. Benincasa, A. Marciano, and L. Modesto, *Spectral Dimension from Nonlocal Dynamics on Causal Sets*, *Phys. Rev.* **D93** (2016), no. 4 044017, [arXiv:1507.0033].

[78] F. Dowker and L. Glaser, *Causal set d'Alembertians for various dimensions*, *Class. Quant. Grav.* **30** (2013) 195016, [arXiv:1305.2588].

[79] A. Chandran, C. Laumann, and R. D. Sorkin, *When is an area law not an area law?*, *Entropy* **18** (2016) 240, [arXiv:1511.0299].

[80] H. Casini and M. Huerta, *A Finite entanglement entropy and the c-theorem*, *Phys. Lett.* **B600** (2004) 142–150, [hep-th/0405111].

[81] G. Evenbly and G. Vidal, *Entanglement renormalization in free bosonic systems: real-space versus momentum-space renormalization group transforms*, *New J. Phys.* **12** (2010) 025007, [arXiv:0801.2449].

[82] W. G. Unruh, *Comment on "proof of the quantum bound on specific entropy for free fields"*, *Phys. Rev. D* **42** (Nov, 1990) 3596–3597.

[83] T. He, J. M. Magan, and S. Vandoren, *Entanglement Entropy of Periodic Sublattices*, *Phys. Rev.* **B95** (2017), no. 3 035130, [arXiv:1607.0746].

[84] A. J. Speranza, *Entanglement entropy of excited states in conformal perturbation theory and the Einstein equation*, *JHEP* **04** (2016) 105, [arXiv:1602.0138].

[85] J. Pye, W. Donnelly, and A. Kempf, *Locality and entanglement in bandlimited quantum field theory*, *Phys. Rev.* **D92** (2015), no. 10 105022, [arXiv:1508.0595].

[86] H. Casini and M. Huerta, *Entanglement and alpha entropies for a massive scalar field in two dimensions*, *J. Stat. Mech.* **0512** (2005) P12012, [cond-mat/0511014].

[87] K. Mallayya, R. Tibrewala, S. Shankaranarayanan, and T. Padmanabhan, *Zero modes and divergence of entanglement entropy*, *Phys. Rev.* **D90** (2014), no. 4 044058, [arXiv:1404.2079].

[88] E. Abdalla, M. Abdalla, and K. Rothe, *Non-perturbative Methods in 2 Dimensional Quantum Field Theory*. World Scientific, 2001.

[89] M. Headrick and T. Takayanagi, *A Holographic proof of the strong subadditivity of entanglement entropy*, *Phys. Rev.* **D76** (2007) 106013, [arXiv:0704.3719].

[90] A. Kitaev and J. Preskill, *Topological entanglement entropy*, *Phys. Rev. Lett.* **96** (2006) 110404, [hep-th/0510092].

APPENDICES

Appendix A

Causal Sets in terms of Scalar Field Propagators

In this appendix we summarize a result from [36] which is an extension to the case of $2d$ causal sets of some of the results of [9] for continuum theories. In that work it was shown that the metric tensor can be reconstructed from the inhomogeneous propagators of a scalar quantum field. We ask whether a causal set can be determined from knowledge of only the propagator of the scalar field theory on the causal set. We specifically consider the Feynman propagator defined in Chapter 2 (2.13):

$$G_F = G_R + i\mathrm{Pos}\, i(G_R - G_R^\dagger). \tag{A.1}$$

It is clear that given a G_R there is a unique corresponding G_F. Is the reverse also true? Given a G_F is there a unique G_R it will correspond to? Let us assume that there exists another retarded Green's function $\tilde{G}_R$ from which G_F could also be constructed:

$$G_F = \tilde{G}_R + i\mathrm{Pos}\, i(\tilde{G}_R - \tilde{G}_R^\dagger). \tag{A.2}$$

G_R and $\tilde{G}_R$ can be made to be strictly upper triangular while $\mathrm{Pos}\, i(G_R - G_R^\dagger)$ and $\mathrm{Pos}\, i(\tilde{G}_R - \tilde{G}_R^\dagger)$ are Hermitian. Therefore the difference between G_R and $\tilde{G}_R$ cannot be compensated for by the difference between $\mathrm{Pos}\, i(G_R - G_R^\dagger)$ and $\mathrm{Pos}\, i(\tilde{G}_R - \tilde{G}_R^\dagger)$. It follows that $\tilde{G}_R = G_R$ and there is a unique G_R corresponding to each G_F. Therefore, knowledge of G_F indeed implies complete knowledge of the causal set.

Operationally, the Feynman propagator G_F, being central to the Feynman rules, can in principle be measured through suitable particle physics experiments. This would mean

that we can measure G_F, deduce G_R and therefore the causal matrix C through (2.7). Once we have C we know what the causal set is.

Figures A.1 and A.2 show the imaginary and real parts of the Feynman propagator with respect to one point fixed near the center. Larger dots correspond to larger magnitudes for G_F. As shown in Figure A.1, the magnitude of the imaginary part, $\mathrm{Im}[G_F]$, decays with the distance away from the lightcone of this point. As evident from Figure A.2, the magnitude of the real part, $\mathrm{Re}[G_F]$, is either close to zero (the light dots have a magnitude $< 10^{-10}$) outside of the lightcone of this point, or $\frac{1}{4}$ inside its lightcone. Thus the imaginary part of the propagator tells us the distance of the second point from the lightcone of the first point, while the real part indicates whether or not the second point is inside or outside the lightcone of the first (i.e., it indicates the causal structure). Figures A.1 and A.2 therefore illustrate the intuition that the Feynman propagator effectively provides a measure of the distance (or metric) between spacetime events of the causal set. The fact that knowledge of the Feynman propagator is to know metric distances helps explain why knowledge of the Feynman propagator is to know the spacetime manifold, i.e., in this case the causal set.

It is not yet known whether an extension of this relation to the case of $4d$ causal sets is possible. Equation (A.1) continues to hold, but the general relation between G_R and C in $4d$ is not yet known. Therefore, given G_F we can still deduce G_R but we would not in general know how to deduce the causal matrix C from it in $4d$.

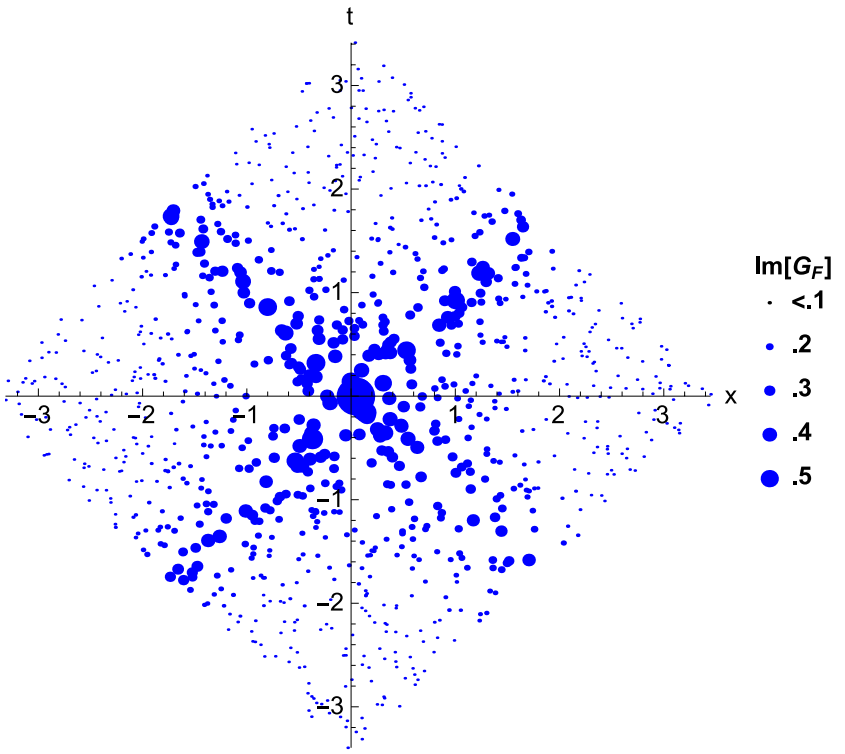

Figure A.1: The imaginary part of the massless Feynman Propagator from an event at the center to other events indicated by dots. The background causal set is a sprinkling of 1000 elements into a finite interval in $1+1$-dimensional Minkowski spacetime, with x, t coordinates shown on the axes. The magnitude of its imaginary part, $\mathrm{Im}[G_F]$, is indicated by the radius of the dots. The magnitude of $\mathrm{Im}[G_F]$ decays with the distance away from the lightcone of the point at the center. This shows that the imaginary part of the Feynman propagator contains the information about the amount of invariant distance that there is between two events - except that it does not tell us if this distance is spacelike or timelike.

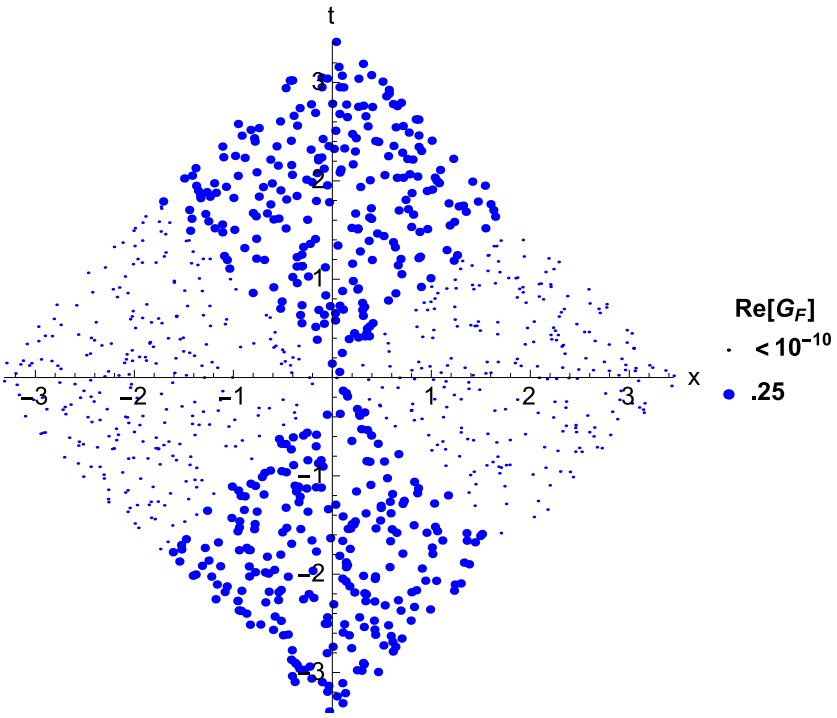

Figure A.2: The real part of the massless Feynman propagator from an event near the center to other events indicated by dots. The background causal set is a sprinkling of 1000 elements into a finite interval in $1+1$-dimensional Minkowski spacetime, with x, t coordinates shown on the axes. The magnitude of its real part, $\mathrm{Re}[G_F]$, is indicated by the radius of the dots. The magnitudes are $\frac{1}{4}$ inside the lightcone and close to zero (the light dots have a magnitude $< 10^{-10}$) outside of the lightcone of the event near the center. This shows that the real part of the Feynman propagator carries the information about whether two events are spacelike or timelike.

Appendix B

Spectral Geometry for Causal Sets

In this appendix we summarize some of the results of [36]. We consider the spectral geometry of causal sets in $2d$. Traditional spectral geometry [58–60], asks how much geometric information about a compact Riemannian manifold is contained in the spectra of Laplacians on that manifold (or also, for example, how much of the shape of a drum one can hear in its spectrum [61]). See [62] for a review. The spectral geometry of spacetimes, i.e., of Lorentzian manifolds, however, is still in its infancy.

Here, we consider spacetimes described by causal sets and we calculate the spectra of their correlators and d'Alembert operators, or more accurately, of their self-adjoint and anti self-adjoint parts. We find numerical evidence that these spectra contain a large amount of geometric information: It occurs relatively rarely that, for example, the d'Alembertian spectra of two distinct causal sets coincide. Indeed, we find numerical evidence that, in general, the more geometrically different two causal sets are, the more their spectra differ. This means that the spectral distances of causal sets could serve as a measure of their geometric similarity.

B.1 Towards Lorentzian Spectral Geometry

As the Lorentzian counterpart to the Laplacian is the d'Alembertian, it is a natural operator to consider for spectral geometry on a causal set. For causal sets, it is known that d'Alembertians that have the correct continuum limit are nontrivially related to Green functions that have the correct continuum limit (i.e, they are generally not simply inverses of each other), [27]. D'Alembertians that are known to possess the correct continuum limit

can be constructed at a point by summing over values of the field on a few layers of elements to the past of that point. In this direction, there is a class of non-local d'Alembertians defined on causal sets [52, 63, 64]. We will focus on the original $2d$ d'Alembertian, B, introduced in [52].

If we fix an element $x \in \mathcal{C}$, at which we would like to know the value of $\Box\phi$ in the causal set, this will be

$$B\phi(x) = \frac{4}{\ell_\rho^2}\left(-\frac{1}{2}\phi(x) + \left(\sum_1 -2\sum_2 + \sum_3\right)\phi(y)\right), \tag{B.1}$$

where ℓ_ρ is the discreteness scale and we are summing over y. We have separated the elements that precede x into *layers* according to the number of intervening elements between them and x. The first layer consists of those y which are linked to x such that $y \prec* x$, the second layer consists of those $y \prec x$ with only a single element z such that $y \prec* z \prec* x$, etc. The causal set prescription for $\Box\phi(x)$, (B.1), is then to take a combination of the first few layers, with alternating signs and suitable coefficients. The three sums $\sum$ in (B.1) extend over the first three layers as just described.

As a matrix at point x, B is

$$\frac{\ell_\rho^2}{4}B_{xy} = \begin{cases} -1/2, & \text{for } x = y \\ 1, -2, 1, & \text{for } n(x,y) = 0, 1, 2, \text{ respectively, for } x \neq y \\ 0 & \text{otherwise} \end{cases} \tag{B.2}$$

where $n(x, y)$ is the cardinality of the order-interval $\langle y, x\rangle = \{z \in \mathcal{C} | y \prec z \prec x\}$, or the number of elements of $\mathcal{C}$ causally between y and x.

B is linear, retarded, and invariant under relabelling of the causal set elements. It can also be applied to any causal set, with or without curvature.

In the continuum limit ($\ell_\rho \to 0$) the average of B over all sprinklings on a spacetime reduces to the continuum d'Alembertian plus a term proportional to the Ricci scalar curvature [65]:

$$\lim_{\ell_\rho \to 0} \bar{B}\,\phi(x) = (\Box - \frac{1}{2}R(x))\,\phi(x). \tag{B.3}$$

Interestingly, as we will now show, given B, one can reconstruct L (or C) and therefore the entire causal set. To this end, we search for matrix elements of value 1 in $\frac{\ell_\rho^2}{4}B$, which

denote links as well as cardinality 2 intervals. Checking for other relations between the elements, we can then distinguish between the links and intervals of cardinality 2. Once we have all the links, we have the link matrix L and the causal set.

We conclude that there is a one-to-one correspondence between the link matrices for each causal set and their respective d'Alembertian. B uniquely determines L, and L uniquely determines a causal set. Hence this is a promising direction in which to explore spectral geometry. There are four levels of spectral geometry we can consider: 1) Whether the spectrum of B or some other related operator can be used to distinguish "manifoldlike" causal sets (i.e. ones that can be faithfully embedded into a Lorentzian manifold) from non-manifoldlike causal sets, 2) Whether the spectrum of B or some other operator related to L can be used to distinguish causal sets that are different sprinklings into the same spacetime manifold, 3) Whether the spectrum of B or some other operator related to L can be used as a measure of how "close" two causal sets sprinkled into the same spacetime manifold are to one another, and 4) Whether the spectrum of B or some other operator related to L can be used to distinguish causal sets sprinkled into spacetime manifolds of differing curvature. In the latter case, causal sets obtained by sprinklings into a particular spacetime manifold should all possess the same (or approximately the same) spectra. As mentioned in Chapter 2, a fundamental conjecture of causal set theory (called the "Hauptvermutung" [18]) is that two very different manifolds could not approximate the same causal set. Likewise, we do not expect to get similar spectra arising from very different manifolds. In Section B.2 we find numerical evidence that the spectra are weakly able to distinguish different sprinklings into the same spacetime and that they are strongly able to distinguish sprinklings into different spacetimes. We also find some cases where the spectra can be used to distinguish causal sets that can be embedded into $1+1$d Minkowski spacetime from those that cannot.

Now the d'Alembertian B itself is not self-adjoint. It is lower triangular, and its spectrum consists of eigenvalues that are all $-\frac{1}{2}$. Thus the spectrum of B itself is trivial and is not useful for spectral geometry. Let us, therefore, consider operators such as $(B \pm B^\dagger)$ and $(L \pm L^\dagger)$. We find that the spectra of such operators do indeed carry large amounts of geometric information.

Concretely, for a small causal set, for example with 6 or 7 elements, we can enumerate all possible L's and therefore all possible B's. There are 318 possibilities with 6 elements and 2045 with 7 elements, including some that do not embed in $1+1$d flat spacetime (such as the 6 element "crown" at the top right corner of Figure B.1). Hasse diagrams for a sample set of such 6 elements causal sets are shown in Figure B.1.

We will use the set of 6 and 7 element causal sets (or 6-orders and 7-orders) as one indication of the degree of uniqueness of the spectra of various causal set operators for a

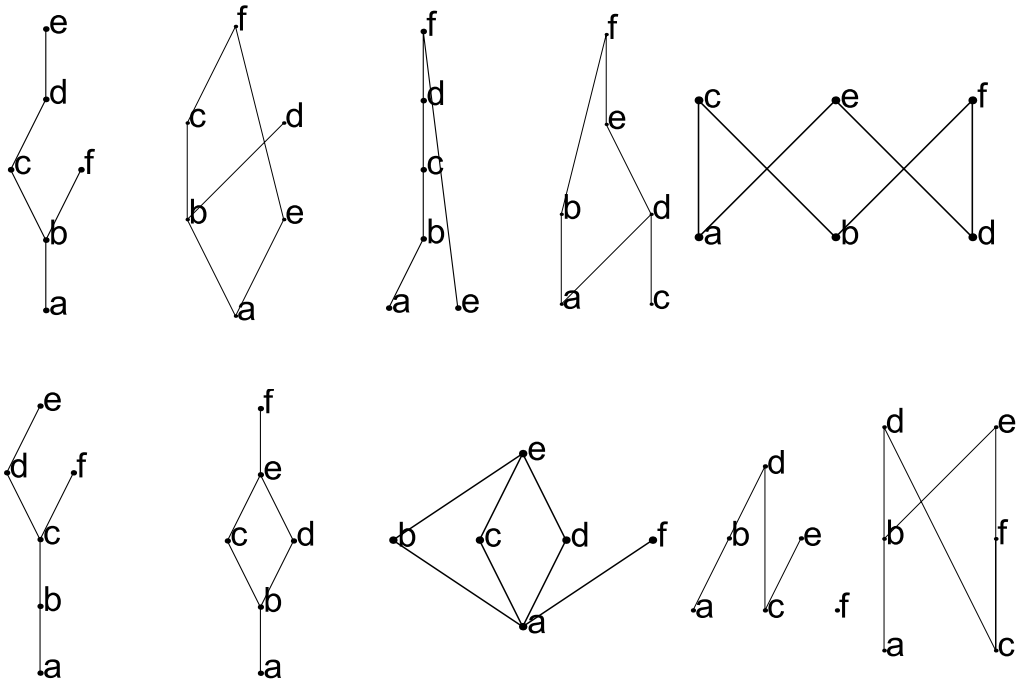

Figure B.1: Hasse diagrams for a sample of 6 element causal sets.

free massless scalar field in $2d$. Table 1 summarizes (in order of uniqueness) the results for the operators we considered: G_F, $G_F \pm G_F^\dagger$, $B \pm B^\dagger$, $i\Delta$, and $G_R + G_R^\dagger$.

Out of the operators we considered, the spectrum of $i(B - B^\dagger)$ does best[1] at distinguishing between causal sets. It has the most number of unique spectra for the 6- and 7-orders. The degeneracy for some of the operators in Table 1 (G_F, $B + B^\dagger$, $G_F + G_F^\dagger$, and $G_R + G_R^\dagger$) is never between spectra of causal sets that can be embedded into $1 + 1$d Minkowski spacetime and spectra of those that cannot (this is not the case for the remaining operators in Table 1, such as $i(B - B^\dagger)$ which has a small number of its degeneracies between manifoldlike and non-manifoldlike causal sets). Thus the spectrum of one or more of these operators might be a useful tool for distinguishing manifoldlike causal sets from non-manifoldlike ones.

We here only work with 1+1d manifolds. In general, the asymptotics of the spectrum of the Laplacian is in one-to-one correspondence with the dimension of the manifold, according

[1]Since the degeneracies for different operators do not in general overlap with one another, a combination of the spectra of two or more operators could be used to distinguish between even more causal sets.

Operator	6-orders: 318 total	7-orders: 2045 total
$i(B - B^\dagger)$	264	1709
$i\Delta$	210	1316
G_F	201	1155
$B + B^\dagger$	178	1013
$G_F + G_F^\dagger$	163	923
$G_R + G_R^\dagger$	162	921
$i(G_F - G_F^\dagger)$	105	512

Table B.1: Approximate number of unique spectra for various causal set operators on 6- and 7-orders.

to Weyl's asymptotic formula [66]. If this asymptotic behavior can be translated into a property of also the d'Alembertian then one could envisage a constraint in the action that enforces a certain asymptotic behavior to obtain causal sets that can be embedded in 3+1 dimensional continuous spacetimes and energetically penalizes others. It should be very interesting to explore how natural such a constraint term may be.

Another interesting observation that can be made from the data in Table 1, is that the ratio of the number of different spectra of $i(B - B^\dagger)$ to the number of different causal sets, is 0.830 and 0.836 for $n = 6$ and $n = 7$ respectively. This might suggest that the degeneracy could be removed for larger causal sets. Larger causal sets are necessary to test this conjecture, and we defer this investigation to future work.

We will next look more closely at the properties of the spectrum of $i(B - B^\dagger)$.

B.2 The Spectrum of $i(B - B^\dagger)$

Let us ask how the spectra of $i(B - B^\dagger)$ differ for sprinklings into different manifolds. We will consider 4 different manifolds: 1) A causal diamond in $2d$ Minkowski (Figure 2.1, and $\Diamond$ in Figure B.5), 2) A patch of a $2d$ spacetime whose volume measure grows exponentially with time (Figure B.2, and e^t in Figure B.5), 3) A patch of a $2d$ spacetime whose conformal factor is $\frac{1}{1+x}$ (Figure B.3, and *inv* in Figure B.5), and 4) A patch of a $2d$ spacetime whose conformal factor is the oscillating function $2 + cos\, t$ (Figure B.4, and *cos* in Figure B.5).

We will work with 20 sprinklings of 200 elements into each of these spacetimes. Figure B.5 shows the sum of the difference squared of the spectra of $i(B - B^\dagger)$ for pairs of sprinklings within each spacetime and across each pair of different spacetimes. The numbers

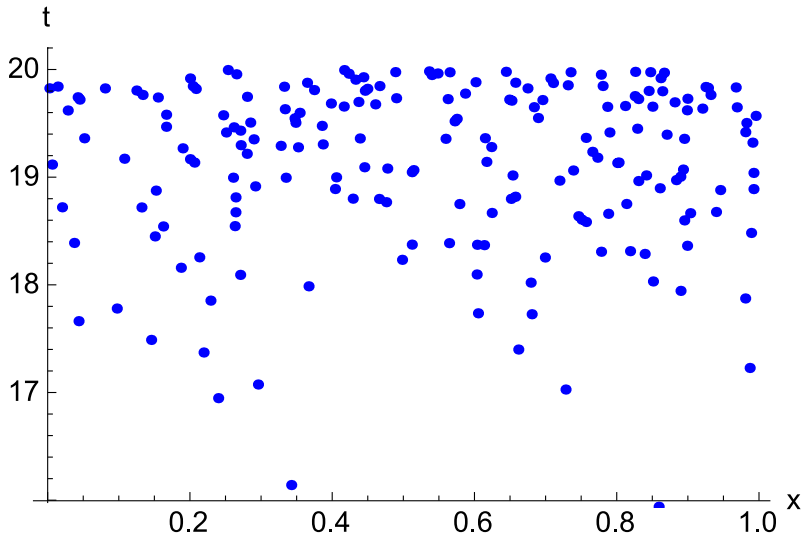

Figure B.2: A causal set formed by sprinkling 200 elements into a finite interval in a conformally flat $2d$ spacetime with conformal factor e^t.

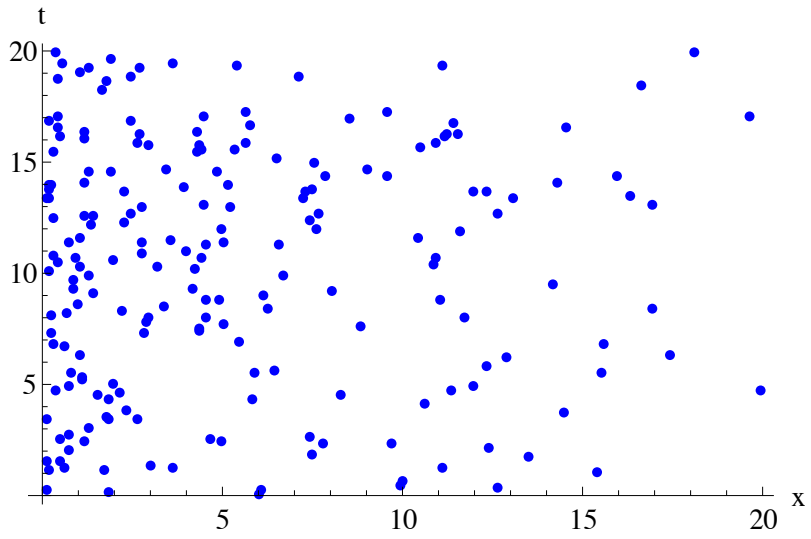

Figure B.3: A causal set formed by sprinkling 200 elements into a finite interval in a conformally flat $2d$ spacetime with conformal factor $\frac{1}{1+x}$.

on the horizontal axis label the pairs of spectra in the comparisons, and the spectral

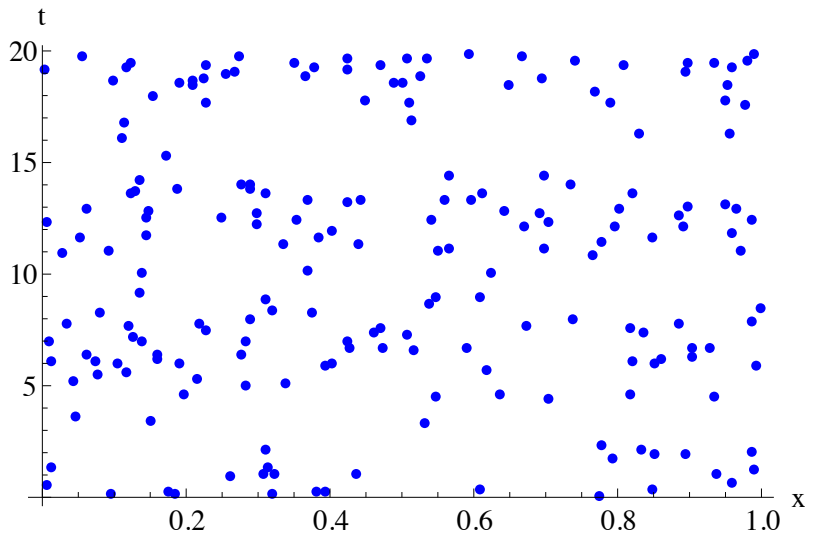

Figure B.4: A causal set formed by sprinkling 200 elements into a finite interval in a conformally flat $2d$ spacetime with conformal factor $2 + \cos t$.

differences are sorted in increasing order for ease of comparison. The differences across two different spacetimes are clearly more pronounced. This means that if we are given two spectra and we find their difference to be large, we can say that there is a greater probability that they will correspond to different spacetimes than the same spacetime.

The second most unique operator in Table 1, $i\Delta$, also shows the same trend of spectral differences being larger across different spacetimes.

We have shown that the d'Alembertian B contains the complete information about the causal set, at least for the 2-dimensional case. In Appendix A we showed that this is also true of the Feynman Green function G_F. It would be very interesting to generalize these results to the 4-dimensional case. It can be shown that the $4d$ analogue of the B we worked with in Section 4, introduced in [52], also uniquely determines L. A challenge in exploring some of the other operators in Table 1 is that the general relation between G_R and L (or C) is not yet known in $4d$. Furthermore, while it is known that the $2d$ d'Alembertian B that we have worked with leads to stable evolution, its $4d$ analogue has been shown to be unstable [63]. It is not known yet whether any of the $4d$ d'Alembertians in [63] lead to stable evolutions. We defer further investigation of the $4d$ case to future work.

That all geometric information is encoded in G_F or B means, in particular, that it should be possible to pursue the development of causal set kinematics, dynamics and

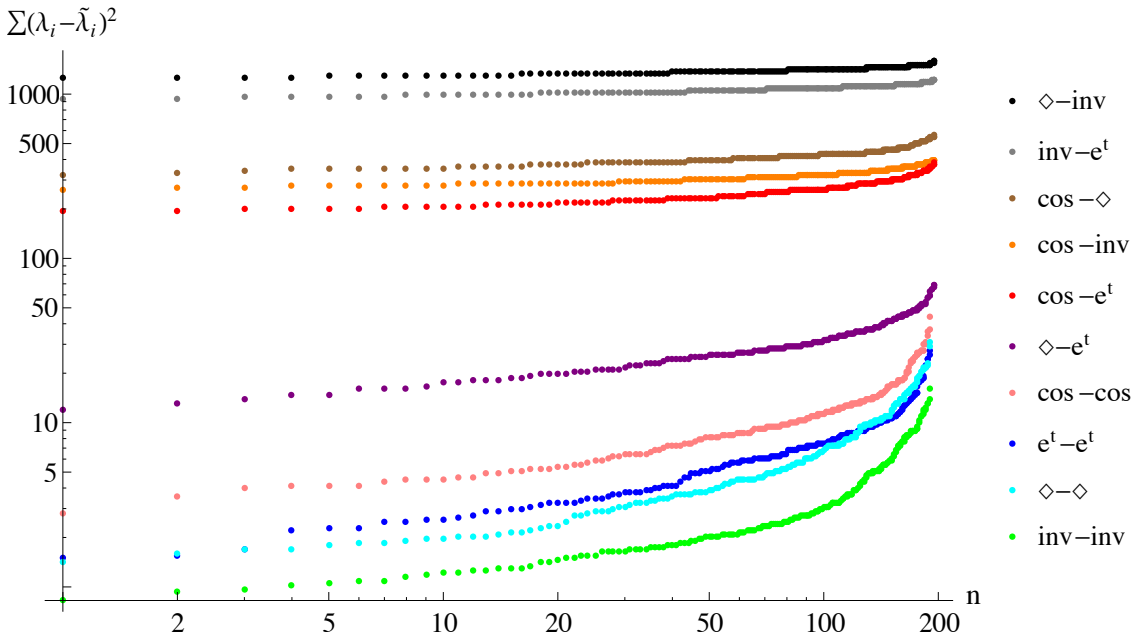

Figure B.5: Spectral differences $\sum(\lambda_i - \tilde{\lambda}_i)^2$ for different sprinklings into the same and different manifolds. The horizontal axis labels the pair of sprinklings and the spectral differences are sorted in increasing order. $\Diamond$ corresponds to the spacetime of Figure 2.1, e^t corresponds to the spacetime of Figure B.2, *inv* refers to Figure B.3 and *cos* refers to Figure B.4. The legend labels the curves from top to bottom.

quantization with the geometric degrees of freedom expressed in terms of B or G_F. The spectra of covariant operators such as d'Alembertians and correlators are geometric invariants, i.e., since they are labeling independent (analogously to diffeomorphism invariance). Therefore these spectral degrees of freedom could be easier to handle, for example, in a path integral where no modding out of spurious gauge (relabeling) degrees of freedom is required. Some ideas from [67–74] may prove useful in this direction.

In a number of approaches to quantum gravity, the phenomenon of the reduction of the spectral dimension on small scales has been observed [75]. Work on the causal set approach to quantum gravity by Eichhorn and Mizera [76] has indicated that, based on random walks and meeting probabilities, the spectral dimension increases at small distances. In contrast, Belenchia et al. [77] computed the spectral dimension from the regularized Laplace transform of (causal set inspired) continuum non-local d'Alembertians using conventional heat kernel methods, and they find the usual spectral reduction to two dimensions in all

cases. It should be interesting to pursue this question with the methods of the present paper, where we use spectral methods to capture the detailed shape of a spacetime, with the short distance structure expected to be encoded in the large eigenvalues.

We have shown numerical evidence that the spectra alone of correlators and d'Alembert operators already possess a large amount of geometric information about the underlying causal set: causal sets from sprinklings on the same manifold tend to have significantly closer spectra than causal sets from sprinklings on geometrically differing manifolds. Intuitively, listening to the spectrum of the quantum noise on a causal set tends to tell about the causal set's geometric shape. The spectral distances of causal sets may therefore be useful for describing the dynamics or quantization of causal sets.

Appendix C

Miscellaneous Calculations and Observations Involving Entanglement Entropy in Causal Set and Continuum Diamonds

Along the way to reconciling the continuum and causal set entropy results, several analyses regarding both were carried out. Some of these were altered versions of the calculations carried out in Chapters 4 and 5 in an attempt to make them more similar to one another, while others were attempts at gaining more insight into certain properties of the entropy in either setting. Here we report on some of these calculations and their results. Throughout we will be using the untruncated operators, except where explicitly stated otherwise. Some of these results attest to the generiticity of the volume-law scaling in the causal set, while others shed light on the subtlety of this result. We only discuss the setups and results. We do not, however, dwell too much on the implications of each of the calculations.

C.1 Entanglement Entropy with Nonlocal Propagators

As mentioned in Appendix B, it is known that causal set d'Alembertians that have the correct continuum limit are not merely inverses of Green functions that have the correct continuum limit [28]. D'Alembertians that are known to possess the correct continuum

limit can be constructed at a point in the causal set by summing over values of the field on a few layers of elements to the past of that point [52, 63, 78].

In this subsection we investigate whether or not working with the Green function obtained by inverting a causal set d'Alembertian also leads to a spacetime volume law for the entanglement entropy.

Recall from Chapter 2 that in setting up the scalar field theory, the starting point was G_R. From G_R we obtained $i\Delta$ and then took its positive part (the SJ prescription) to get W. In short we had $G_R \to i\Delta \to W$. The entropy in turn was obtained from W and $i\Delta$. Now we are going to add one more step to this path: $B \to \tilde{G}_R \to i\tilde{\Delta} \to \tilde{W}$, where B is the causal set d'Alembertian. We have placed a $\sim$ over G_R and the subsequent functions derived from it as a reminder that these functions will not be the same as the one we were working with before.

The d'Alembertian in (B.1) is only a good approximation to $\Box$ when averaged over a collection of causal sets [52]. Fluctuations in (B.1) grow with N and any given realization of it may not produce the correct continuum limit. It remains to be seen whether or not the presence of these fluctuations has any important implications. Under the assumption that we would not like to have such fluctuations, however, a broader class of d'Alembertians, B_k, have been defined in which a non-locality scale ℓ_k (larger than the discreteness scale) is introduced [52]. With a nonlocality scale equal to the discreteness scale ($\ell_k = \ell_\rho$) the result of (B.1) is obtained. For general $\ell_k > \ell_\rho$ we have

$$B_k\phi(x) = \frac{4\epsilon}{\ell_\rho^2}\left(\frac{1}{2}\phi(x) + \epsilon\sum_{y\prec x} f\left(n(x,y),\epsilon\right)\phi(y)\right), \tag{C.1}$$

where $\epsilon \equiv \ell_\rho^2\ell_k$, and

$$f(n,\epsilon) = (1-\epsilon)^n\left(1 - \frac{2\epsilon n}{1-\epsilon} + \frac{\epsilon^2 n(n-1)}{2(1-\epsilon)^2}\right). \tag{C.2}$$

Any given realization of (C.1) is a good approximation to $\Box$ and its fluctuations decrease with N [52], as desired. We will take as our Green function the inverse of the d'Alembertian above, (C.1), with $\ell_k = 5\ell_\rho$ and diamond size ratio of $\ell/L = 1/4$. The result is shown in Figure C.1 along with the original result using $G_R = \frac{1}{2}C$. As evident from the figure, using the inverse of the d'Alembertian (C.1), with non-locality scale larger than the discreteness scale, still produces a linear scaling of the entropy with N, i.e a spacetime volume law. The result is slightly different from the one with $G_R = \frac{1}{2}C$ (different slopes and intercepts) but the general scaling result is the same.

Therefore, it seems that we cannot avoid the spacetime volume law of the causal set entropy even if we use the nonlocal d'Alembertians intrinsic to it. It may be interesting to explore how the results change as we consider different choices within the space of all the d'Alembertian operators defined so far for a causal set (including varying ℓ_k in the above box operator). It is possible that the volume term would have a weaker presence in one case over another. Some work in this direction is being pursued [57].

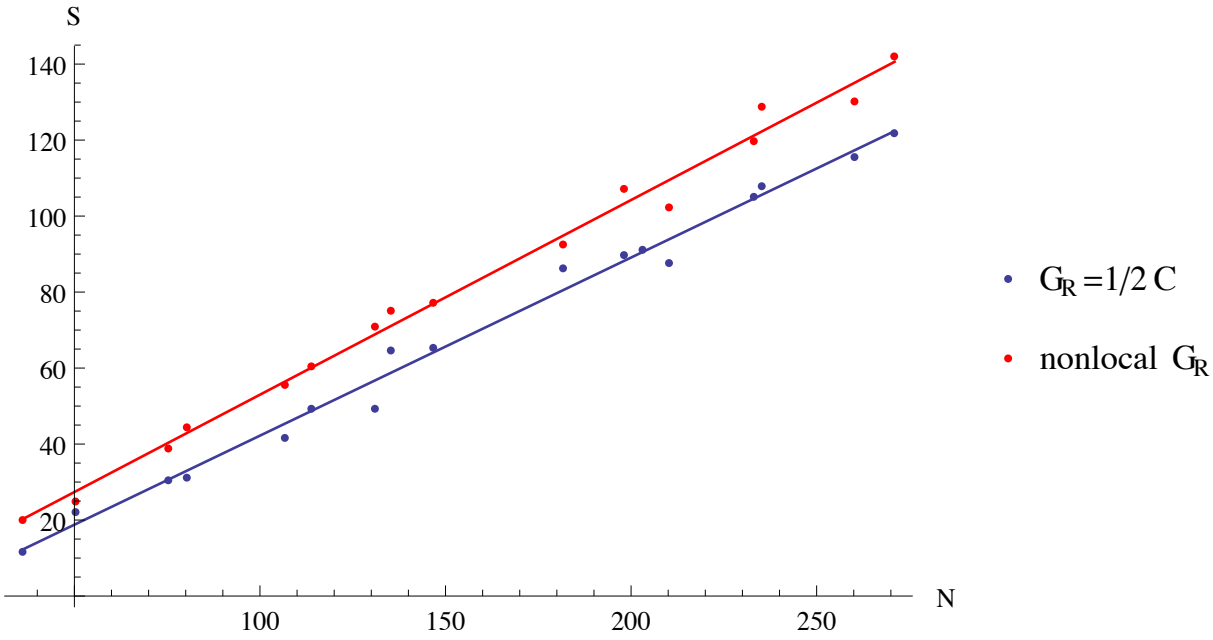

Figure C.1: Entanglement entropy with the inverse of a nonlocal d'Alembertian, along with that from $G_R = \frac{1}{2}C$.

C.2 Regular Lattices

In order to explore whether or not the stochastic nature of a causal set could be the source of extra entropy, we can consider regular lattices. The same setup as in Chapters 4 and 5 but with regular lightcone lattices is pictured in Figure C.2. This is the background we consider in this subsection. We use the causal set retarded Green function (2.7) evaluated at the lattice points and carry out the entropy calculation as before. The results are shown in Figures C.3 and C.4 for $\ell/L = 1/4$ and $\ell/L = 1/2$ respectively. In the former case the

best fit of the data to $S = aN + b$ yields $a = 6.6 \times 10^{-3}$ and $b = 4.96$, while in the latter case it yields $a = 6.6 \times 10^{-3}$ and $b = 4.96$. N here is the number of lattice elements in the smaller diamond. The data does not display a linear scaling with N as strongly as in the causal set case, but it certainly does not fit a logarithmic scaling well either.

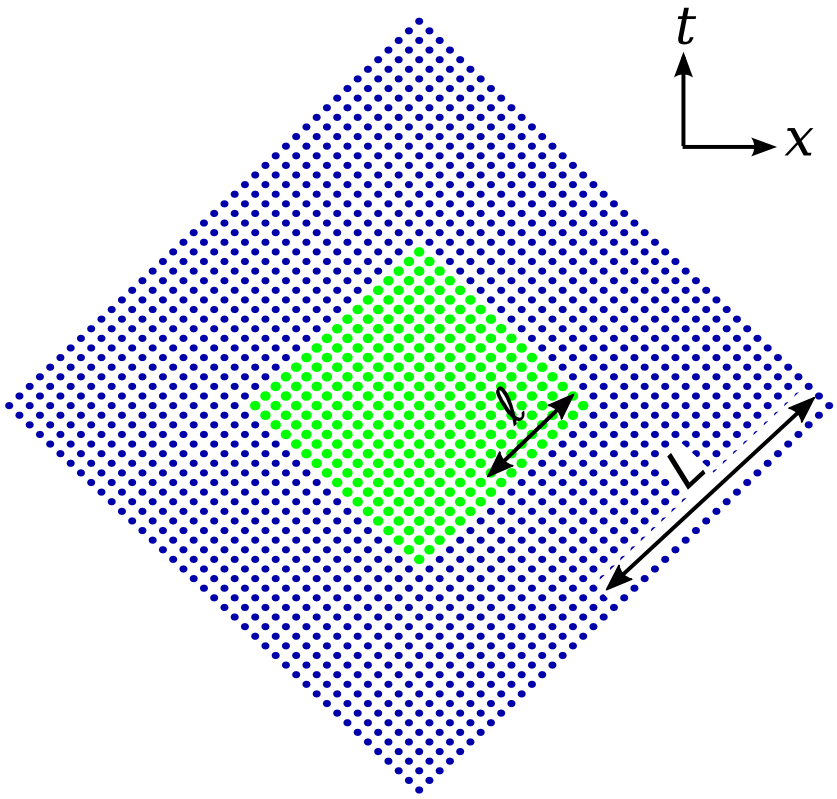

Figure C.2: Two concentric regular lightcone lattice causal diamonds.

One can also try and use the continuum $i\Delta$ and W functions evaluated at the regular lattice elements in solving (3.14). The difficulty in doing this is that W (see (4.2)) is divergent when proper time vanishes, such as on its diagonal (when $x = x'$). We could regularize this divergence by using a different expression at these points or by introducing a minimum proper time, but it is ambiguous how to do this and the final results are sensitive to this choice. The same challenge exists if one wishes to evaluate the continuum $i\Delta$ and W functions at the causal set elements.

It is also worth mentioning here that "discreteness" by itself does not seem to be the

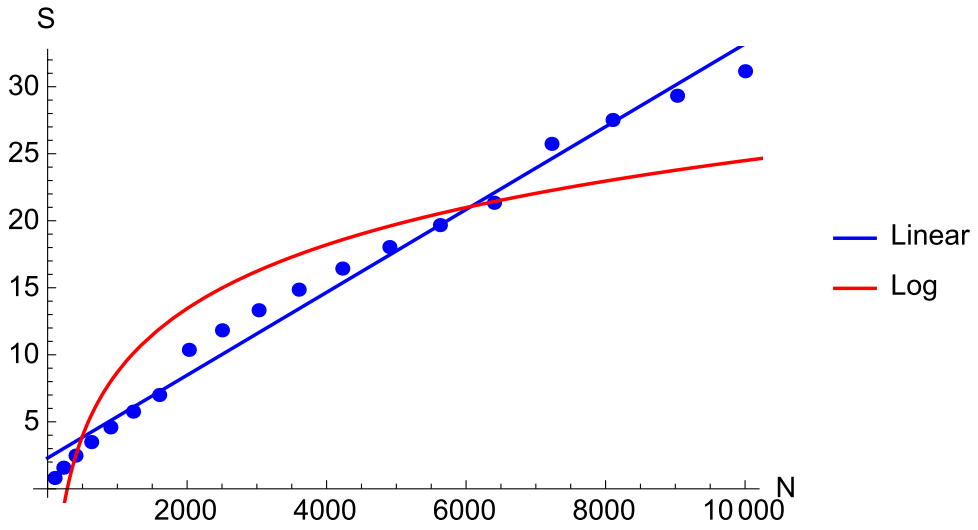

Figure C.3: Entanglement entropy vs. number of lattice points in a regular lightcone lattice, for $\ell/L = 1/4$. The data fits $S = aN + b$ with $a = 6.6 \times 10^{-3}$ and $b = 4.96$, where N is the number of lattice points in the smaller diamond. A best fit logarithm is also shown for comparison.

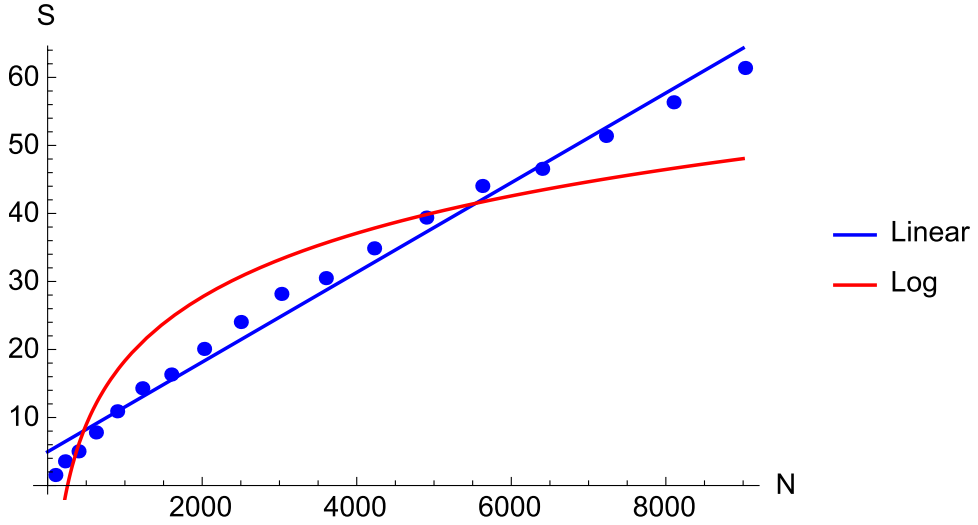

Figure C.4: Entanglement entropy vs. number of lattice points in a regular lightcone lattice, for $\ell/L = 1/2$. The data fits $S = aN + b$ with $a = 6.6 \times 10^{-3}$ and $b = 4.96$, where N is the number of lattice points in the smaller diamond. A best fit logarithm is also shown for comparison.

source of extra entropy. In Appendix D we will study a 1d chain of harmonic oscillators with nearest neighbour couplings, which can be used to model a scalar field theory. This system is an example of a theory with spatial discreteness and there we recover the expected scaling of the entropy. It is also the case that if we consider a single harmonic oscillator on a 1d stretch of randomly sprinkled times and consider the entanglement entropy associated to a subinterval within it that the entropy vanishes as expected[1]. Therefore it seems that by discretizing either time or space we obtain conventional results. It remains an open question whether some extra subtlety arises when one discretizes both space and time.

C.3 Massive Scalar Field Theory

In order to rule out the spacetime volume law being an artifact of the massless theory[2], we also considered the entanglement entropy of a massive scalar field theory on a causal set causal diamond. The retarded Green function is (2.7). We set $m = 1$ for this calculation. The expected entropy scaling in this case is (3.18). The results are shown in Figures C.5 and C.6 for $\ell/L = 1/4$ and $\ell/L = 1/2$. As evident from the figures, the spacetime volume law persists in the massive theory and the entropy grows linearly with the number of causet elements N. In the $\ell/L = 1/4$ case the data fits $S = aN + b$ with $a = 0.47$ and $b = -3.9$, while for $\ell/L = 1/2$ it fits $S = aN + b$ with $a = 0.32$ and $b = 0.13$. N here is the number of causal set elements in the smaller diamond.

C.4 Renormalization: $S = S_{lin} + S_{log}$?

It could be possible that the causal set entanglement entropy could be normalized in some suitable manner, such as by directly removing the linear part of its scaling with N. In other words, it might be possible to separate the entanglement entropy into a linear and logarithmic part $S = S_{lin} + S_{log}$.

[1] This was a calculation suggested by Niayesh Afshordi to ensure that discretizing time gives the expected result.

[2] We have previously encountered surprising results in studying the massless scalar field theory on a causal diamond, which we think is an aspect of the infrared pathology of the massless theory and will be absent in the massive theory. This surprising result was that the SJ vacuum near the left (right) corner of the diamond is the vacuum of Minkowski spacetime with a static mirror placed at the left (right) corner instead of the Rindler vacuum (which was our expectation). See [33] for details, and also Appendix D for a discussion of zero modes and entanglement entropy.

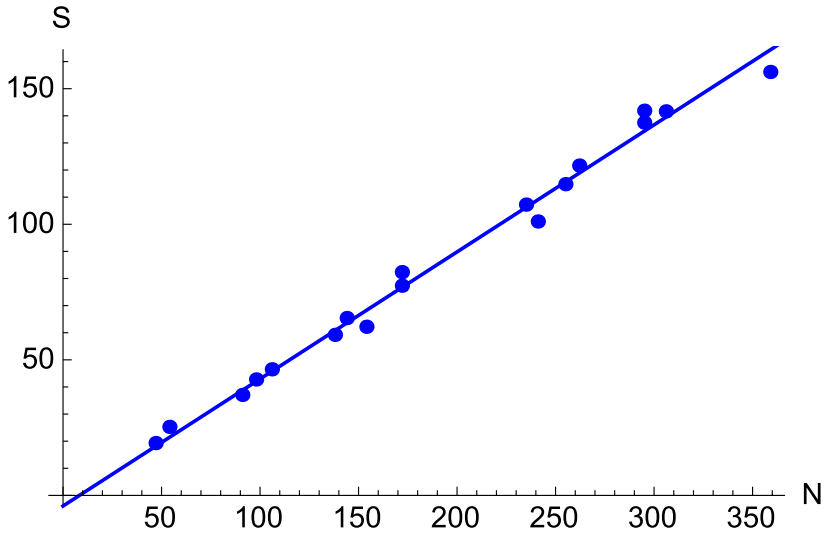

Figure C.5: Entanglement entropy vs. number of causal set elements in the smaller diamond, for $\ell/L = 1/4$. The data fits $S = aN + b$ with $a = 0.47$ and $b = -3.9$.

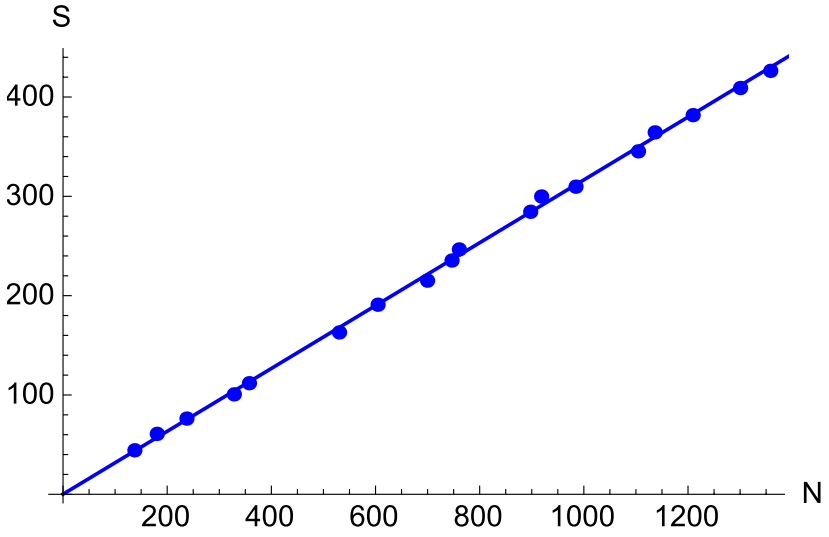

Figure C.6: Entanglement entropy vs. number of causal set elements in the smaller diamond, for $\ell/L = 1/2$. The data fits $S = aN + b$ with $a = 0.32$ and $b = 0.13$.

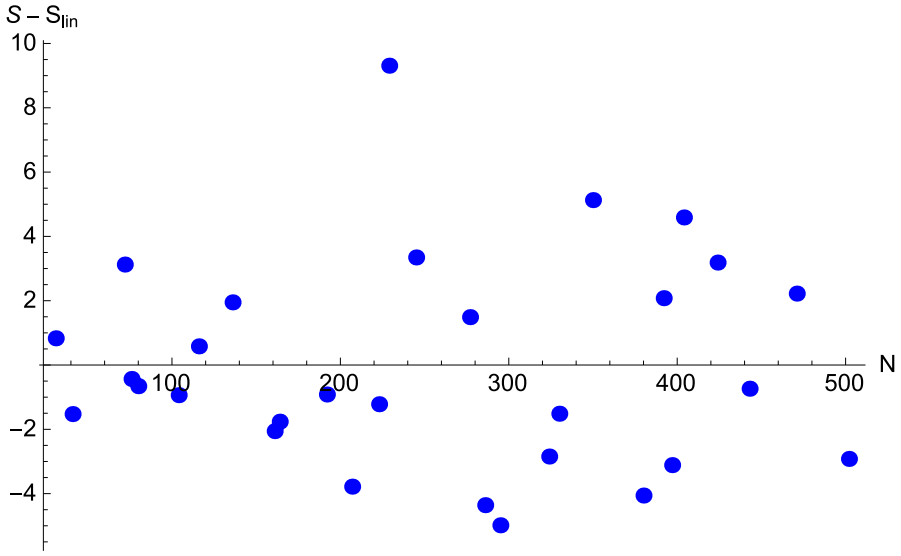

Figure C.7: A typical result after removing the linear part of the scaling from S.

A typical result after removing the linear part from S is shown in Figure C.7. It does not resemble any function and looks like noise. This is only one example, however. It remains plausible that when considering a large number of such samples, careful statistics might show evidence favouring a logarithmic scaling over others. We will not pursue this further here.

C.5 Area Ratio Relation

There is also a simple relation between the (untruncated) entanglement entropy and the ratio of the areas, a/A, of the diamonds in the causet. Figure C.8 shows the results for a causal set with density $\rho = 225$. The relation is quadratic and in this case fits $S = d\ (a/A)^2 + b\ a/A + c$ with $d = -781.84, b = 779.35, c = 9.28$

The relation between S and $e \equiv a/A$ can therefore in general be expressed as

$$\begin{aligned} S &\sim bN_{tot}e(1-e) \\ &= bN_1(N_{tot} - N_1)/N_{tot} \\ &= bN_1N_2/N_{tot} \end{aligned} \tag{C.3}$$

where N_1 is the number of elements in the smaller diamond, N_2 the number of elements excluding N_1, and N_{tot} the total number of elements. $b \sim 0.4$ and is independent of N_{tot},

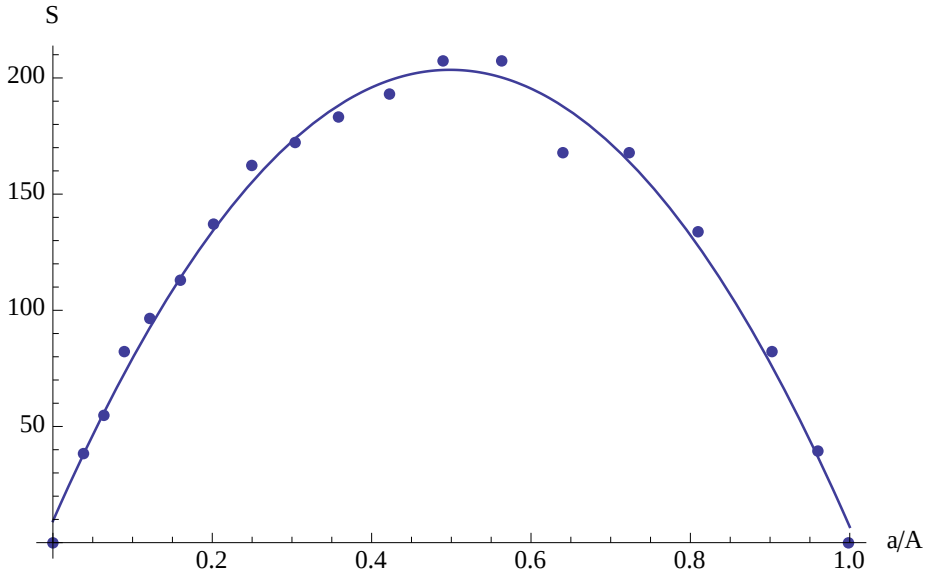

Figure C.8: S vs. a/A (ratio of areas) for a causet diamond with density $\rho = 225$.

so this entropy could also be thought of as a kind of entropy per pair. This result together with the linear scaling of entropy at fixed ratio e, lets us determine an expression for the slope of the linear scaling [3]: this slope is $\sim b\, e(1-e)$.

C.6 Single Truncation of the Spectrum of $i\Delta$

When we first realized (thanks to Siavash Aslanbeigi) that the near zero but finite part of the spectrum of $i\Delta$ was very likely the source of the extra entropy, we focussed on removing these extra contributions in the smaller diamond. This was because it is in the smaller diamond that the generalized eigenvalue problem $Wv = i\lambda\Delta v$, whose eigenvalues go into (3.13), is solved. The generalized eigenvalue problem can also be written as an ordinary eigenvalue problem for the operator $-i\Delta^{-1}W$. Our initial intuition was that the major contribution from the small eigenvalues is entering at this stage due to the inversion of Δ^{-1} here.

We found that indeed if we truncate the spectrum of $i\Delta$ (by throwing away a certain number of its smallest (in magnitude) eigenvalues and the projections of their eigenfunctions in W), a logarithmic dependence on $\sqrt{N_\ell}$ (or N_ℓ), is obtained. Furthermore, the

[3] Fay Dowker pointed this out.

correct coefficient of $\frac{1}{3}$ can be obtained by truncating Δ by "just the right amount". Two examples of the logarithmic shape of the data points after the truncation of $i\Delta$ in the smaller diamond are shown in Figures C.9 and C.10. In figure C.9, $\ell/L = 1/4$ and the spectrum of Δ has been truncated from from N_ℓ to $\frac{1}{4}\sqrt{N_\ell}$ eigenvalues. A fit to $S = b\ln(\sqrt{N_\ell}) + c$ of this data was also made and included in the figure and the best fit parameters were $b = 0.29$ and $c = 0.24$. In figure C.10, $\ell/L = 0.4$ and the spectrum of Δ has been truncated from from N_ℓ to $0.4\sqrt{N_\ell}$ eigenvalues. A fit to $S = b\ln(\sqrt{N_\ell}) + c$ of this data was also made and included in the figure and the best fit parameters were $b = 0.35$ and $c = -0.18$. N in the figures is the number of elements in the smaller diamond.

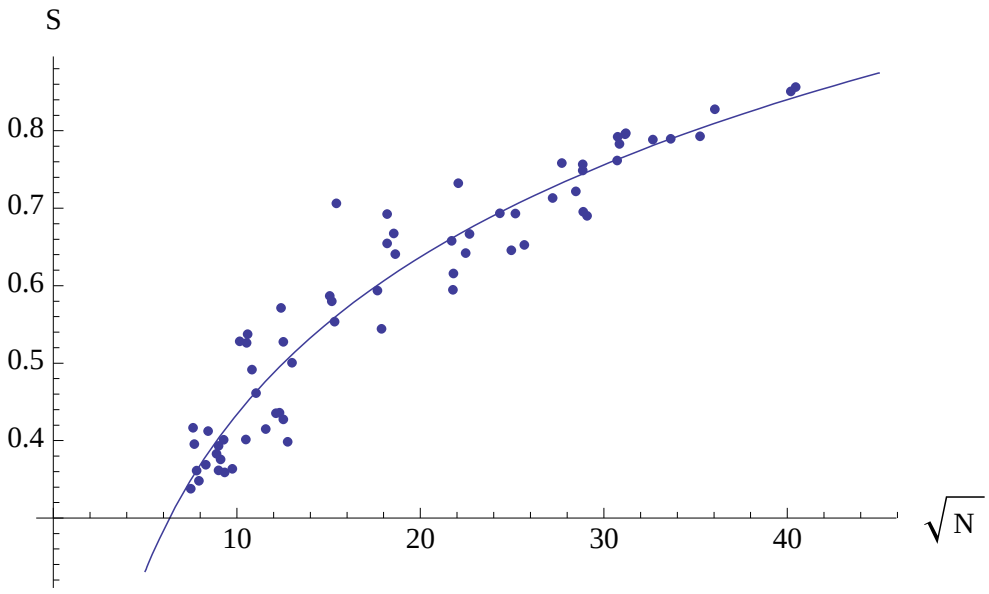

Figure C.9: S vs. $\sqrt{N}$, after the spectrum of Δ has been truncated from from N to $\frac{1}{4}\sqrt{N}$ eigenvalues. $\ell/L = 1/4$ in this example, and N is the number of elements in the smaller diamond. A fit to $S = b\ln(\sqrt{N}) + c$ of this data yields best fit parameters $b = 0.29$ and $c = 0.24$.

In general it seems that to get the expected answer we can truncate the spectrum of $i\Delta$ in the smaller diamond, by keeping approximately $\ell/L\sqrt{N_\ell}$ of its (largest in magnitude) eigenvalues. We already expected an order of $\sqrt{N_\ell}$ terms to contribute[4], but how can we justify the $\sim \ell/L$ factor? We lack a physical understanding of how this particular

[4]For a cutoff $k_{max} = n_{max}\pi/\ell$ in the continuum, approximately n_{max} terms contributed. In the causal set the cutoff is $\sqrt{\rho} = \sqrt{N_\ell}/2\ell$, so we expect approximately $\sqrt{N_\ell}$ terms to contribute.

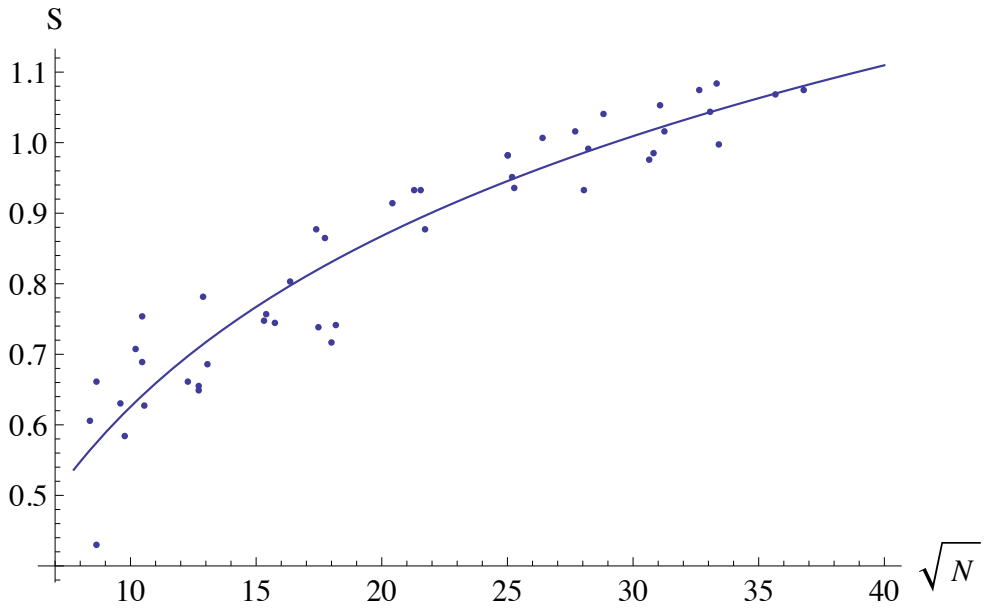

Figure C.10: S vs. $\sqrt{N}$, after the spectrum of Δ has been truncated from from N to $0.4\sqrt{N}$ eigenvalues. $\ell/L = 0.4$ in this example, and N is the number of elements in the smaller diamond. A fit to $S = b\ln(\sqrt{N}) + c$ of this data yields best fit parameters $b = 0.35$ and $c = -0.18$.

truncation scheme leads to results consistent with the continuum calculation.

A possibility is that perhaps the two sets of eigenfunctions (the ones we keep and the ones we throw away) could be distinguished via a suitable measure of smoothness. The eigenfunctions of $i\Delta$ resemble linear combinations of two plane waves. Similarly, the large eigenvalue (long wavelength) eigenfunctions in the causal set resemble plane waves as well. Of course the causal set eigenfunctions are not smooth functions, but if one interpolates between the values at each causal set element, a typical large eigenvalue eigenfunction looks as shown in Figure C.11; it demonstrates smooth oscillation. In contrast, a typical small eigenvalue eigenfunction looks fairly jagged, as shown in Figure C.12. We did not pursue further this possibility of using a meaningful smoothness measure to dictate where the truncation must take place.

Further investigation into this single truncation scheme eventually led to the double truncation scheme presented in Chapter 5, whereby contributions from the small eigenvalue part of the spectrum of $i\Delta$ need to be removed from *both* the larger and the smaller

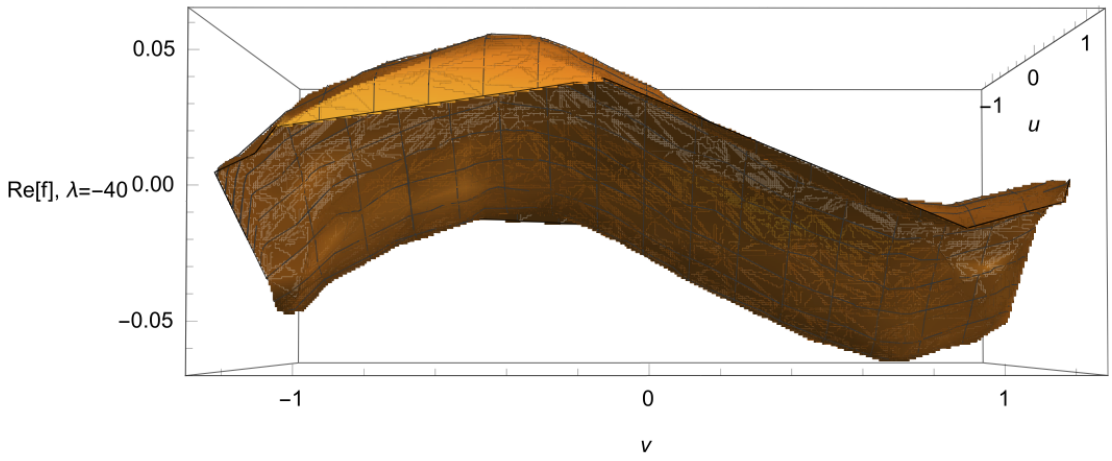

Figure C.11: The real part of a typical large eigenvalue eigenfunction of $i\Delta$ in the causet, with interpolation between the values at each causet element. The other two axes are the lightcone coordinates u and v. The eigenfunction resembles a smooth function that is a linear combination of plane waves.

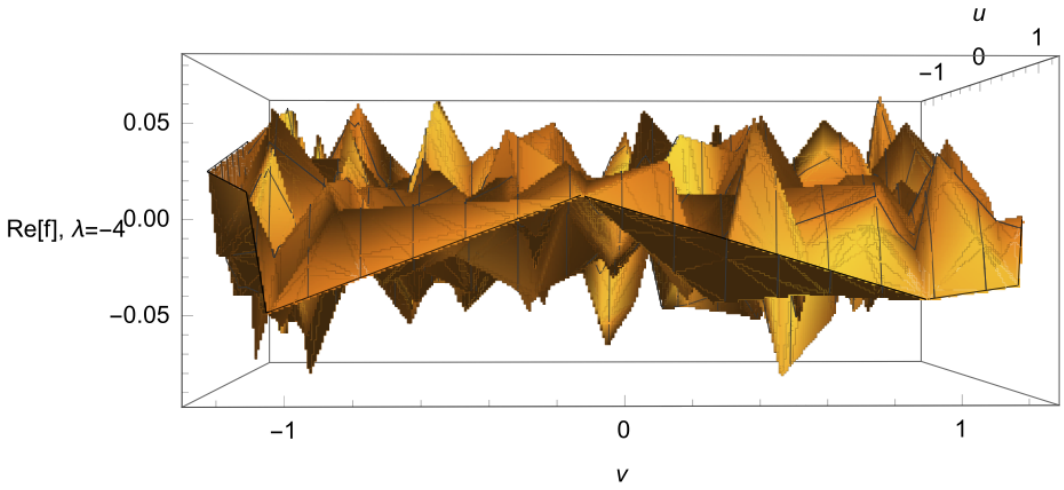

Figure C.12: The real part of a typical small eigenvalue eigenfunction of $i\Delta$ in the causet, with interpolation between the values at each causet element. The other two axes are the lightcone coordinates u and v. The eigenfunction does not resemble a smooth function that is a linear combination of plane waves and instead looks very jagged.

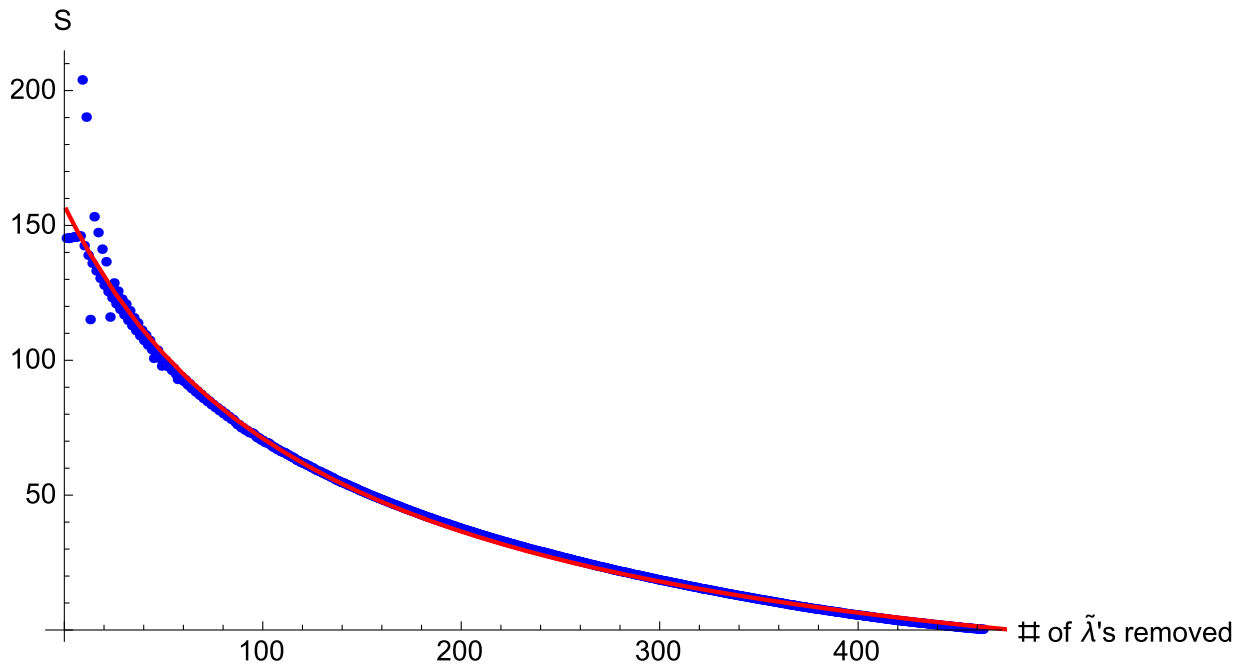

Figure C.13: Entanglement entropy vs. number of smallest eigenvalues ($\tilde{\lambda}$'s) removed from $i\Delta$. In this causal set there were 2000 elements in the larger diamond and 520 in the smaller. The data fits $S = c_0/(c_1 + \tilde{\lambda}) + c_2$ with $c_0 = 30400$ and $c_1 = 144$ and $c_2 = -44.7$.

diamonds. Here, we do have a physical understanding of why the truncations need to take place where they do, in order for agreement with the continuum calculation (see Chapter 5 for details).

Another potentially useful relation is how the entropy decreases as a function of how many of the smallest (in magnitude) eigenvalues of $i\Delta$ are removed. A sample result for a causal set with 2000 elements in the larger diamond, $\ell/L = 1/2$, and 520 elements in the smaller diamond is shown in Figure C.13. The fit shown is $S = c_0/(c_1 + \tilde{\lambda}) + c_2$ with $c_0 = 30400$ and $c_1 = 144$ and $c_2 = -44.7$.

C.7 Modifying the Continuum Calculation

So far we have been primarily discussing the causal set calculation and asking how we can modify our setup or interpretation of results to recover the area law. In this subsection, we approach reconciling the causal set and continuum calculations from the other direction:

we ask how we can modify the setup and calculation in the continuum to obtain a volume law.

One difference between the continuum and causal set calculations of Chapters 4 and 5 respectively, was that in the causal set case we have a UV cutoff in the theory from the very start, whereas in the continuum case we only introduce a cutoff after the restriction to the subregion. In other words, the UV cutoff is already present when the state is defined in the larger diamond in the causal set but this is not the case in the continuum. The UV cutoff is only introduced at the stage where the generalized eigenvalue problem is being solved for the entropy, (3.14).

The question then arises, what if we introduce a UV cutoff in the larger diamond in the continuum? We can do this by representing W and Δ in a truncated basis in the larger diamond:

$$\begin{aligned} W_{SJ,L}(u,v;u',v') = & \sum_{n=1}^{N_{max}} \frac{L^2}{\pi n} \frac{1}{||f_k||^2} f_k(u,v) f_k^*(u',v') \\ & + \sum_{k\in\mathcal{K},k>0}^{k_{max}} \frac{L}{k} \frac{1}{||g_k||^2} g_k(u,v) g_k^*(u',v'). \end{aligned} \tag{C.4}$$

and similarly

$$\begin{aligned} i\Delta(u,v;u',v') = & \sum_{n=-N_{max},n\neq 0}^{N_{max}} \frac{L^2}{\pi n} \frac{1}{||f_k||^2} f_k(u,v) f_k^*(u',v') \\ & + \sum_{k=-k_{max},k\in\mathcal{K}}^{k_{max}} \frac{L}{k} \frac{1}{||g_k||^2} g_k(u,v) g_k^*(u',v'), \end{aligned} \tag{C.5}$$

where as before, $\mathcal{K} = \{k \in \mathbb{R} \,|\, \tan(k\ell) = 2k\ell \text{ and } k \neq 0\}$. Carrying out the rest of the calculation as was done in Chapter 4 we find that we still obtain the logarithmic scaling with the UV-cutoff with a $\frac{1}{3}$ coefficient.

C.8 Extra Coarse-Graining Relations

If we repeat the entropy calculation of Chapter 5 but for a causal set which is a 50% coarse-grained version of the original sprinkling, we find that $S(N, 50\%)$ still scales linearly with N. Therefore, coarse-grained causal sets share some of the scaling properties of un-coarse-grained causal sets.

Now let M be a fixed (large) number. We then vary N and calculate $S(N, M/N \times 100\%)$, such that the causet one is calculating the entropy for is of fixed size (on average) but is a more and more dilute sampling of a denser causet. The result is that $S(N, M/N \times 100\%)$ grows logarithmically with N.

C.9 Entanglement Entropy as a Sum of Pairwise Contributions?

Perhaps if we could understand entanglement entropy in terms of a sum of contributions from pairwise constituents (one in each of the two subsystems which compose the entire system), we would better understand why there is more entropy in the causal set calculation of Chapter 5. In this manner of thinking of entanglement entropy, there would need to be more such pairs contributing to the entropy in the causet.

To this end, let us consider such a possibility in the context of a 1d chain of harmonic oscillators, such as the one studied in Chapter 6 and Appendix D. We divide the chain of oscillators into two connected subintervals A and B. We will label each oscillator in A with a_i and each oscillator in B with b_j. Now, we wish to investigate whether the total entanglement entropy associated to region A, S_A, can be expressed in terms of a sum of contributions from pairs of oscillators where one is in A and the other in B. For this we will need to know the pairwise entropy coming from the entanglement between an oscillator a_i and another one b_j. Let us call this entropy $S_E(a_i, b_j)$. We wish to investigate whether

$$S_A \stackrel{?}{=} \sum_{i \in A, j \in B} S_E(a_i, b_j). \tag{C.6}$$

A challenge we immediately face is that it is not clear how to define the entanglement entropy associated to two parts within a three (or more) part system. We can make a guess as to what $S_E(a_i, b_j)$ may look like. One guess is that it is the mutual information:

$$2S_E(a_i, b_j) \equiv S_{a_i} + S_{b_j} - S_{a_i b_j}. \tag{C.7}$$

Any successful definition of $S_E(a_i, b_j)$, which would reproduce S_A via (C.6), would have to fall off as the inverse square of the separation between each oscillator pair going into the sum (C.6). This is in order that it yield the expected logarithmic scaling relation for S_A.

With our guess (C.7), we find that $S_E(a_i, b_j)$ does not have the required scaling behaviour with the separation between the oscillators. Figure C.14 shows $S_E(a_i, b_j)$ versus ℓ/a (on a log-log scale) for a chain of 500 oscillators and periodic boundary conditions. $S_E(a_i, b_j)$ does not seem to have a power law dependence on ℓ/a. A Plot of

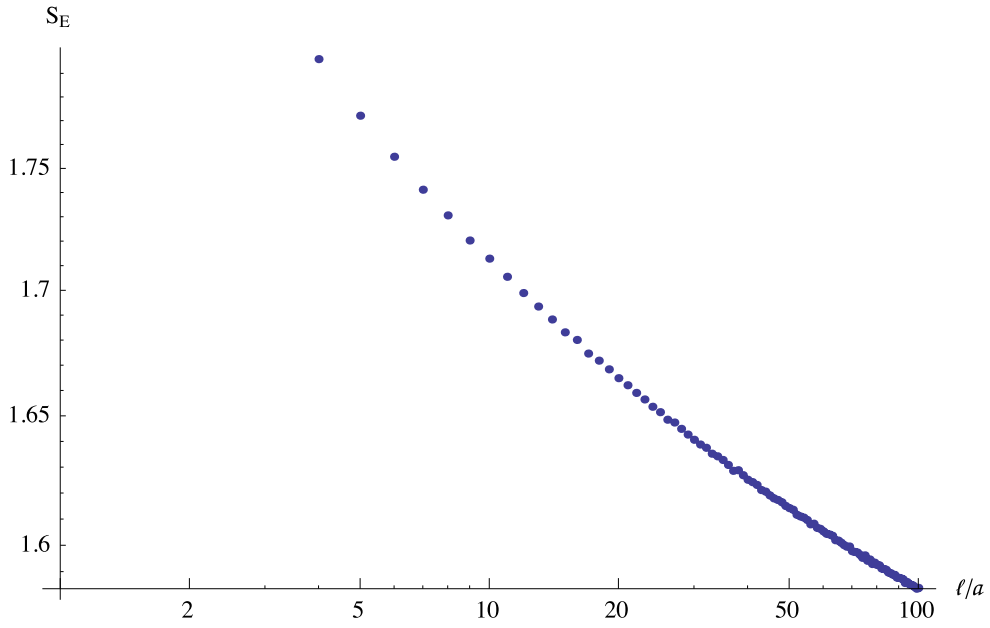

Figure C.14: Log-log plot of S_E vs. ℓ/a for a chain of 500 oscillators for a range of ℓ/a up to 100 oscillators.

$S_A = \sum_{i\in A, j\in B} S_E(a_i, b_j)$ is shown in Figure C.15. S_A does not have the required logarithmic scaling and instead grows nearly linearly with ℓ/a.

Here we have only considered one possibility for $S_E(a_i, b_j)$, namely that it is the mutual information. It is possible that with a different and more suitable definition of $S_E(a_i, b_j)$, the reconstruction of S_A as in (C.6) would be possible. If this were done, it might shed light on the causal set volume law result. More broadly, if such an understanding was achieved, it would be an important insight about entanglement entropy in general.

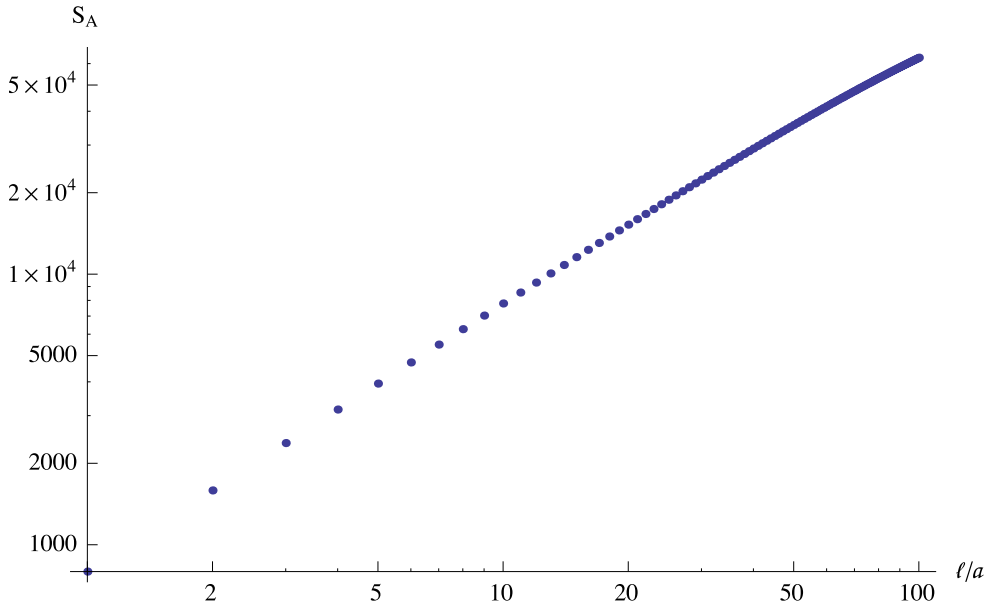

Figure C.15: Log-log plot of $S_A \equiv \sum S_E$ vs. ℓ/a for a chain of 500 oscillators for a range of ℓ/a up to 100 oscillators.

Appendix D

Zero Modes and Entanglement Entropy

While the ultraviolet divergences of entanglement entropy are widely discussed, infrared divergences are much less studied. A simple example of an infrared divergence in $1+1$d occurs in a massless theory of a chain of harmonic oscillators or scalar field on an interval with periodic boundary conditions [79–83]. Interesting new work is also being done where IR divergences arise, such as in entanglement entropy of excited states in conformal perturbation theory [84], entanglement in bandlimited quantum field theory [85], and others [47, 86, 87]. It is therefore worth understanding more rigorously in simple systems.

In this appendix we study in detail the divergence of the entanglement entropy in a simple theory as a result of a zero mode. Zero modes, analogous to free particles, do not have normalizable ground states. Theories that possess zero modes, such as the massless scalar field on a circle (spacetime cylinder), therefore do not have well-defined ground states [88]. One may still define a ground state for such a theory by either ignoring the zero mode solution *ad hoc*, or else by somehow regulating it. If it is included in the theory and not regulated, it can lead to infrared divergences, for example in the entanglement entropy. We study an example of this below.

Casini and Huerta [47, 86] have found infrared divergences in the massless limit of a scalar field theory on a finite interval within an infinite line. In this appendix, the system we study is an interval of a chain of harmonic oscillators within a *finite* chain with periodic boundary conditions (i.e., a circle). It is interesting that the infrared divergence found by [47, 86] on the infinite line is a double logarithm of the mass, while we find a

single logarithm divergence on the finite circle. Additionally, in the present appendix we pinpoint the source of the infrared divergence as a giant eigenvalue of an operator derived from the Lagrangian. This giant eigenvalue additionally has the interesting property that it also contributes to the scaling of the entanglement entropy with the UV cutoff in our finite system. Thus this eigenvalue cannot simply be discarded, as it contributes to the UV scaling of the entanglement entropy, and must therefore be regulated appropriately.

The results of this appendix appear in [54].

D.1 Entropy of Oscillators

We consider a chain of harmonic oscillators, with nearest-neighbour couplings. To find the entanglement entropy associated to a subchain (a connected subset of the full chain) of this system, we follow the procedure laid out in [6], which we now review.

The Lagrangian for our chain of oscillators is

$$\mathcal{L} = \frac{1}{2}\left(\sum_{N=1}^{N_{max}} G_{MN}\hat{\dot{q}}^M\hat{\dot{q}}^N - \sum_{N,M=1}^{N_{max}} V_{MN}\,\hat{q}_N\,\hat{q}_M\right) = \frac{1}{2}\sum_{N=1}^{N_{max}}[G_{MN}\hat{\dot{q}}^M\hat{\dot{q}}^N - m^2\hat{q}_N^2 - k(\hat{q}_{N+1}-\hat{q}_N)^2], \tag{D.1}$$

where k is the coupling strength between the oscillators, and in terms of the spatial UV cutoff a, $k = 1/a^2$ [53]. We define the positive, symmetric matrix W using the potential of this Lagrangian:

$$W_{MA}W^A{}_N = V_{MN}, \tag{D.2}$$

where the symmetric, positive definite metric G_{MN} and its inverse G^{MN} given by $G^{MP}G_{PN} = \delta^M{}_N$, is used to raise the index in (D.2). G_{MN} is a metric on the configuration space of the coupled harmonic oscillators. Now we consider the division of our chain of harmonic oscillators into a subchain whose oscillators will be labelled with Greek indices, and the remainder of the chain whose oscillators will be labelled with Latin indices. It is convenient to rewrite W in terms of blocks referring to these two divisions:

$$W_{AB} = \begin{pmatrix} W_{ab} & W_{a\beta} \\ W_{\alpha b} & W_{\alpha\beta} \end{pmatrix}.$$

Following the convention of [6], the inverse of W_{AB} will be expressed as

$$W^{AB} = \begin{pmatrix} W^{ab} & W^{a\beta} \\ W^{\alpha b} & W^{\alpha\beta} \end{pmatrix},$$

and the inverse of each block will be expressed with tildes (for example $\widetilde{W}^{ab}$ is the inverse of W_{ab}). It was shown in [6] that when ρ is the density matrix for the vacuum state, the reduced density matrix ρ_{red} associated to a subchain of oscillators (say, the Latin-indexed ones) can be expressed in terms of these blocks we have just defined, as

$$\rho_{red}(q^a, q'^b) = \sqrt{det(\widetilde{W}_{ab})}\exp[-\frac{1}{2}W_{ab}(q^a q^b + q'^a q'^b))]\exp[\frac{1}{4}\widetilde{W}^{\alpha\beta}W_{\alpha a}W_{\beta b}(q+q')^a(q+q')^b]. \tag{D.3}$$

Furthermore, it was shown that the entropy $S = -\mathrm{Tr}\rho_{red}\ln\rho_{red}$ can be expressed in terms of the eigenvalues λ_n of the operator $\Lambda^a_b \equiv W^{ac}W_{c\alpha}\widetilde{W}^{\alpha\beta}W_{\beta b}$, as

$$S = \sum_n \{\ln(\frac{1}{2}\sqrt{\lambda_n}) + \sqrt{1+\lambda_n}\ln(\sqrt{1+1/\lambda_n} + 1/\sqrt{\lambda_n})\}. \tag{D.4}$$

An alternative method to compute the entanglement entropy involves a matrix $C = \sqrt{XP}$, where X_{ij} are the field correlators at sites i and j, and P_{ij} are the conjugate momentum correlators at sites i and j in the region corresponding to the reduced density matrix. The entanglement entropies calculated using that method should match those found in this paper[1]. Below we compute the entanglement entropy associated to a shorter subchain within a longer chain of oscillators with periodic boundary conditions, using the formula (D.4). We will study the zero mode in this model and show that it leads to an infrared divergence. We single out the source of the divergence as a giant eigenvalue in the spectrum of Λ. We also consider the entanglement entropy associated to a subchain within a longer chain of oscillators with one fixed boundary. We show that no infrared divergences arise when setting the mass to zero in this case, since there are no zero modes.

D.1.1 Periodic Boundary Conditions

We consider the Lagrangian (D.1), with periodic boundary conditions $\hat{q}_{N+1} = \hat{q}_1$. If we set the mass to zero, the entropy diverges logarithmically, as we will show. If we set m to a

[1] See e.g. Section 2.2.1 of [47] for further details.

small but finite number, the entropy is finite and obeys the expected asymptotic form (as also reviewed in Section 3.1) for $a \to 0$ of logarithmic scaling with the UV cutoff [8, 38, 49]

$$S \sim \frac{1}{3} \ln[L \sin(\pi \ell / L)/\pi a] + c_1, \tag{D.5}$$

where ℓ and L are the physical lengths (number of oscillators times the spacing a) of the subchain and total chain respectively, and c_1 is a non-universal constant whose exact form is known for a few systems (eg. [89, 90]). In the limit that the length of the smaller subchain is much shorter than the length of the full chain ($\frac{\ell}{L} \to 0$), the entropy simplifies to

$$S \sim \frac{1}{3} \ln(\ell/a) + c_1. \tag{D.6}$$

(This was also reviewed in Chapter 3). The entropy in (D.5) or (D.6) is only well-defined with respect to an overall vacuum state. In referring to this result for the massless theory on a circle, one has to be careful to address the fact that this theory does not have a well-defined ground state due to the zero mode. Before moving on to a discussion of this zero mode, we first verify that by regulating the zero mode with a small mass, the result of (D.5) can indeed be obtained.

We regulate the zero mode with a small mass $m^2 = 10^{-6}$ and set $k = 10^6$. Our chain of oscillators contains 500 oscillators. We hold k fixed and vary ℓ. The result is shown in Figure D.1, where the solid curve is the function $S = b_1 \ln(\sin(\pi \ell / L)) + c_1$ being fit to the data. The best fit parameters are $b_1 = 0.3337$ and $c_1 = 5.9316$, in agreement with (D.5).

The contribution of the regulated zero mode to the entanglement entropy can be seen in the spectrum of Λ. It contributes a giant eigenvalue (relative to the other eigenvalues). A sample spectrum for a subchain of 10 oscillators within a chain of 500 oscillators, with $k = 10^6$ and $m^2 = 3 \times 10^{-8}$ is $\{31400, 0.470, 0.0321, 2.03 \times 10^{-3}, 9.82 \times 10^{-5}, 3.49 \times 10^{-6}, 8.88 \times 10^{-8}, 1.53 \times 10^{-9}, 1.66 \times 10^{-11}, 2.91 \times 10^{-13}\}$. The size of the giant eigenvalue is inversely proportional to the size of the mass regulator ($\lambda_{giant} \propto m^{-1}$). This leads to a power law divergence in the giant eigenvalue as $m \to 0$, as illustrated in Figure D.2 for the 10-subchain. The form of (D.4) then suggests that we should expect a logarithmic divergence of the entropy with the size of this mass regulator. This is indeed what we find. Figures D.3 and D.4 show the results for varying m in the limit $m \to 0$, while holding all other variables and parameters fixed. We considered subchains of 50 and 10 oscillators, within a chain of 500 oscillators. The 50-subchain result fits $S = b_2 \ln(m\ell) + c_2$ with $b_2 = -0.496$ and $c_2 = 0.624$, while the 10-subchain result fits the same function with $b_2 = -0.494$ and $c_2 = -0.674$. The infrared divergence is therefore logarithmic, with a universal coefficient of $\sim -\frac{1}{2}$.

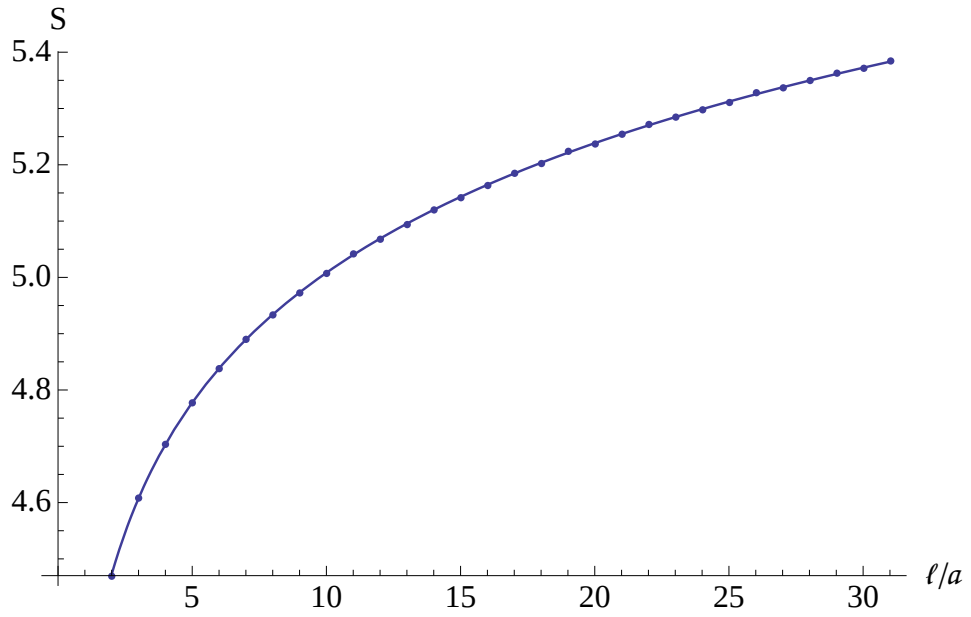

Figure D.1: S vs. ℓ/a for a chain of harmonic oscillators with periodic boundary conditions.

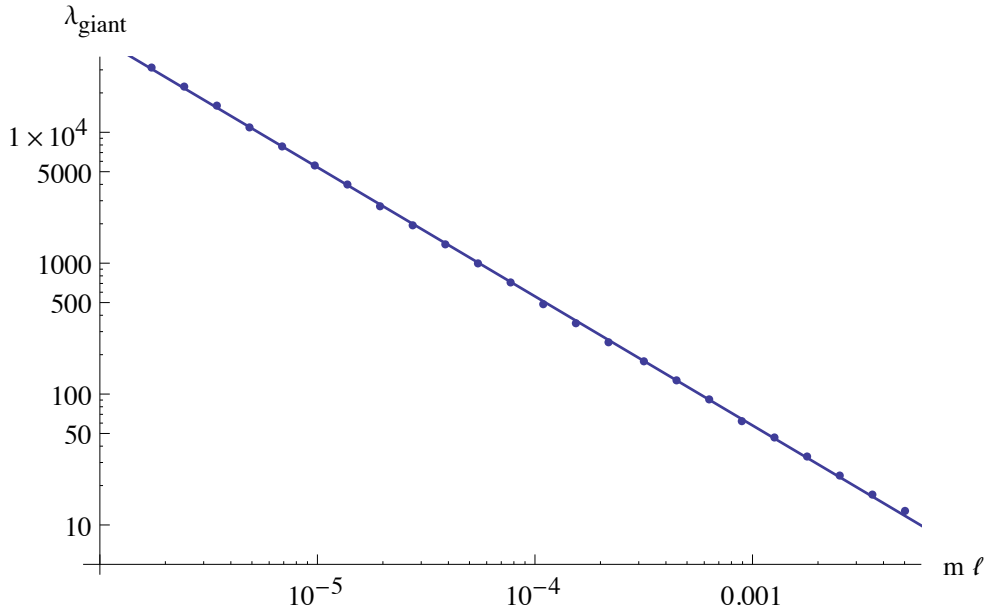

Figure D.2: λ_{giant} vs. $m\ell$ on a log-log scale for a subchain of 10 harmonic oscillators within a longer chain of 500 oscillators with periodic boundary conditions.

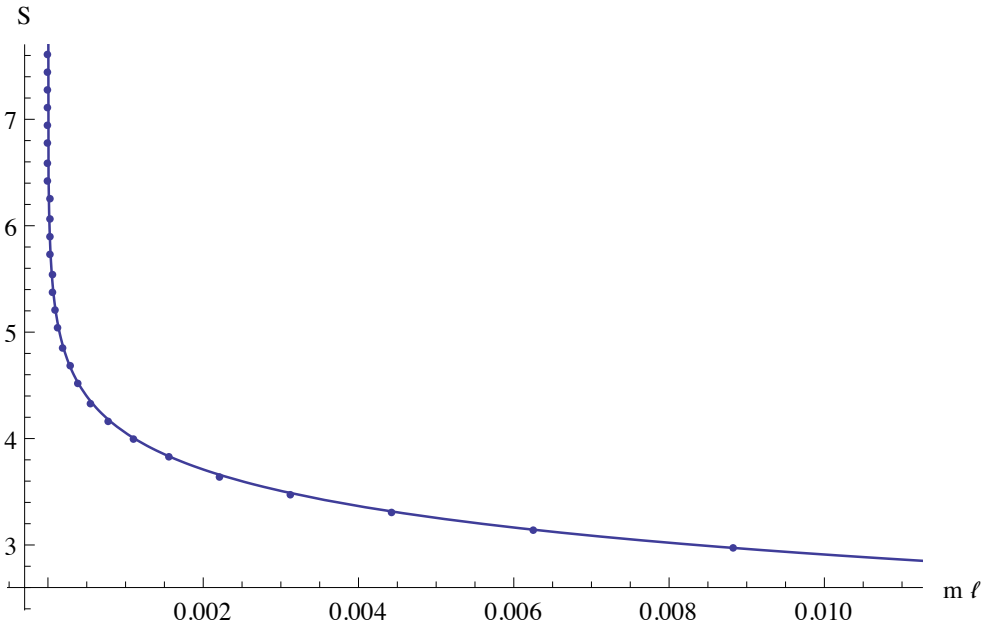

Figure D.3: S vs. mℓ for a subchain of 50 harmonic oscillators within a longer chain of 500 oscillators with periodic boundary conditions.

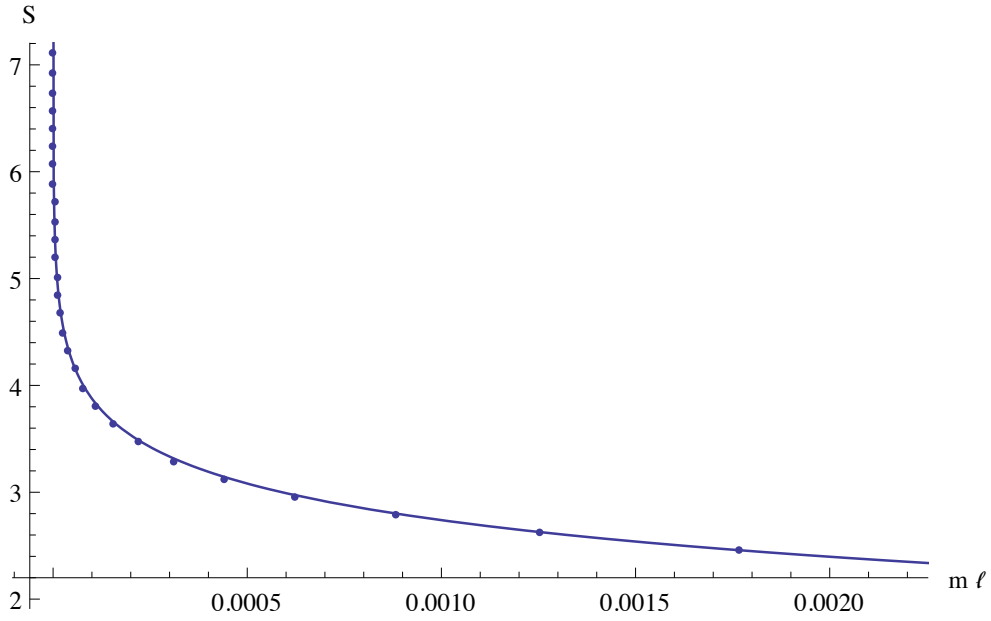

Figure D.4: S vs. mℓ for a subchain of 10 harmonic oscillators within a longer chain of 500 oscillators with periodic boundary conditions.

Surprisingly, the size of the giant eigenvalue also has a dependence on the UV cutoff. This dependence is logarithmic: $\lambda_{giant} = b_3 \ln(ma) + c_3$ (keeping m fixed), with b_3 and c_3 being non-universal constants that are inversely proportional to the length of the entire chain L. Figure D.5 shows the result for $\ell = \frac{5}{100\sqrt{10}}$ [2], $L = 10\ell$, and $m^2 = 10^{-6}$ and is fit by $\lambda_{giant} = b_3 \ln(ma) + c_3$ with $b_3 = -3985$ and $c_3 = -36093$.

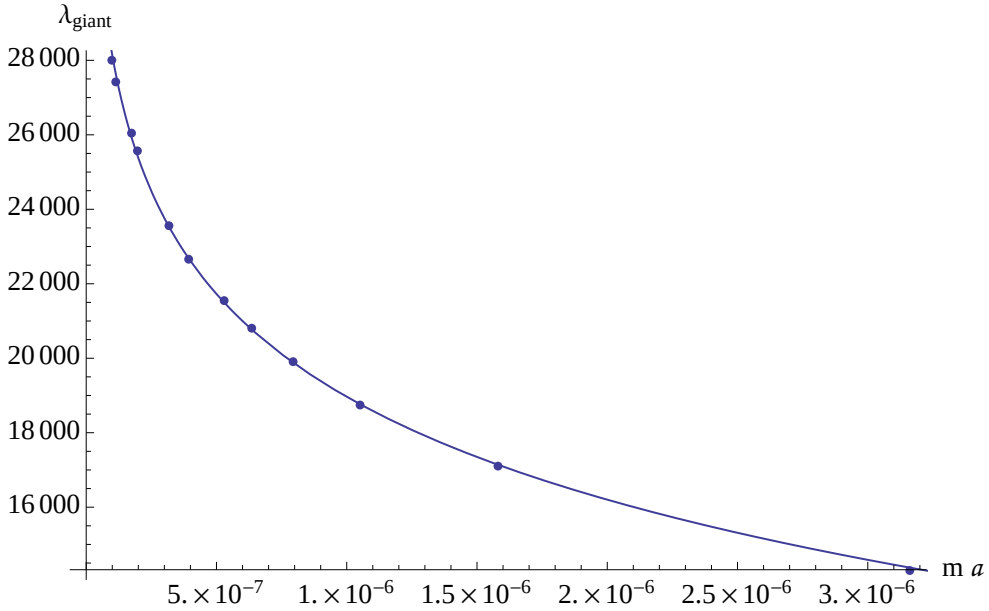

Figure D.5: S vs. ma for a subchain of length $\ell = \frac{5}{100\sqrt{10}}$ within a longer chain of length $L = 10\ell$, with fixed mass $m^2 = 10^{-6}$ and periodic boundary conditions.

Figure D.6 shows the scaling of b_3 and c_3 with the length of the entire chain L. We set $\ell = \frac{5}{100\sqrt{10}}$, $m^2 = 10^{-6}$, and impose periodic boundary conditions on the chain of oscillators. We set L/ℓ to different values, and for each of these values find b_3 and c_3 from the UV scaling. The fits correspond to $-b_3 = d_1 \frac{\ell}{L}$ with $d_1 \sim 4.0 \times 10^4$, and $-c_3 = d_2 \frac{\ell}{L}$ with $d_2 \sim 8.6 \times 10^4$. Therefore, we see that indeed $b_3 \propto L^{-1}$ and $c_3 \propto L^{-1}$, resulting in the

[2] In the numerical code for the computations of Figures D.5 and D.6, our initial value for the square of the oscillator spacing was $a^2 = 1/k = 1/10^5$ or $a = 1/(100\sqrt{10})$, and $\ell = na$ (with $n = 5$). As stated after (D.1), a is related to the constant k by $k = 1/a^2$, which is why a contains the $\sqrt{10}$ in its expression. For each subsequent data point we divide a^2 by y^2 and multiply n by y, where y is an integer, such that we keep ℓ fixed.

UV dependence of the zero mode becoming sub-leading compared to the total contribution of all the other eigenvalues in the limit $L \to \infty$. This is consistent with other works, such as [47, 86], that do not see a significant contribution from the zero mode to the UV scaling in the limit $L \to \infty$.

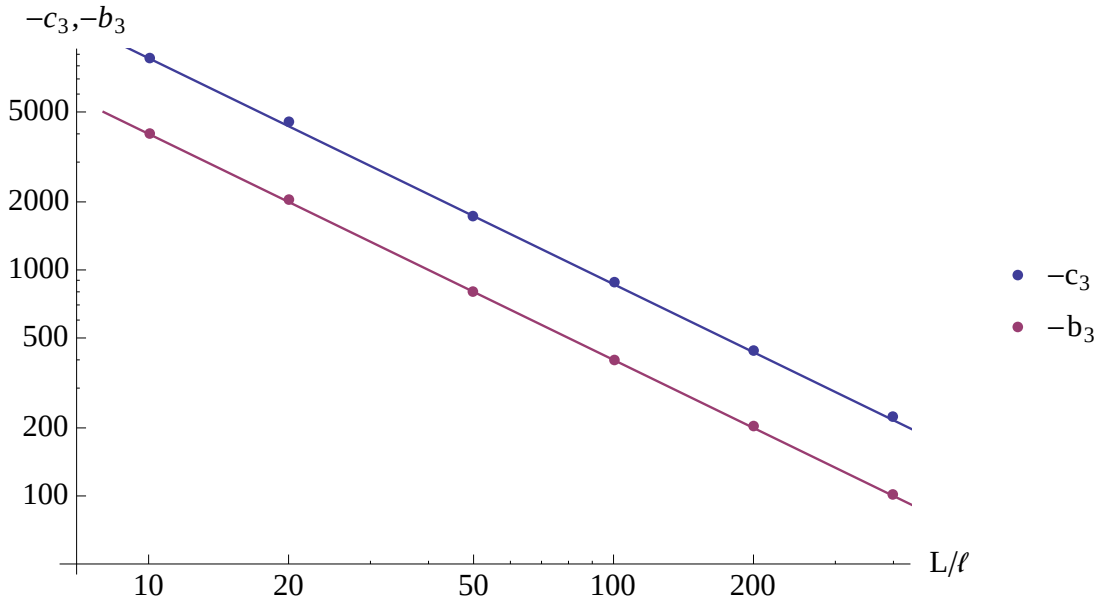

Figure D.6: $-b_3$ and $-c_3$ vs. L/ℓ on a log-log scale for a subchain of length $\ell = \frac{5}{100\sqrt{10}}$, $m^2 = 10^{-6}$, and periodic boundary conditions.

D.1.2 One Fixed Boundary

The chain of harmonic oscillators with Dirichlet boundary conditions at one end no longer possesses a zero mode (translation symmetry is broken), and as a result of this we do not expect there to be any infrared divergences for the massless theory. The Lagrangian for the oscillators is again (D.1), but with boundary condition $\hat{q}_{N+1} = 0$. Since a mass regulator is no longer needed, we set $m = 0$, and $k = 10^6$ as before.

The expected asymptotic form for the entanglement entropy, with $a \to 0$, is [8, 38, 49]

$$S \sim \frac{1}{6} \ln(L \sin(\pi\ell/L)/\pi a) + c_1. \tag{D.7}$$

Our result for the harmonic oscillators with one fixed boundary is shown in Figure D.7, and $S = b_1 \ln(\sin(\pi\ell/L)) + c_1$ is fit to this data. The best fit parameters are $b_1 = 0.1567$ and $c_1 = 0.9150$, in agreement with (D.7). Also, as expected, there is no longer a giant eigenvalue in the spectrum of Λ. A sample spectrum for a subchain of 10 oscillators within a chain of 500 oscillators, with $k = 10^6$ and $m = 0$ is $\{0.738, 7.72 \times 10^{-3}, 5.98 \times 10^{-5}, 2.56 \times 10^{-7}, 6.06 \times 10^{-10}, 6.98 \times 10^{-13}, 6.66 \times 10^{-14}, 2.44 \times 10^{-14}, -1.62 \times 10^{-15}, -1.98 \times 10^{-15}\}$.

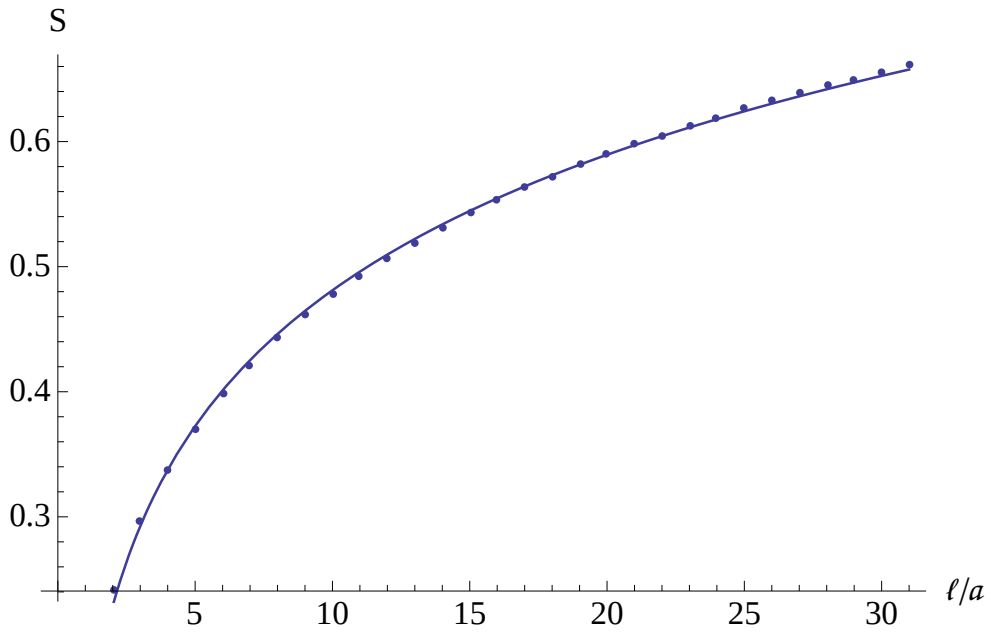

Figure D.7: S vs. ℓ/a for a chain of harmonic oscillators with one fixed boundary.

We have just established that there is no infrared divergence for the chain with one fixed boundary, but we will nevertheless examine more closely the small mass limit of this case. Figure D.8 shows the result for varying m in its limit $m \to 0$, while holding all other variables and parameters fixed. The subchain consists of 50 oscillators, within a longer chain of 500 oscillators. The entropy remains finite for all small m including $m = 0$. The data fits $S = b_4 \ (m\ell)^2 + c_4$ with best fit parameters $b_4 = -0.532$ and $c_4 = 0.741$.

We have thus demonstrated through our specific example, the importance of correctly regulating a theory containing zero modes in order to get physically meaningful scalings for entanglement entropy. We saw that the unregulated theory has an IR divergence in the entanglement entropy, and thus obscures all interesting UV physics. Finally, we

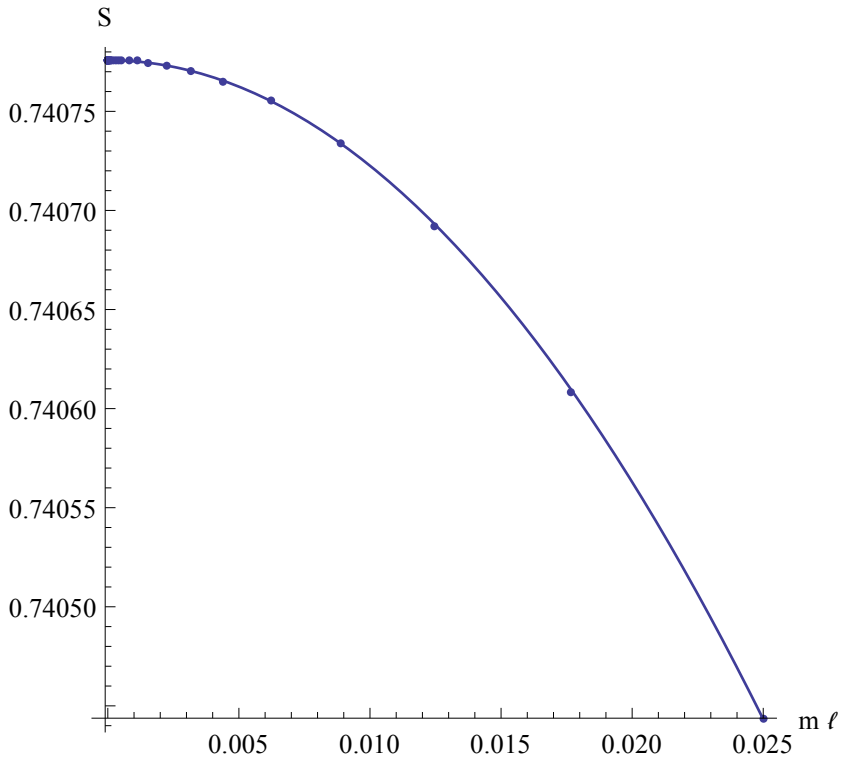

Figure D.8: S vs. $m\ell$ for a subchain of 50 harmonic oscillators within a longer chain of 500 oscillators with one fixed boundary.

demonstrated the resolution of this problem by introducing a mass regulator to the theory, revealing the interesting behaviour of the entropy. We also found that the zero mode has a dependence on the UV cutoff which makes a significant contribution to the entanglement entropy for finite L and becomes sub-leading in the limit $L \to \infty$.

Another example of an IR regulation of the zero mode is described in [33]. There, the regulation is done by placing a massless scalar field in a causal diamond instead of infinite Minkowski space.